

# Sheffield Hallam University

*Micro-mechanics modelling of smart materials.*

SHAH, Syed Asim Ali.

Available from the Sheffield Hallam University Research Archive (SHURA) at:

<http://shura.shu.ac.uk/20349/>

## A Sheffield Hallam University thesis

This thesis is protected by copyright which belongs to the author.

The content must not be changed in any way or sold commercially in any format or medium without the formal permission of the author.

When referring to this work, full bibliographic details including the author, title, awarding institution and date of the thesis must be given.

Please visit <http://shura.shu.ac.uk/20349/> and <http://shura.shu.ac.uk/information.html> for further details about copyright and re-use permissions.

Sheffield Hallam University  
Learning and Information Services  
Adsetts Centre, City Campus  
Sheffield S1 1WD

102 113 360 4



**REFERENCE**

ProQuest Number: 10700995

All rights reserved

INFORMATION TO ALL USERS

The quality of this reproduction is dependent upon the quality of the copy submitted.

In the unlikely event that the author did not send a complete manuscript and there are missing pages, these will be noted. Also, if material had to be removed, a note will indicate the deletion.



ProQuest 10700995

Published by ProQuest LLC (2017). Copyright of the Dissertation is held by the Author.

All rights reserved.

This work is protected against unauthorized copying under Title 17, United States Code  
Microform Edition © ProQuest LLC.

ProQuest LLC.  
789 East Eisenhower Parkway  
P.O. Box 1346  
Ann Arbor, MI 48106 – 1346

**SHEFFIELD HALLAM UNIVERSITY**

**MICRO-MECHANICS MODELLING OF SMART MATERIALS**

**Syed Asim Ali Shah**

**A Thesis submitted in partial fulfilment of the requirements of  
Sheffield Hallam University  
For the degree of Doctor of Philosophy**

**2016**

# TABLE OF CONTENTS

PREFACE.....	vi
ACKNOWLEDGEMENTS .....	vii
NOMENCLATURE.....	viii
LIST OF FIGURES .....	xi
LIST OF TABLES .....	xiv
ABSTRACT.....	xv
<b>CHAPTER 1</b>	
<b>Introduction .....</b>	<b>1</b>
1.1 Knowledge Gap .....	2
1.2 Aims and Objectives .....	5
<b>CHAPTER 2</b>	
<b>Literature Review .....</b>	<b>7</b>
2.1 History of Composites.....	7
2.1.1 Composite Building Materials .....	8
2.1.2 Fiber-Reinforced Composite .....	9
2.1.3 Metal Matrix Composites .....	11
2.1.4 Ceramic Matrix Composites.....	14
2.1.5 Aluminum Matrix Composites .....	14
2.2 Reinforcement in Matrix.....	18
2.3 Types of Reinforcements.....	21
2.4 Matrix Materials and Key Composites .....	22
2.5 Advantages and Disadvantages of MMCs .....	24
2.6 Characteristics and Design Considerations of MMCs.....	25
2.7 Fabrication Methods .....	28
2.7.1 MMCs Fabrication – Processing Routes.....	29
2.7.2 Liquid State Processing .....	30
2.7.3 Stir-Casting Approach.....	32

2.7.4 Solid State Processing.....	33
2.8 Applications of MMCs .....	34
2.9 Limitations of MMCs .....	35
2.10 Role of Interface: Matrix-Reinforcement Interface in an MMC .....	36
2.11 Scope of SiC Reinforced Al Composites .....	37
2.12 Numerical Modelling: A Unit Cell Approach .....	39

### **CHAPTER 3**

#### **An Empirical Method of Calculating Interfacial Strength in a Second Phase**

<b>Reinforced Alloy.....</b>	<b>43</b>
3.1 Introduction.....	44
3.2 Estimation of Interfacial Stress and Strain using Numerical Modelling .....	46
3.2.1 Interfacial Fracture Strength Model.....	46
3.2.2 Interfacial Stress / Strain Behaviour of Reinforced Alloy System.....	49
3.2.3 Constants Calculation.....	53
3.3 Interfacial Strengthening Behaviour of Reinforced Alloy System.....	55
3.3.1 Strengthening Behaviour in MMCs .....	55

### **CHAPTER 4**

<b>Finite Element Analysis of a Unit Cell Using ANSYS .....</b>	<b>57</b>
4.1 Introduction.....	57
4.2 Analysis Using ANSYS .....	58
4.2.1 Unit Cell Concept.....	58
4.2.2 Finite Element Analysis of Interfacial Characteristics of Al/SiC Metal Matrix Composite.....	61
4.3 Al/SiC Stress Strain Simulations using ANSYS .....	65
4.4 Empirical Model of a Unit Cell: Young's Modulus at the Interface.....	69
4.5 Correlation with Empirical Model .....	71
4.6 Modelling and Analysis of Cohesive Zone Element at Matrix-Reinforcement Interface.....	73
4.7 Observations from the CZE Analysis .....	76
4.7 Conclusion.....	79

## CHAPTER 5

<b>Strengthening Behaviour with T6 and HT1 Heat Treatments .....</b>	<b>80</b>
5.1 Introduction .....	80
5.2 T6 Heat Treatment.....	82
5.3 HT1 Heat Treatment .....	83
5.4 Materials Considered for Simulations .....	83
5.5 Microstructure of Al/SiCp .....	85
5.6 Unit Cell - FEA Analysis.....	85
5.6.1 Modelling the Unit Cell from the Interface .....	85
5.6.2 Comparing Different Heat Treatments with Same Volume Percent of SiCp	87
5.6.3 Varying the Volume Percent of SiCp: Keeping the same Heat Treatment...	89
5.6.4 Effects of Dislocation Pile Up upon Strengthening in A359/SiCp.....	91
5.6.5 Predictions and Correlations.....	92

## CHAPTER 6

<b>Simulating Linear Response of SiC Reinforced Aluminium Alloy (VAMUCH)..</b>	<b>96</b>
6.1 VAMUCH Simulation of Al/SiC.....	97
6.2 Inputs to VAMUCH code.....	98
6.3 VAMUCH Outputs.....	102
6.4 Predictions and Correlations.....	107
6.5 Conclusions .....	109

## CHAPTER 7

<b>Modelling Non-Linear Response of SiC Reinforced Aluminum Alloy .....</b>	<b>111</b>
7.1 Introduction.....	111
7.1.1 Different Hardening models .....	114
7.2 Modelling of the Composite .....	117
7.2.1 Finite Element Modelling .....	118
7.2.2 Boundary Conditions .....	119
7.3 Methodology .....	120
7.3.1 3D Unit Cell.....	120
7.3.2 Chaboche Kinematic Hardening Model .....	122
7.4 Results and Discussion .....	124

7.5 Conclusions .....	131
<b>CHAPTER 8</b>	
<b>Conclusions and Future Works .....</b>	<b>133</b>
8.1 Conclusions .....	133
8.2 Key Contributions to Knowledge.....	136
8.3 Future Work.....	137
<b>REFERENCES .....</b>	<b>139</b>
<b>Appendix A: Getting to know ANSYS.....</b>	<b>161</b>
<b>Appendix B: Initial Experiments on the Unit Cell Concept.....</b>	<b>166</b>
<b>Appendix C: ANSYS APDL Code for Non-Linear Analysis.....</b>	<b>174</b>
<b>Appendix D: ANSYS APDL Code with Cohesive Zone Element Analysis .....</b>	<b>186</b>
<b>Appendix E: Fatigue Analysis .....</b>	<b>188</b>
<b>Appendix F: List of Publications and Posters .....</b>	<b>201</b>

## **PREFACE**

This report describes PhD work carried out at Sheffield Hallam University, Sheffield, United Kingdom from November 2013 to January 2016. The submission of the report is in accordance with the requirements for the award of the degree of Doctorate of Philosophy in Computer Simulation and Modelling under the auspices of Sheffield Hallam University.

## **ACKNOWLEDGEMENTS**

At this point, I would like to thank my family and friends for their valuable support at every level. I have a real debt of gratitude to my Mother and Father for their unremitting zeal and helpfulness. Also special thanks to my wife Kiran, and my daughters Ibba and Zoha for helping and encouraging me to achieve my goals, to broaden my horizons and realize my ambitions. I hope to give them more joy and happiness in the future. Finally, I would like to thank my supervisors Dr. Syed Hasan and Dr. Mike Bramhall who truly believed in me all these years, for giving me the chance to start fulfilling my dreams.

I would also like to thank Dr. Wenbin Yu, Dr. Liang Zhang and Mr. Hamsasew M Sertse from Purdue University, USA for their kind help.

## NOMENCLATURE

$T$	-	Absolute temperature
$A_i$	-	Area of interface
$A_m$	-	Area of matrix
$A_p$	-	Area of particulate
$A_{uc}$	-	Area of unit cell
$V_f$	-	Volume fraction of reinforcement
$a$	-	Aspect ratio of the reinforcement
$\bar{r}$	-	Average diameter of the particle
$\bar{h}$	-	Average length of the particle
$R$	-	Crack Propagation Resistance
$n$	-	Cyclic strain hardening exponent
$K$	-	Cyclic strength coefficient
$Z$	-	Density of interface sites
$\rho_s$	-	Density of the interface region
$d$	-	Diameter of the particle
$A$	-	Dislocation pile up
$\varepsilon_e$	-	Elastic energy involved with inserting atom into a matrix
$G$	-	Elastic energy release rate
$K_t$	-	Elastic stress concentration factor
$E_R$	-	Energy consumed in crack propagation
$\varepsilon_p$	-	Energy required to create two fracture surfaces
$d_e$	-	Equivalent dimension of the particle
$\varepsilon_f$	-	Fatigue ductility coefficient
$C$	-	Fatigue ductility exponent
$\sigma_f$	-	Fatigue strength coefficient

B	-	Fatigue strength exponent (Basquin's exponent)
$\epsilon_f$	-	Formation energy of the impurity in the bulk
$K_{IC}$	-	Fracture toughness
$K_{int}$	-	Fracture toughness at the interface
$\epsilon_{gb}$	-	Grain boundary energy
R	-	Gas constant
$a_i$	-	Impurity atomic radius
$\sigma_{int}$	-	Interfacial fracture strength
$G_k$	-	Intergranular fracture
$a_m$	-	Matrix atomic radius
B	-	Modification of the boundary energy by impurities using Zuchovitsky Eq.
E	-	Modulus of elasticity
$\epsilon_a$	-	New interfacial energy caused by segregation
$\sigma_N$	-	Normal stress
$N_f$	-	Number of cycles of failure
$2N_f$	-	Number of reversals to failure
s	-	Overall dimension of the cubic unit cell
d	-	Particle thickness
$\nu$	-	Poisson's ratio
$p_c$	-	Properties of the composite
$p_m$	-	Properties of the matrix
$p_f$	-	Properties of the reinforcement
c	-	Segregate constant needed to cause embrittlement
G	-	Shear modulus
$G_{int}$	-	Strain energy
L	-	Stress carrying capability
$L_m$	-	Stress carrying capability of matrix

$L_p$	-	Stress carrying capability of particulate
$K$	-	Stress intensity factor
$\epsilon_s$	-	Surface energy required in forming the impurity atom
$\sigma_T$	-	Tensile stress
$D = d_i$	-	Thickness of the interface region
$v_m - v_{in}$	-	Volume fractions for interface failure
$v_m$	-	Volume fraction for matrix
$v_f$	-	Volume fraction for particulate
$v_{\bar{f}}$	-	Volume fraction of particles including interphase
$n$	-	Work hardening exponent
$E$	-	Young's modulus
$E_{int}$	-	Young's modulus of interface
$E_i$	-	Young's modulus of the inhomogeneity
$E_m$	-	Young's modulus of the matrix
$\Delta\sigma$	-	2 X the stress amplitude

# LIST OF FIGURES

FIGURE 1: SOME INDUSTRIA AMCS APPLICATIONS:(A) BRAKE ROTORS FOR HIGH SPEED TRAIN, (B) AUTOMOTIVE BRAKING SYSTEMS, (C) AUTOMOTIVE PUSHRODS AND (D) CORES FOR HV ELECTRICAL WIRES. .... 16

FIGURE 2: METALLIC MATRIX REINFORCEMENT TYPES, (A) REINFORCEMENT BY LONG, CONTINUOUS FIBRES, (B) REINFORCEMENT BY WISKERS, (C) REINFORCEMENT BY PARTICULATES. .... 21

FIGURE 3: OVERVIEW FLOW CHART OF MMC PROCESSING ROUTES ..... 30

FIGURE 4: A CUBIC UNIT CELL WITH ITS 8 NODES AT THE CORNERS ..... 40

FIGURE 5: SCHEMATIC OF THE MODEL UNIT CELL SHOWING WHERE THE FORCES WERE ACTING AND THE FIXED SUPPORTS ..... 41

FIGURE 6: (A) CRACK PROPAGATING THROUGH THE INTERFACE (B) CRACK PROPAGATING THROUGH THE PARTICULATE..... 45

FIGURE 7: THE GRID PATTERN SHOWING THE MESHING USED IN THIS MODEL ..... 59

FIGURE 8: (A) THE GRID PATTERN SHOWING THE TETRAHEDRAL MESHING (B) MAGNIFIED MESH AT THE INTERFACE ..... 60

FIGURE 9: (A) THE CONTACT PLANE BETWEEN ALUMINIUM MATRIX AND SICP REINFORCEMENT (B) THE FIXED SUPPORTS AND THE FORCES BEEN APPLIED (C) THE COORDINATE SYSTEM (D) MESHING OF THE MODEL USED. .... 62

FIGURE 10: THE GIRD PATTERNS SHOWING STRAINS RECORDED AT 77, 147, 149, 151, 155, 193, 232, 310 MPA ..... 63

FIGURE 11: THE GIRD PATTERNS SHOWING STRESSES RECORDED AT 77, 147, 149, 151, 155, 193, 232, 310 MPA..... 64

FIGURE 12: COMPARISION OF THE STRESS/STRAIN VALUES AT THE CENTER, INTERFACE AND THE EDGE OF THE UNIT CELL. .... 66

FIGURE 13: COMPARISON OF INTERFACIAL STRESS / STRAIN CURVES OF AL/SIC COMPOSITE UNIT CELL AND THE EMPIRICAL RESULTS..... 67

FIGURE 14: COMPARISON OF INTERFACIAL STRESS / STRAIN CURVES OF AL/SIC COMPOSITE UNIT CELL AT 0° AND 90° OF THE APPLIED LOAD AND THE EMPIRICAL RESULTS.. 68

FIGURE 15: COMPARISON OF INTERFACIAL STRESS / STRAIN CURVES OF AL/SIC COMPOSITE UNIT CELL AND THE EMPIRICAL RESULTS..... 69

FIGURE 16: CONVERSION OF A SPHERICAL PARTICLE TO A CUBIC PARTICLE ..... 70

FIGURE 17: INTERFACIAL STRESS STRAIN CURVES OF AL/SIC UNIT CELL AT 0° ..... 72

FIGURE 18: STRESS STRAIN CURVES OF AL/SIC UNIT CELL AT 90° ..... 72

FIGURE 19: (A) 3D-UNIT CELL LINES,(B) NODES 3D, (C) NODES 2D, (D) 3D-COMPLETE UNIT CELL, (E) INTERFACE WITH SAME PROPERTIES AS THE MATRIX, (F) INTERFACE WITH DIFFERENT PROPERTIES. .... 74

FIGURE 20: (A) CZE (B) HALF SECTION UNIT CELL WITH CZE..... 75

FIGURE 21: STRESS/STRAINS AT THE CZE FOR 20% VOL FRACTION SIC AT T1, HT1 AND T6... 76

FIGURE 22: STRESS/STRAINS AT THE CZE FOR 31% VOL FRACTION SIC AT T1, HT1 AND T6... 76

FIGURE 23: STRESS/STRAINS AT THE CZE FOR 20% AND 31% VOLUME FRACTION SIC AT T1. 77

FIGURE 24: STRESS/STRAINS AT THE CZE FOR 20% AND 31% VOLUME FRACTION SIC AT T1 COMPARED WITH STRESS/STRAINS AT THE INTERFACE WITHOUT THE CZE FOR 20% VOLUME FRACTION SIC AT T1. ....	78
FIGURE 25: A BLOWN UP UNIT CELL SHOWING THE INTERFACE AS A RING WITH ONE UNIT ON THE INTERFACE WHICH IS FURTHER BLOWN UP IN (B).....	86
FIGURE 26: COMPARING STRESS VS STRAIN OF THE EXPERIMENTAL RESULTS VS ANSYS FEA SIMULATION RESULTS FOR AL A359/SiC <sub>p</sub> , 20% VOL FOR T6 HEAT TREATMENT, HT1 HEAT TREATMENT AND THE AS RECEIVED SAMPLE. ....	88
FIGURE 27: COMPARING STRESS VS STRAIN OF THE EXPERIMENTAL RESULTS VS ANSYS FEA SIMULATION RESULTS FOR AL A359/SiC <sub>p</sub> , 31% VOL FOR T6 HEAT TREATMENT, HT1 HEAT TREATMENT AND THE AS RECEIVED SAMPLE. ....	88
FIGURE 28: COMPARING EXPERIMENTAL RESULTS VS ANSYS FEA SIMULATION RESULTS FOR AL A359/SiC <sub>p</sub> , 20% VOL AT T1 VS 31% VOL SIC AT T1.....	90
FIGURE 29: COMPARING EXPERIMENTAL RESULTS VS ANSYS FEA SIMULATION RESULTS FOR AL A359/SiC <sub>p</sub> , 20% VOL AT T1 VS 31% VOL SIC AT T6.....	90
FIGURE 30: COMPARING EXPERIMENTAL RESULTS VS ANSYS FEA SIMULATION RESULTS FOR AL A359/SiC <sub>p</sub> , 20% VOL AT T1 VS 31% VOL SIC AT HT1.....	91
FIGURE 31: COMPARING EXPERIMENTAL RESULTS VS ANSYS FEA SIMULATION STRESS/STRAIN RESULTS FOR AL A359/SiC <sub>p</sub> , 20% VOL AND 31% VOL AT T1. ....	93
FIGURE 32: PARTICULATE SHEARING, FORMING NEW SURFACES. ....	94
FIGURE 33: EXPERIMENTAL RESULTS PLOTTED FOR STRESS / STAINS FOR AL SIC FOR 20% AND 31 % VOL FRACTION AT TEMPERATURES T1, HT1 AND T6 .....	104
FIGURE 34: COMPARISON OF EXP AND VAMUCH LINEAR RESULTS FOR AL/SiC 31% AT T1... ..	104
FIGURE 35: COMPARISON OF EXP AND VAMUCH LINEAR RESULTS FOR AL/SiC 31% AT HT1. ....	105
FIGURE 36: COMPARISON OF EXP AND VAMUCH LINEAR RESULTS FOR AL/SiC 31% AT T6... ..	105
FIGURE 37: COMPARISON OF EXP AND VAMUCH LINEAR RESULTS FOR AL/SiC 20% AT T6... ..	106
FIGURE 38: COMPARISON OF EXP AND VAMUCH LINEAR RESULTS FOR AL/SiC 20% AT HT1. ....	106
FIGURE 39: COMPARISON OF EXP AND VAMUCH LINEAR RESULTS FOR AL/SiC 20% AT T1... ..	107
FIGURE 40: EXPERIMENTAL RESULTS AND VAMUCH RESULTS PLOTTED FOR STRESS / STAINS FOR AL SIC FOR 20% AND 31 % VOL FRACTION AT TEMPERATURES T1, HT1 AND T6 ALONG WITH THE T6.....	108
FIGURE 41: LINEAR SECTION (SECTION MARKED RED IN FIG 34) OF THE EXPERIMENTAL RESULTS AND VAMUCH RESULTS PLOTTED FOR STRESS / STAINS FOR AL SIC FOR 20% AND 31 % VOL FRACTION AT TEMPERATURES T1, HT1 AND T6.....	108
FIGURE 42: (A) KINEMATIC HARDENING (B) ISOTROPIC HARDENING .....	112
FIGURE 43: BAUSCHINGER EFFECT .....	113
FIGURE 44: UNIT CELL MODEL. (A) SQUARE ARRAY ARRANGEMENT OF PARTICLES; (B) UNIT CELL .....	117
FIGURE 45: A CROSS SECTION CUT FROM A UNIT CELL TO VISUALLY SEE THE SILICON CARBIDE PARTICLES .....	121
FIGURE 46: SIC PARTICLES IN 20% VOLUME FRACTION INSTANCE WITHOUT THE MATRIX BLOCK. ....	121
FIGURE 47: GRID OF THE SINGLE 3D UNIT CELL SHOWING THE REINFORCEMENT AND THE MATRIX.....	122

FIGURE 48: STRESS-STRAIN BEHAVIOUR FOR LINEAR KINEMATIC HARDENING ILLUSTRATED ..... 123

FIGURE 49: HYSTERESIS LOOP FOR 5-50% VOLUME FRACTION SiC IN AL MATRIX (400 SUB STEPS)..... 126

FIGURE 50: HYSTERESIS LOOP FOR AL-SiC 20% VOL FRACTION ..... 127

FIGURE 51: HYSTERESIS LOOP FOR AL-SiC 31% VOL FRACTION ..... 127

FIGURE 52: HYSTERESIS LOOP FOR AL-SiC 20% AND 31% VOL FRACTION ..... 128

FIGURE 53: HYSTERESIS LOOP DEFINING THE DUCTILITY DIFFERENCES FOR 5-50% VOLUME FRACTION SiC IN AL MATRIX. (EACH RESULT CONSISTING OF 400 SUBSETS PER ONE CYCLE)..... 131

## LIST OF TABLES

TABLE 1: MECHANICAL PROPERTIES OF AL AND SIC .....	61
TABLE 2: THE CHEMICAL COMPOSITION OF THE MATRIX ALLOY AND THE AMOUNT OF SiC <sub>p</sub> .	84
TABLE 3: YOUNGS MODULUS OF AL A359-SiC <sub>p</sub> -20P AND 31P AT DIFFERENT HEAT TREATMENTS .....	86
TABLE 4: VALUES OF STRESS AND STRAIN AS MEASURED IN THE SIMULATIONS AND EXPERIMENTALLY WITH THEIR DIFFERENCE FOR AL A359/SiC <sub>p</sub> 20% VOL .....	93
TABLE 5: VALUES OF STRESS AND STRAIN AS MEASURED IN THE SIMULATIONS AND EXPERIMENTALLY WITH THEIR DIFFERENCE FOR AL A359/SiC <sub>p</sub> 31% VOL .....	93
TABLE 6: VALUES OF E1 FOR DIFFERENT HEAT TREATMENTS FOR DIFFERENT VOLUME FRACTIONS FROM VAMUCH .....	100
TABLE 7: VALUES OF v12 FOR DIFFERENT HEAT TREATMENTS FOR DIFFERENT VOLUME FRACTIONS FROM VAMUCH .....	100
TABLE 8: VAMUCH VALUES TO BE PLOTTED .....	103
TABLE 9: EXPERIMENTAL RESULTS FOR STRESS / STAINS FOR AL SIC FOR 20% AND 31 % VOL FRACTION AT TEMPERATURES T1, HT1 AND T6.....	103

## ABSTRACT

Metal Matrix ceramic-reinforced composites are rapidly becoming strong candidates as structural materials for many high temperature and engineering applications. Metal matrix composites (MMC) combine the ductile properties of the matrix with a brittle phase of the reinforcement, leading to high stiffness and strength with a reduction in structural weight. The main objective of using a metal matrix composite system is to increase service temperature or improve specific mechanical properties of structural components by replacing existing super alloys.

The purpose of the study is to investigate, develop and implement second phase reinforcement alloy strengthening empirical model with  $\text{SiC}_p$  reinforced A359 aluminium alloy composites on the particle-matrix interface and the overall mechanical properties of the material.

To predict the interfacial fracture strength of aluminium, in the presence of silicon segregation, an empirical model has been modified. This model considers the interfacial energy caused by segregation of impurities at the interface and uses Griffith crack type arguments to predict the formation energies of impurities at the interface. Based on this, model simulations were conducted at nano scale specifically at the interface and the interfacial strengthening behaviour of reinforced aluminium alloy system was expressed in terms of elastic modulus.

The numerical model shows success in making prediction possible of trends in relation to segregation and interfacial fracture strength behaviour in  $\text{SiC}$  particle-reinforced aluminium matrix composites. The simulation models using various micro scale modelling techniques to the aluminum alloy matrix composite, strengthened

with varying amounts of silicon carbide particulate were done to predict the material state at critical points with properties of Al-SiC which had been heat treated.

In this study an algorithm is developed to model a hard ceramic particle in a soft matrix with a clear distinct interface and a strain based relationship has been proposed for the strengthening behaviour of the MMC at the interface rather than stress based, by successfully completing the numerical modelling of particulate reinforced metal matrix composites.

# CHAPTER 1

## Introduction

The satisfactory performance of metal matrix composites (MMCs) depends critically on their integrity, the heart of which is the quality of the matrix-reinforcement interface. The nature of the interface depends in turn on the processing of the MMC component. At the micro-level the development of local deformation gradients around the reinforcement can be very different to the nominal conditions and play a crucial role in important microstructural events such as segregation and precipitation at the matrix-reinforcement interface. These events dominate the cohesive strength and mechanical properties of the interface and hence the overall performance of the metal matrix composite (MMC).

The subject of this thesis is to predict the interfacial strengthening mechanism at the matrix-reinforcement interface in a metal matrix composite. To determine such a mechanism will help the design engineers to incorporate advanced MMC's in real life applications. To this end simulation has been done on a unit cell and a numerical method then proposed to predict the interfacial strengthening of a metal matrix composite. These analyses have been complimented with experimental data determined from previous studies by Dr.S.T.Hasan and his group of researchers.

A literature review is first presented in chapter 2, which includes the different types of composites, the advantages and disadvantages of MMCs, along with the different fabrication techniques used to make the MMCs. Basic structure of the unit cell used in this study is also explained in this chapter.

Chapter 3 then describes an empirical method of calculating interfacial strength in a second phase reinforced alloy. In this chapter the basic model presented will be used in the rest of the study. Chapter 4 looks at the finite element analysis of a unit cell of a metal matrix particulate composite of aluminium silicon carbide, in which a number of stress / strain simulations are conducted, predictions are made, along with correlations of the simulated results to the empirical model.

Chapter 5 looks at the strengthening behaviour of the Al/SiC composite with different volume fractions of SiC, along with different heat treatments, finite element analysis is used for comparing the different heat treated Al-SiC MMCs, material properties of whom were taken from previous studies. The analysis and simulations are continued in chapter 6 with Variational Asymptotical Method for Unit Cell Homogenization (VAMUCH), which is also explained in detail in this chapter, comparisons are made for stress and strain values and a closer look is taken at the interface.

Chapter 7 is mainly the modelling and simulation of the non-linear response of silicon carbide reinforced aluminium alloy with the consideration of a hardening model on a unit cell method. Chapter 8 focuses on the fatigue analysis on the unit cell of our chosen composite, and predictions and correlations are made. In the end the conclusions are made with the recommendations for future work.

## **1.1 Knowledge Gap**

At the present time the relationship between the strength properties of MMCs and the characteristics of the reaction products at the matrix-reinforcement interface are not well understood. The purpose of this project is to define the features that

significantly affect the interfacial strength of an aluminium/silicon carbide system. Models for segregation and precipitation of second phase particles are used to predict the nature and properties of the matrix-reinforcement interface.

The key objective of this study is "To predict the interfacial strengthening mechanism at the matrix-reinforcement interface in a metal matrix composite."

An attempt has been made to predict the atomic movements in the materials on the 1 to 100 nm scale in the region of internal interfaces in MMCs. The work has built on the knowledge and skills acquired in mathematically predicting materials behaviour when the following mechanisms are in operation.

- (i) Interfacial segregation
- (ii) Precipitation on interfaces and intragranular precipitation
- (iii) Combined grain boundary precipitation and segregation
- (iv) Relation of grain boundary and interfacial structure to cohesive strength.

The kinetics of precipitation in the solid state has been the subject of much attention. Early work on growth kinetics has been developed by Aaron and Aaronsson [1] for the grain boundary case and by Aaron et al [2] for intragranular precipitation. Quantification of nucleation kinetics has been well treated by Russell's group [3]. These approaches have been integrated to produce a unified description of the inter and intragranular nucleation and growth mechanisms by Shercliff and Ashby [4] and Carolan and Faulkner [5].

More recently successful attempts have been made to combine models of precipitate growth at interfaces with concurrently occurring segregation in aluminium alloys [3]. Studies of the relation between interfacial cohesive strength and structure have only recently become possible. This is due to the remarkable advances in physical examination techniques allowing direct viewing of interface structure and improved theoretical treatments of grain boundary structure. Recent advances relating the strength of boundaries to structure have been made by Lim and Watanabe [6].

The effect of stress and strain history on the micro-modelled mechanisms is likely to be of greatest importance to the segregation and precipitation phenomena and thus indirectly affect cohesive strength. The methods of incorporating stress into the description of the segregation process are based on the Rauh-Bullough theory [7] and the concept of misfit-related impurity-boundary binding energies developed by Carolan and Faulkner [8]. The precipitation kinetics modelling are reconsidered using Russell's arguments [9] and by evaluating the effect of the misfit term in the free energy of nucleus formation equation. Attempts have been made to quantify the effects of strain, on diffusion constants using the saddle point configuration volume method [10]. By performing an iteration loop using the diffusion constant data with the stress induced segregation data, a complete picture of the effect of strain on precipitate growth is possible.

Particle reinforced metal matrix composites (MMCP) are of interest for a variety of industrial applications due to their higher stiffness and strength than the matrix alloys. Deep understanding of the strengthening behaviour of the MMCP is a critical issue in the development of these materials [11,12]. Experimental observations [11] indicate that the fine particles yield increased strengthening and hardening effects. The

continuum models [13,14] based on the classical plasticity theories could explain the load transfer effect from the composite matrix to the reinforcing particle and successfully predict the plastic work hardening behaviour of the MMCP depending on the particle volume fraction and other non-dimensional parameters (e.g. particle aspect ratio), but they all failed to explain the particle size dependent strengthening, since their constitutive laws possessed no intrinsic material lengths[15].

It is proposed to apply the various micro scale modelling techniques reviewed above to the aluminium alloy matrix composite, strengthened with varying amounts of silicon carbide particulate. The simulation models are then to predict the material state at critical points during heat treatment of the material. Predictions of the models for segregation and precipitation and effect on cohesive strength are then studied and compared with the experimental results.

## **1.2 Aims and Objectives**

The proposal is to apply the various micro scale modelling techniques to the aluminium alloy matrix composite, strengthened with varying amounts of silicon carbide particulate to develop a composition model to predict the interfacial strengthening behaviour of particulate reinforced alloy for which the following aims will be dealt with;

1. Estimate the interfacial fracture energy.
2. Predict the composition variation at matrix reinforcement interface.

3. Develop an algorithm to model a hard ceramic particle in a soft matrix with a clear distinct interface and set the boundary conditions.
5. Numerical simulation of reinforced alloy deformation under a point load.
6. Study the impact of cyclic loading on the reinforced alloy deformation behaviour.
7. Predict and correlate the interfacial strengthening behaviour of ceramic particle reinforced metallic alloy.

## **CHAPTER 2**

### **Literature Review**

#### **SUMMARY**

This chapter starts off with the history of the composites defining different types of MMCs along with different reinforcements used in industry with their advantages and disadvantages. Metal Matrix Composites (MMC) are then discussed, giving emphasis to the Aluminium Metal Matrix Composites and the Silicon Carbide reinforcements (SiC). Advantages of using Al-SiC MMCs have also been listed. The design considerations are then discussed with the fabrication methods. A brief introduction to the structure of the unit cell concept is also explained which is used later in this study.

#### **2.1 History of Composites**

A composite material is composed of two or more materials that results in better properties than those of the individual components used alone. In contrast to metallic alloys, each material retains its separate chemical, physical, and mechanical properties. The two major constituents are known as the reinforcement and the matrix [16].

The idea of making composite materials came from the need for stronger and stiffer yet lighter composites in fields as diverse as aerospace, energy, automotive and civil construction [17]. Research into these composite materials date back to the early

1960's and a lot of developmental efforts have been made since. Some examples of composites which are used every day and which are not engineered materials are steel rods in concrete, cement mixed with sand, carbon black in rubber, fiberglass in resin etc [18]. Today, because of the research and development and given the most efficient designs, new materials and manufacturing processes, composite materials that meet or even exceed the performance requirements in various industries can be made. Most of the savings from the introduction of these materials are in weight and cost. These are measured in terms of ratios such as stiffness/weight, strength/weight and cost/weight ratios [19].

It has been documented that very attractive physical and mechanical properties such as high specific modulus, strength, and thermal stability for metal matrix composites can be achieved [20-24].

There are different man-made engineered composite materials categorized by the different reinforcements and matrix combinations which include:

- Composite building materials like concrete and cements.
- Reinforced plastics like fiber-reinforced polymer (PMC or FRP)
- Metal Matrix Composites (MMC)
- Ceramic Matrix Composites (CMC)

### **2.1.1 Composite Building Materials**

One of the earliest man-made composite materials documented was straw and mud combined to form bricks for building construction. Ancient brick-making was documented by Egyptian tomb paintings. Wattle and daub is one of the oldest man-

made composite materials, at over 6000 years old, in which a woven lattice of wooden strips called wattle is daubed with a sticky material usually made of some combination of wet soil, clay, sand, animal dung and straw. Many historic buildings include wattle and daub construction, and the technique is again becoming popular in more developed areas as a low-impact sustainable building technique [25]. Concrete is also a composite material, composed of aggregate (a broad category of coarse particulate material used in construction, including sand, gravel, crushed stone, slag and recycled concrete) bonded together with a fluid cement which hardens over time. Concrete can be formulated with high compressive strength, but always has lower tensile strength. For this reason it is usually reinforced with materials that are strong in tension (often steel). Concrete is used more than any other man-made material in the world. As of 2014, about 4.18 billion metric tons concrete was made [26].

### **2.1.2 Fiber-Reinforced Composite**

Fiber-reinforced composite materials (FRC) can be divided into two main categories normally referred to as short fiber-reinforced materials and continuous fiber-reinforced materials. Continuous reinforced materials often constitute a layered or laminated structure. The woven and continuous fiber styles are typically available in a variety of forms, being pre-infused with the given matrix. Short fibre reinforced composites on the other hand provide similar stiffness levels achievable with continuous fibres while at the same time being mouldable into complex shapes. [25]

Short fibre reinforced composites were initially developed basically to fill the gap between continuous fibre laminates which were used as primary structures by the aerospace industry and unreinforced ceramics on the other hand were used largely in non-load bearing applications. By the introduction of the short fibre systems which benefit from each of these property bounding engineering materials like, if the fibres are sufficiently long, stiffness levels can approach those of a continuous fibre system, while having the ability of the unreinforced ceramic to be moulded into complex shapes. Hence the short fibre reinforced composites are now used in lightly loaded secondary structures, in which stiffness dominates the design, along with a notable increase in strength over the unreinforced ceramics is required [27].

Common fibers used for reinforcement include glass fibers, carbon fibers, cellulose (wood/paper fiber and straw) and high strength polymers. Fiber-reinforced plastics (FRP) are commonly used in the aerospace, automotive, marine, and construction industries. Along with the various advantages structural failure can also occur when using FRP materials, this happens when, the tensile forces acting on the composite, stretch the matrix more than the fibers, causing the material to shear at the interface between matrix and fibers, or if the tensile forces near the end of the fibers exceed the tolerances of the matrix, separating the fibers from the matrix, or if the tensile forces exceed the tolerances of the fibers causing the fibers themselves to fracture, leading to material failure [28].

Hence, FRPs are best suited for any design in which one wants to save weight, do precision engineering, finite tolerances, and the simplification of parts in both production and operation. According to price a molded polymer artefact is cheaper,

faster, and easier to manufacture than cast aluminum or steel artefact, and maintains similar and sometimes better tolerances and material strengths.

### **2.1.3 Metal Matrix Composites**

A metal matrix composite (MMC) is a composite material with at least two constituent parts a matrix and a reinforcement, it is typically made by dispersing a reinforcement metal material into a monolithic (a single crystal solid material in which the crystal lattice of the entire sample is continuous) metal matrix. In structural applications, the matrix is usually a lighter metal such as aluminum, magnesium, or titanium [29], whereas the reinforcement which is usually a strong material does not always serve a purely structural task of reinforcing the compound but is also used to change physical properties such as wear resistance, friction coefficient, and/or thermal conductivity.

The MMC's are becoming more and more popular in manufacturing of space systems, aircraft components, top end sports equipment, electronic substrates, bicycles, automobiles and a variety of other applications. While the vast majorities are aluminum matrix composites, a growing number of applications require the matrix properties of super alloys like, titanium, copper, magnesium or iron [30].

In MMCs two or more materials are engineered by systematic combinations of different constituents in a way to tailor the properties of the overall composite, as monolithic materials they have limitations in respect to the combinations of strength, stiffness and density which can be achieved. MMCs can be either with continuous or discontinuous fibres, whiskers, or particles in a metal matrix of very high specific

strength and specific modulus. Furthermore, with systematic design and synthesis procedures properties like high elevated temperature strength, fatigue strength, damping properties, electrical and thermal conductivities, friction coefficient, wear resistance and expansion coefficient can be achieved. In comparison with cast composites, where the volume and shape of phase is governed by phase diagrams, for example, cast iron and aluminium-silicon alloys, which have been produced by foundries for a long time. The modern composites differ in the sense that any selected volume, shape and size of reinforcement can be artificially introduced in the matrix. The modern composites are non-equilibrium combinations of metals and ceramics, where there are fewer thermodynamic restrictions on the relative volume percentages, shapes and size of ceramic phases. By carefully controlling the relative amounts and distribution of the ingredients constituting a composite as well as the processing conditions, MMCs can be imparted with a tailored set of useful engineering properties which cannot be achieved with conventional monolithic materials. The quest for improved performance has resulted in a number of developments in different fabrication techniques and preparation for the reinforcing phases for MMC fabrication, further explained in section 2.7.

The relationship between the properties and the performance of the composites interface between the matrix and the reinforcing phase (fibre or particle) is of primary importance. Processing of MMCs sometimes allows tailoring of the interface between the matrix and the fibre in order to meet specific property-performance requirements. The cost of producing cast MMCs has come down rapidly, especially with the use of low cost particulate reinforcements like graphite, alumina and silicon carbide.

Composite materials technology offer unique opportunities to tailor the properties of metals and metal alloys. Under ideal conditions, the composite exhibits the principal mechanical, thermal, physical and tribological properties defined by the 'rule-of-mixture' as shown in Eq. 1.

$$p_c = p_m v_m + p_f v_f \quad (1)$$

where  $p_c$  are the properties of the composite materials,  $p_m$  are the properties of matrix phase,  $p_f$  are the properties of reinforcement phase,  $v_m$  is the volume fraction of the matrix phase, and  $v_f = 1 - v_m$  is the volume fraction of the reinforcement phase .

New composite materials can be manufactured by selecting different reinforcing phases and an efficient bonding between the matrix and the reinforcement, which would then exhibit dramatic improvements in strength, elastic modulus, fracture toughness, density, and coefficient of expansion of the overall composite [31-32].

The preceding discussion is based on the assumption that rule-of-mixture is followed by the composite materials. In fact, this can be the case for certain properties like modulus, when continuous filament is used as the reinforcing phase, and matrix to reinforcement phase interfacial reactions are controlled to provide good bonding without degradation of the reinforcing phase.

#### **2.1.4 Ceramic Matrix Composites**

Ceramic matrix composites consist of ceramic fibers embedded in a ceramic matrix, thus forming a ceramic fiber reinforced ceramic (CFRC) material. The matrix and fibers can consist of any ceramic material, whereby carbon and carbon fibers can also be considered a ceramic material. CMCs do not have strength but are used where fracture toughness is required.

As compared to conventional ceramics which have brittle failure, low fracture toughness and limited thermal shock resistance, CMCs overcome these disadvantages and hence find their applications in the fields requiring reliability at high-temperatures and resistance to corrosion and wear. Examples of some of the applications where CMCs are used include heat shield systems for space vehicles, components for high-temperature gas turbines such as combustion chambers and turbine blades, components for burners, flame holders, and hot gas ducts, brake disks and components for slide bearings under heavy loads. In addition CMCs can also be used in applications, which employ conventional ceramics or in which metal components have limited lifetimes due to corrosion or high temperatures.

#### **2.1.5 Aluminum Matrix Composites**

Aluminium is the most popular matrix for the MMCs. Aluminium alloys are quite attractive due to their low density, their capability to be strengthened by precipitation, their high damping capacity, high thermal and electrical conductivity and good corrosion resistance. Like all composites, aluminum-matrix composites (AMCs) are not a single material but a family of materials whose stiffness, strength, density, and

thermal and electrical properties can be tailored. To achieve required properties the matrix alloy, the reinforcement material, the volume of the reinforcement, the shape of the reinforcement, the location of the reinforcement, and the fabrication method can all be varied. Regardless of the variations, however, aluminum composites offer the advantage of low cost over most other MMCs [33].

AMCs are produced by casting, powder metallurgy, in situ development of reinforcements, and foil-and-fiber pressing techniques. High-quality products are now readily available in large quantities, with major producers scaling up production and reducing prices.

AMCs have been widely studied since the 1920s and are now used in a number of industries like sporting goods, armours, electronic packaging and automotive industries. They offer a large variety of mechanical properties depending on the chemical composition of the Al-matrix. They are usually reinforced by  $\text{Al}_2\text{O}_3$ , SiC and C, but  $\text{SiO}_2$ , B, BN and  $\text{B}_4\text{C}$  may also be considered.

In the 1980s, transportation industries began to develop discontinuously reinforced AMCs, because of their low cost and attractive isotropic mechanical properties which are generally higher than their unreinforced alloys. Among the various and numerous applications [34, 35], a few examples, are shown in figure1(a) Brake rotors for German high speed train ICE-1 and ICE-2 developed by Knorr Bremse AG and made from a particulate reinforced aluminium alloy ( $\text{AlSi}_7\text{Mg}+\text{SiC}$  particulates) supplied by Duralcan. Compared to conventional parts made out of cast iron with 120 kg/piece, the 76 kg of the AMC rotor offers an attractive weight saving potential [34]. Figure1 (b) The braking systems (discs, drums, callipers or back-plate) of the New Lupo from Volkswagen is made from particulate reinforced aluminium alloy

supplied by Duralcan [34]. Figure1 (c) AMC continuous fiber reinforced pushrods produced by 3M for racing engines. These pushrods weigh 40% as much as steel, are stronger and stiffer, and have high vibration damping [35]. Figure1 (d) AMC wires also developed by 3M for the core of electrical conductors. The unique properties of this type of conductor offer substantial performance benefits when compared to the currently used steel wire reinforced conductors [35].



Figure 1: Some industrial AMCs applications: (a) brake rotors for high speed train, (b) automotive braking systems, (c) automotive pushrods and (d) cores for HV electrical wires.

The field of Al-SiC whisker composites began in the mid-1960s with the realisation that whiskers, or discontinuous fibre reinforcements, can be competitive with continuous-fibre reinforced material from the standpoint of mechanical properties. Silicon carbide whisker reinforced aluminium alloys show promise as metal matrix composites for stiff and high-strength, light-weight applications requiring adequate corrosion resistance [36].

Silicon Carbide (SiC) also has advantages over other candidate reinforcing whiskers such as boron, graphite, and alumina in Al-matrix alloys. These include the excellent thermal conductivity and corrosion resistance of the SiC, comparatively low whisker cost, high machinability, and good workability of the Al-SiC composites. SiC is also

chemically compatible with aluminium and forms an adequate bond with the matrix without developing intermetallic phases [37].

Interfacial segregation takes place by two mechanisms: equilibrium and non-equilibrium types. Equilibrium segregation occurs as a result of impurity atoms relaxing in disordered sites found at interfaces such as grain boundaries [38]. Non-equilibrium segregation arises because of imbalances in point defect concentrations set up around interfaces during non-equilibrium heat treatment processing [39].

Aluminium-based metal matrix composites (AMCs) are very promising for high temperature and strength as well as wear resistant applications. Aluminium alloys are important materials in many industrial applications. Silicon carbide particulate-reinforced aluminium alloy composites (Al/SiC<sub>p</sub>) are especially attractive due to their superior strength, stiffness, low cycle fatigue properties, corrosion fatigue behaviour, creep and wear resistance compared with corresponding wrought aluminium alloys which are normally used extensively for various critical structural applications [40-43].

An important feature of the microstructure in the SiC particulate reinforced aluminium alloy composites is the higher density of dislocations and larger residual internal stresses in comparison to the unreinforced alloys, which are introduced by the large difference in coefficients of thermal expansion between the reinforcement and the matrix. The introduction of the reinforcement plays a key role in both the mechanical and the thermal ageing behaviour of the matrix alloy, as well as the composite material. Micro-compositional changes which occur during the thermo-mechanical forming processes of these materials may cause substantial changes in mechanical properties such as ductility, fracture toughness and stress corrosion resistance [44-47].

The ability of the work hardening behaviour of particulate reinforced metal matrix composites is crucial in optimising the parameters for deformation processing of these materials. The particulate composite material is not homogeneous; hence material properties are not only sensitive to the constituent properties, but also to the interfacial ones. The strength of the particulate composites depends on the size of the particles, the inter-particle spacing, and the volume fraction of the reinforcement [40].

The strengthening of a pure metal is carried out by alloying and supersaturating, to the extent, the excess alloying additions precipitate (ageing) using suitable heat treatment. The deformation behaviour of precipitate hardened alloy or particulate reinforced metal matrix composites the interaction of dislocation with the reinforcing particles is much more dependent on the particle size, the spacing and the density than on the composition [41]. Furthermore, when a particle is introduced in a matrix, an additional barrier to the movement of dislocation is created and the dislocation must react by either cutting through the particles or by taking a path around the obstacles [48].

## **2.2 Reinforcement in Matrix**

The reinforcement material is embedded into the matrix, this can be achieved in two different ways, blending of the reinforcement throughout the matrix material, or adding shaped forms - known as preforms - both methods are performed prior to consolidation.

The purpose of adding the reinforcement in the matrix can be for multiple reasons; firstly it can be structural reason to make the overall composite strong. But it can purely be because of non-structural reasons as well like to change the physical properties such as wear resistance, thermal conductivity or friction coefficient [49].

The reinforcement can be of two types either continuous or discontinuous.

Continuous reinforcement uses fibers such as carbon fiber or silicon carbide. This results in an anisotropic (directionally dependent) structure as the fibers are embedded into the matrix in a certain direction.

Discontinuous reinforcement on the other hand uses whiskers, particles or short fibers this results in an isotropic (identical properties in all directions) structure and can be worked with standard metalworking techniques, such as extrusion, forging, or rolling. In addition, they may be machined using conventional techniques. Mostly alumina and silicon carbide are used.

MMCs with discontinuous reinforcements are usually less expensive to produce than continuous fibre reinforced MMCs, although this benefit is normally offset by their inferior mechanical properties. Consequently, continuous fibre reinforced MMCs are generally accepted as offering the ultimate in terms of mechanical properties and commercial potential.

The family of discontinuously reinforced MMCs includes both particulates and whiskers or short fibres. More recently, this class of MMCs has attracted considerable attention as a result of (a) availability of various types of reinforcement at competitive costs, (b) the successful development of manufacturing processes to produce MMCs with reproducible structure and properties, and (c) the availability of

standard or near-standard metal working methods which can be utilized to fabricate these MMCs [53]. The particulate-reinforced MMCs are of particular interest due to their ease of fabrication, lower costs, and isotropic properties.

Traditionally, discontinuously reinforced MMCs have been produced by several processing routes such as powder metallurgy, spray deposition, mechanical alloying and various casting techniques, i.e. squeeze casting, rheocasting and compocasting [50-57].

In the blending approach, reinforcement particles are uniformly dispersed in the matrix by stirring in molten aluminum for the manufacture of Aluminum MMCs. The particles are slurred with alumina and spray dried for the manufacture of Al-CMCs [58]. In the preform approach used for Aluminum MMCs, reinforcements, typically in the form of fibers, chopped fibers, particulates or whiskers, are blended with low and high temperature binders and formed into the desired selective reinforcement shape or preform using vacuum forming, pressing or injection molding forming techniques. Vacuum forming is the most common method for manufacturing simple shaped preforms, such as the plates/disks, rings or cylinders used in the manufacture of Aluminum MMCs for pistons and cylinder liners.

Pressing of plastic or granulated reinforcements is currently being developed to make more complex preform shapes required for new applications. Injection molding has also been used to some extent to make very complex preform shapes, but preform density is limited, based on the need to maintain a flow able plastic body, which is then heated or cooled to provide adequate green strength for removal from the die without distortion [59].

## 2.3 Types of Reinforcements

Reinforced composites can be generally classified into following three types as shown in figure 2.

- (i) Reinforcement by long, continuous fibers.
- (ii) Reinforcement by whiskers.
- (iii) Reinforcement by particulates.

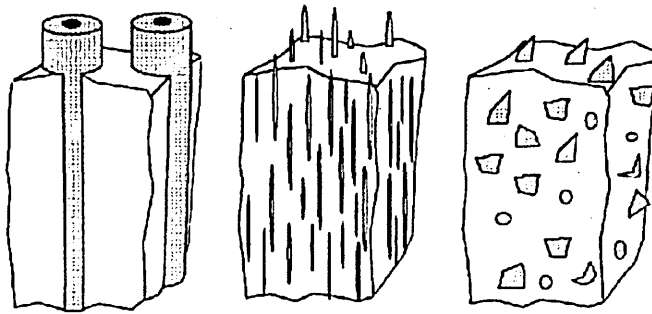


Figure 2: Metallic matrix reinforcement types, (A) Reinforcement by long, continuous fibres, (B) Reinforcement by whiskers, (C) Reinforcement by particulates [60].

Key continuous fibers include boron, graphite (carbon), alumina, and silicon carbide. Boron fibers are made by chemical vapor deposition (CVD) of this material on a tungsten core. Carbon cores have also been used. These relatively thick monofilaments are available in various diameters (like 4.0, 5.6, 8.0 mm, etc). To retard reactions that can take place between boron and metals at high temperature, fiber coatings of materials such as silicon carbide or boron carbide are sometimes used.

Silicon carbide monofilaments are also made by a CVD process, using a tungsten or carbon core. Continuous alumina fibers are available from several suppliers. Chemical compositions and properties of the various fibers are significantly different. Graphite fibers with a wide range of strengths and moduli are available. Efforts to make graphite fibers from coal-based pitch are under way.

The leading discontinuous fiber reinforcements at this time are alumina and alumina-silica. Both originally were developed as insulating materials. Silicon carbide and boron carbide, the key particulate reinforcements, are obtained from the commercial abrasives industry. Silicon carbide particulates are also produced as a by-product.

A number of metal wires including tungsten, beryllium, titanium, and molybdenum have been used to reinforce metal matrices. Currently, the most important wire reinforcements are tungsten wire in super-alloys and superconducting materials incorporating niobium-titanium and niobium-tin in a copper matrix. The reinforcements cited above are the most important at this time. Many others have been tried over the last few decades, and still others undoubtedly will be developed in the future.

## **2.4 Matrix Materials and Key Composites**

Numerous metals have been used as matrices. The most important have been aluminum, titanium, magnesium, copper alloys and super-alloys. Matrices can be used in a number of different forms like continuous fiber, discontinuous fiber, whiskers and particulates, the following shows the materials used in the above mentioned forms in metal matrix composites;

## **ALUMINUM MATRIX**

- Continuous fibers: boron, silicon carbide, alumina, graphite
- Discontinuous fibers: alumina, alumina-silica
- Whiskers: silicon carbide
- Particulates: silicon carbide, boron carbide

## **MAGNESIUM MATRIX**

- Continuous fibers: graphite, alumina
- Whiskers: silicon carbide
- Particulates: silicon carbide, boron carbide

## **TITANIUM MATRIX**

- Continuous fibers: silicon carbide, coated boron
- Particulates: titanium carbide

## **COPPER MATRIX**

- Continuous fibers: graphite, silicon carbide
- Wires: niobium-titanium, niobium-tin
- Particulates: silicon carbide, boron carbide, titanium carbide.

## **SUPERALLOY MATRICES**

- Wires: tungsten

## 2.5 Advantages and Disadvantages of MMCs

MMC's have numerous advantages over non-reinforced ceramics, some of them are listed as they are resistant to fire, they can operate in wider range of temperatures, they do not absorb moisture, have better electrical and thermal conductivity and are resistant to radiation damage. In addition, they offer excellent thermal conductivity, high shear strength, excellent abrasion resistance, minimal attack by fuels and solvents, and the ability to be formed and treated on conventional equipment. Some of the advantages of MMC when compared with other metals are listed as follows;

Compared to unreinforced metals, MMCs have:

- Increased specific strength
- Increased specific stiffness
- Increased elevated temperature strength
- Improved wear resistance
- Lower density
- Improved damping capabilities
- Tailor able thermal expansion coefficients
- Good corrosion resistance

Compared to monolithic metals, MMCs have:

- Higher strength-to-density ratios
- Higher stiffness-to-density ratios
- Better fatigue resistance
- Better elevated temperature properties
- Higher strength

- Lower creep rate
- Lower coefficients of thermal expansion
- Better wear resistance

The advantages of MMCs over polymer matrix composites are:

- Higher temperature capability
- Fire resistance
- Higher transverse stiffness and strength
- No moisture absorption
- Higher electrical and thermal conductivities
- Better radiation resistance
- No outgassing
- Fabricability of whisker and particulate-reinforced MMCs with conventional metalworking equipment.

Some of the disadvantages of MMCs compared to monolithic metals and polymer matrix composites are:

- Higher cost of some material systems
- Relatively immature technology
- Complex fabrication methods for fiber-reinforced systems (except for casting)

## **2.6 Characteristics and Design Considerations of MMCs**

An important characteristic of MMCs, along with their superior mechanical properties, and one they share with other composites, is that by appropriate selection of matrix

materials, reinforcements, and layer orientations, it is possible to tailor the properties of a component to meet the needs of a specific design. For example, within broad limits, it is possible to specify strength and stiffness in one direction, coefficient of expansion in another, and so forth. This is rarely possible with monolithic materials, as monolithic metals tend to be isotropic. Some processes such as rolling, however, can impart anisotropy, so that properties vary with direction. The stress-strain behaviour of monolithic metals is typically elastic-plastic. Most structural metals have considerable ductility and fracture toughness.

The wide variety of MMCs have properties that differ dramatically. Factors influencing their characteristics include:

- Reinforcement properties, form, and geometric arrangement
- Reinforcement volume fraction
- Matrix properties, including effects of porosity
- Reinforcement-matrix interface properties
- Residual stresses arising from the thermal and mechanical history of the composite
- Possible degradation of the reinforcement resulting from chemical reactions at high temperatures, and mechanical damage from processing, impact, etc.

Particulate-reinforced MMCs, like monolithic metals, tend to be isotropic. The presence of brittle reinforcements and perhaps of metal oxides, however, tends to reduce their ductility and fracture toughness. Continuing development may reduce some of these deficiencies.

The properties of materials reinforced with whiskers depend strongly on their orientation. Randomly oriented whiskers produce an isotropic material. Processes such as extrusion can orient whiskers, however, resulting in anisotropic properties. Whiskers also reduce ductility and fracture toughness.

MMCs reinforced with aligned fibers have anisotropic properties. They are stronger and stiffer in the direction of the fibers than perpendicular to them. The transverse strength and stiffness of unidirectional MMCs (materials having all fibers oriented parallel to one axis), however, are frequently great enough for use in components such as stiffeners and struts. This is one of the major advantages of MMCs over PMCs, which can rarely be used without transverse reinforcement because the modulus and strength of metal matrices are significant with respect to those of most reinforcing fibers, their contribution to composite behaviour is important. The stress-strain curves of MMCs often show significant nonlinearity resulting from yielding of the matrix.

Another factor that has a significant effect on the behaviour of MMCs is the frequently large difference in coefficient of expansion between the two constituents. This can cause large residual stresses in composites when they are subjected to significant temperature changes. In fact, during cool down from processing temperatures, matrix thermal stresses are often severe enough to cause yielding. Large residual stresses can also be produced by mechanical loading.

Although fibrous MMCs may have stress-strain curves displaying some nonlinearity, they are essentially brittle materials, as are PMCs. In the absence of ductility to reduce stress concentrations, joint design becomes a critical design consideration.

Numerous methods of joining MMCs have been developed, including metallurgical and polymeric bonding and mechanical fasteners.

## **2.7 Fabrication Methods**

Since as described earlier the properties can be adjusted for MMCs by the way they are made, hence the fabrication methods are an important part of the design process for all structural materials especially MMCs. A lot of work has been done in this respect in this critical area and significant improvements in existing processes and development of new ones appear likely [60].

Current methods for the fabrication of MMCs can be divided into two major categories, primary and secondary. Primary fabrication methods are used to create the MMCs from its constituents [61]. The resulting material may be in a form that is close to the desired final configuration, or it may require some additional processing, called secondary fabrication, such as forming, rolling, metallurgical bonding, and machining. The processes used depend on the type of reinforcement and matrix.

During the fabrication process reactions can occur between the reinforcement and matrices at high temperatures, these impose limitations on the kinds of constituents that can be combined by the various processes. Cast MMCs now consistently offer improved stiffness, strength, and compatibility with conventional manufacturing techniques. They are also consistently lower in cost than those produced by other methods.

### **2.7.1 MMCs Fabrication – Processing Routes**

The important factors for processing good MMCs are, firstly, the reinforcement must be distributed in a controlled manner in the metal matrix and minimal porosity and full density would result in the final component. Typically, volume fractions of 10% – 40% of reinforcement need to be incorporated in the matrix. Reactions at the reinforcement/matrix interface should be controlled to promote optimum bond strength and avoid reinforcement degradation. The route should be capable of producing components with a high degree of reproducibility with minimum product variability, minimum cost and maximum productivity. Highly desirable flexibility in a variety of shapes can be produced [62-63].

Processing of Metal Matrix Composites can be broadly divided into three categories of fabrication techniques, Solid, Liquid and Vapour State Processing [59], according to whether the matrix is in the liquid, solid or vapour phase while it is being combined with the reinforcement, as depicted in figure 3. The individual composite production operations are briefly outlined below under these groupings by Mortensen et al [65].

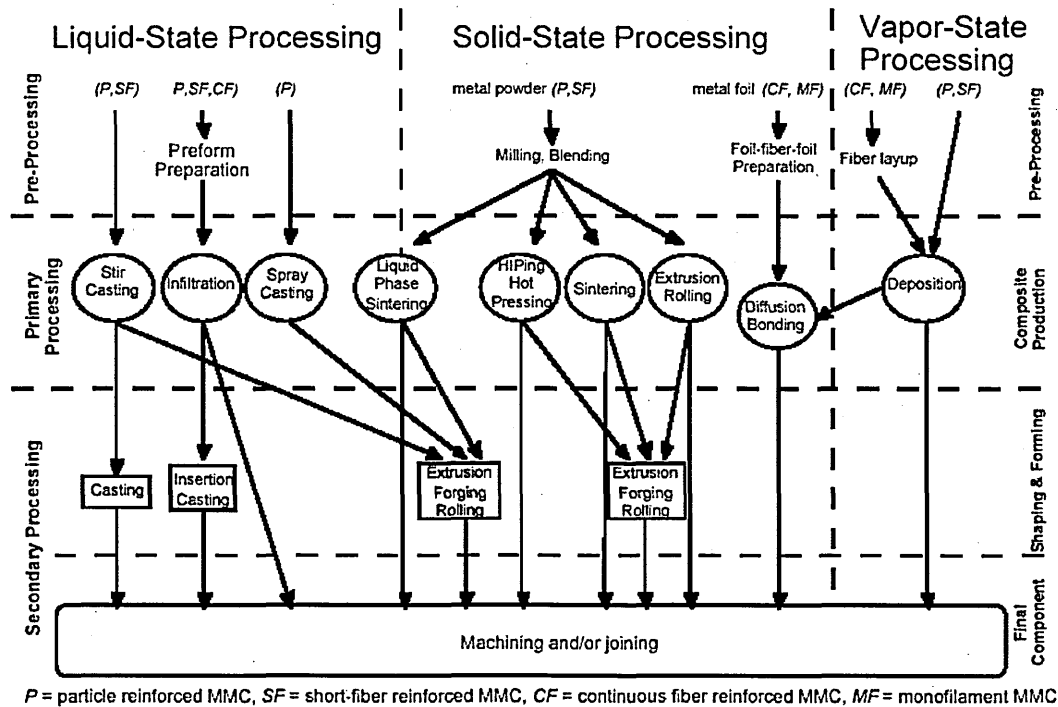


Figure 3: Overview flow chart of MMC processing routes [65].

### 2.7.2 Liquid State Processing

Liquid State processing technologies can be divided into three main sub categories, infiltration, dispersion and spraying.

Composites can be made by penetrating liquid metal into a fabric or pre-arranged fibrous configuration called a preform, this process is called infiltration and can be carried out under vacuum, pressure or both. The final composite phases consist of the reaction products and the remaining matrix material. By this method, a dense composite shape is usually achieved [66-67]. Squeeze infiltration [74] is another method for liquid state processing of short fibres.

In dispersion processes the reinforcement is incorporated in loose form into the metal matrix, but due to poor wetting characteristic of metal-reinforcement systems, mechanical force is required to combine these phases. The simplest dispersion process is the Vortex method, which consists of vigorous stirring of the liquid metal and the addition of particles in the vortex [75]. Difficulties, such as the segregation/settling of secondary phases in the matrix, particulate fracture during agitation, and extensive interfacial reactions, are often encountered [76]. For the fabrication of MMCs by stir casting, a requirement for a good stirring unit is to provide intimate contact while minimising gas absorption [77].

Mixing of particles and metal can also be achieved while the alloyed metal is kept between solidus and liquids temperature. This process is known as compocasting or rheocasting. The advantage of using semi-solid metal is the increase in the apparent viscosity of the slurry. This process permits the introduction of the pre-treated particulate or short fibres into the solidifying, highly viscous dendritic slurry of the molten matrix by agitation. This mechanically entraps the ceramic reinforcements and prevents any form of segregation. Continued stirring then reduces the viscous mass to low-viscous, fine, non-dendritic slurry. This results in a mutual interaction between the matrix melt and the filler phase, which enhances wetting and bonding between the two phases.

In spray processes, as the name suggests, droplets of molten metal are sprayed together with the reinforcing phase and collected on a substrate where metal solidification is completed. Alternatively the reinforcement may be placed on the substrate and molten metal may be sprayed onto it. One of the drawbacks of the process is the amount of residual porosity and normally the resulting materials need further processing. Spray Deposition (SD) is gaining recognition in the synthesis of

discontinuously reinforced MMCs. [78]. Adaptation to particulate MMC production by injection of ceramic powder into the spray has been extensively explored, although with limited commercial success. MMC material produced in this way often exhibits inhomogeneous distributions of ceramic particles [79].

### **2.7.3 Stir-Casting Approach**

The experimental results which are compared in this study with the simulated results are from Myriounis [9] experiments. All the material samples used for his experiments were provided by a company MC-21. MC-21 uses a stir-casting approach in which, the desired aluminium alloy is melted, and carefully sized ceramic silicon carbide particles are stirred in by means of an efficient vacuum-assisted mixing process. The process allows good wetting and a very strong bond between the ceramic particles and aluminium matrix and uses inexpensive raw materials, this method allows them to produce MMCs containing different volume fractions of ceramic particulate and of aluminium alloy matrices, this can usually be done using fairly conventional processing equipment and can be carried out on a continuous or semi-continuous basis [68-71].

MC-21 have created improved mixing technology that reduces the time required for uniform incorporation of a wide range of ceramic particle reinforcement volume fractions [72], which allows the mixing to be done in “real time” in the foundry environment, which in turn eliminates the need for careful re-melting of the melt stock currently required for MMC ingot produced by other processes, saving time, minimizing the chance for overheating and ruining of the melt, and reducing energy

consumption. Stir casting is also considered to be the cheapest method to fabricate MMCs [73].

#### **2.7.4 Solid State Processing**

Solid State processes are generally used to obtain the highest mechanical properties in MMCs, particularly in discontinuous MMCs. Since segregation effects and brittle reaction product formation are at a minimum for these processes, especially when compared with liquid-state processes, powder metallurgy is the most common method for fabricating metal – metal composites. With the advent of rapid solidification technology, the matrix alloy is produced in a pre-alloyed powder form rather than starting from elemental blends. After blending the powder with particulate reinforcements, cold isostatic pressing is utilised to obtain a green compact that is then thoroughly degassed and forged or extruded [80]. Although, powder based routes for MMC production tend to be more expensive than liquid based routes and therefore generally occupy the more specialist high cost markets for MMCs [81].

Powder Metallurgy is used in the synthesis of Aluminium Matrix Composites through the relatively low-cost methods of compaction at ambient or hot conditions and mechanical deformation following hot pressing. In these solid-state techniques, subfusion temperature regimes are normally attained in consolidation for optimum results. Depending on the morphology of the reinforcement or the desirable properties, further processing by mechanical-deformation mechanisms is applied [82-83].

## 2.8 Applications of MMCs

Current markets for MMCs are primarily in military and aerospace applications. Experimental MMC components have been developed for use in aircraft, satellites, jet engines, missiles, and the National Aeronautics and Space Administration (NASA) space shuttles. The first production application of a particulate-reinforced MMC in the United States was a set of covers for a missile guidance system [85]. The most important commercial application which was made in the 1980's was the MMC diesel engine piston made by Toyota. This composite piston offered better wear resistance and high-temperature strength than the cast iron piston it replaced. It was estimated that 300,000 such pistons were produced and sold in Japan annually at that time. This development demonstrated that MMCs were at least not prohibitively expensive for a very cost sensitive application. Other commercial applications include cutting tools and circuit-breaker contacts [86].

Metal matrix composites with high specific stiffness and strength could be used in applications in which saving weight is an important factor. In-service performance demands for many modern engineering systems require materials with broad spectrum of properties, which are quite difficult to meet using monolithic material systems [87]. Metal matrix composites (MMCs) have been noted to offer such tailored property combinations which are required in a wide range of engineering applications [86] and [87], included in this category are robots, high-speed machinery, and high-speed rotating shafts for ships or land vehicles. Good wear resistance, along with high specific strength, also favours MMC use in automotive engine and brake parts. Tailor-able coefficient of thermal expansion and thermal conductivity make them good candidates for lasers, precision machinery and electronic

packaging. Based on information now in the public domain, the following military applications for MMCs appear attractive: high-temperature fighter aircraft engines and structures; high-temperature missile structures; and spacecraft structures.

## **2.9 Limitations of MMCs**

It is worth considering the limitations that may hamper the full commercialisation of metal composites.

The first thing is to bridge the gap which is present in understanding between the materials, expert's knowledge of the performance of new material and real engineering applications. This would involve helping the engineering community to design with MMCs by providing property data covering key aspects of performance and to apply appropriate processing techniques.

Next the misconception of the increased cost of replacing conventional components with MMC components for gaining increased performances is also a major disadvantage. It needs to be clarified that for example, if aluminium based MMC is offered against a conventional aluminium component, then a major increase in performance is vital if the significant increase in costs is to be justified. However, it is often the case that an aluminium based MMC is offered in replacement of a titanium or polymeric composite part, competing on both performance and cost.

The MMC component design must also take into account of cost effective processing techniques. MMCs commonly require net shape forming with minimal losses. Selective reinforcement techniques allow the high performance fibre and monofilament materials to be applied in critical areas. However, the major factor is

the high price of the monofilament reinforcement and the costs of its incorporation into a reactive matrix. Moving from development to production scale of these advanced materials will bring big savings but will require a major commitment from end-users and producers alike [77].

## **2.10 Role of Interface: Matrix-Reinforcement Interface in an MMC**

One of the most critical aspects in MMCs is the matrix-reinforcement interface. The nature of which depends on how the MMC has been processed. As the MMC attempts to deform during processing, at micro-level the development of local concentration gradients around the reinforcement can be very different to the nominal conditions and play a crucial role in important micro structural events such as segregation and precipitation at the matrix-reinforcement interface. These events dominate the cohesive strength and subsequent mechanical properties of the interface.

The thermodynamics of vacancy and impurity absorption at interfaces and grain boundaries in solids has been studied in the recent years with theoretical models proposed in order to predict the behaviour of vacancies at interfaces, as well as the interface strength during fracture [88]. It has been reported in literature that the tendency for intergranular fracture is closely related to the type and structure of grain boundaries. Low-energy boundaries are resistant to fracture while high energy or the so-called random boundaries are favoured locations for crack nucleation and propagation. Lim and Watanaby [89] and Faulkner and Shvindlerman [90] have recognised the important role played by the interface in determining the amount of

predicted segregation and hence the change of interfacial energy caused by segregation.

Certain amounts of plastic deformation are involved with crack propagation along an interface. The parameters to be considered are the strain rate sensitivity to stress and the dislocation pile up behaviour at the advancing crack tip. Using this approach, the effective work parameter can be shown to be thousand times larger than the surface energy [91]. This implies that minute changes in surface energy caused by segregation would result in large changes in interfacial fracture stress.

In ductile materials such as metals, plastic deformation occurs at the crack tip. Much work is required in producing a new plastic zone at the tip of the advancing crack. Since the plastic zone has to be produced upon crack growth, the energy for its formation can be considered as energy required for crack propagation [92].

## **2.11 Scope of SiC Reinforced Al Composites**

SiC-reinforced aluminium alloy composites are the typical candidates for engineering applications in aerospace, military, and civil manufacturing industries due to their enhanced mechanical properties over the corresponding aluminium alloys such as high strength, wear resistance, and fatigue resistance [93-96].

Among different shaped reinforcements, the composites reinforced with particulates offer relatively isotropic mechanical properties compared to the composites reinforced with short fibres or whiskers and can be produced using conventional metal manufacturing process with low cost [97-98].

It is widely recognized that the properties of MMCs are controlled by the size and volume fraction of the reinforcements as well as the nature of the matrix-reinforcement interfaces. An optimum set of mechanical properties can be achieved when fine and thermally stable ceramic particulates are dispersed uniformly in the metal matrix

Rack [100] studied the fabrication and damage tolerance performance of some of these lightweight and high performance composites [98]. Matrix-to-reinforcement particle size ratio (PSR) is the main factor governing the homogeneity of the reinforcement particle distribution in composites manufactured by the powder metallurgy route. To improve the homogeneity of the distribution, reinforcements with larger average particle size should be used. At the same time, increasing the reinforcement particle size leads to worsening of the mechanical properties due to lower work hardening and higher damage accumulation rates. It is therefore important to optimize the microstructure somewhere in-between a smaller reinforcement particle size and a more homogeneous spatial distribution [101]. Thus, much research has been conducted on particulate metal matrix composites. Slipenyuk et al. [102] have- investigated the effect of reinforcement particle size (3 and 14  $\mu\text{m}$ ), matrix to reinforcement PSR ranging from 2.9 to 12.9, and volume fraction of the reinforcement (0-20 vol%) on microstructure and mechanical properties (yield stress, tensile strength, elongation to fracture, and Young's modulus) for Al-6Cu- 0.4Mn\SiCp composites manufactured by the powder metallurgy route. Lewandowski et al. [103] observed improvement in the reinforcement distribution and better combination of mechanical properties when PSR ratio was varied from 3.3:1 to 1.4:1 in the Al-7Zn-2Mg-2Cu-0.14Zr 20% vol of SiCp composite. However, change of SiC particle size from 5 to 16  $\mu\text{m}$  for changing the PSR ratio overshadowed the real

effect of changing the PSR ratio. Stone et al. [104] also studied the effect of PSR ratio on the properties of the metal matrix composites (MMCs) in rolled and extruded conditions. Their study could not establish any correlation between PSR ratio and the mechanical properties as both the matrix and reinforcement sizes were varied simultaneously. Sternowsky et al. [105] studied the effect of PSR ratio on the compressive strength of sintered 6061 Al/SiC composites.

During the past two decades, a large number of the investigations have been carried out to reveal the strengthening mechanisms of the metal matrix composites. Strengthening effects in the composites could be classified into direct and indirect mechanisms [96].

Direct strengthening is obtained by the load being transferred from the weaker matrix to the hard reinforcements [96, 99] during deformation. While, indirect strengthening results from the variation of the matrix microstructures, such as grain refinement in the composites, by the addition of reinforcements [106-107].

## **2.12 Numerical Modelling: A Unit Cell Approach**

The complexity of composite analysis requires the use of an accurate model for calculating the properties of various composite patterns. Confidence in the model requires analytical studies that are comparable to accepted published results.

For particle reinforced MMC periodic unit cell methodology (which is the simplest repeating unit in a crystal) has been successfully used to study the room temperature, monotonic tensile loading behaviour, based on idealised and regular microstructural geometries [108-111]. Cyclic loading on a unit cell of particulate

metal matrix composite has been studied by Llorca [112] and bohm [113]. 3D unit cell models have also been used by O'Dowd [114] to study the particle arrangement and loading state effects. Particle distribution effects in MMCs containing multiple particles have also been stated by watt [115], in which he studied a unit cell containing 10 particles.

Rustichelli [116] calculated values for the average stress for the entire matrix and for the reinforcing particles for the 3d multiple particle geometry model and his simulated results were about 25% apart when compared by values obtained by neutron diffraction measurements.

In this study simulations are based on a unit cell. Each unit cell is defined in terms of lattice points, defined as the points in space about which the particles are free to vibrate in a crystal. 2D and 3D simulations have been done in various areas of the metal matrix composites of Aluminium silicon carbide to determine the interfacial strength as compared to the early studies which have suggested unit cell methodology for the determination of the entire matrix simulations.

A cubic unit cell with 8 nodes on its corners was chosen for this study as shown in figure 4.

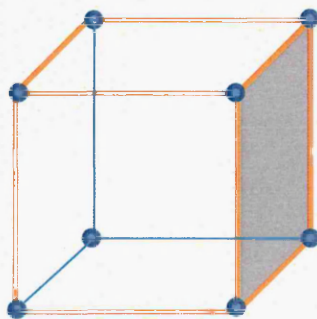


Figure 4: A cubic unit cell with its 8 nodes at the corners

The unit cell was designed in ANSYS, (A complete set of experiments and simulations have been listed step wise in Appendix B covered to come up with the unit cell as used in this study), representing a small part of the composite which has aluminium (Al) as the base material with a hard reinforcement of silicon carbide (SiC) in the centre. The unit cell was assumed to be in symmetry. The dimensions of the unit cell initially was set to 25.4mm x 25.4mm to keep the aspect ratio equal to 1, 12.7mm diameter for the reinforcement was taken and the depth of the unit cell was 0.245mm, as shown in figure 5. In further simulations in chapter 6, the length of the unit cell was then calculated for the 20% and 31% volume fraction of Al-SiC MMC separately and according to the length corresponding to the volume fraction of SiC the depth of the 3D cube was adjusted.

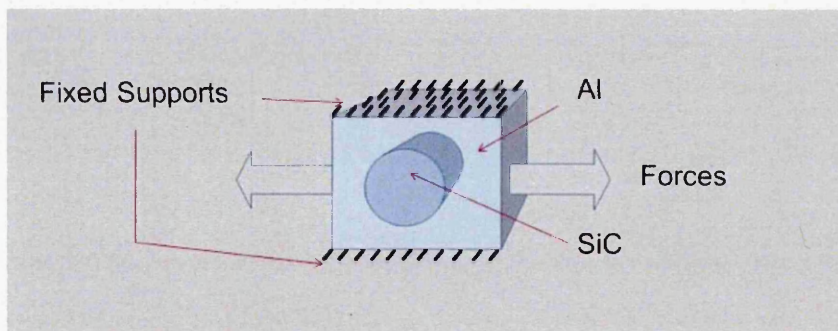


Figure 5: Schematic of the model Unit cell showing where the forces were acting and the fixed supports

Considerable amount of research work has been undertaken to understand the effect of yield of the matrix on the strength of the MMC. The two important characteristic features which complicate the study of MMCs are the high residual stresses arising from manufacture and the influence of the weak interface between reinforcements and matrix. Previous researchers have used finite element micro-

mechanical models to construct initial yield surfaces of unidirectional composites subjected to various external loads [118]. Their procedure was to predict the stresses in the model subjected to load and then scale the load so that the most highly stressed area of the mesh reached yield. Dvorak et al., [119-120] carried out a similar analysis but included the effect of the residual stresses arising from the manufacturing process. They noted that the effect of a uniform temperature change is approximately equivalent to the translation of the yield surface in the direction of the hydrostatic stress axis. Dvorak [121] later showed that uniform thermal changes applied to the composite can be converted to equivalent mechanical loads depending on the thermo-elastic properties of the constituents [117]. Temperature effects on the strengthening of the particulate metal matrix composite with heat treatments were also simulated, further discussions in chapter 5.

Shao, J. C., et al. [15] conducted some simulations in which, since the selection of interface parameters is difficult due to the lack of experimental data on the SiC<sub>P</sub>/Al interface, they choose a representative set of interface parameters to describe the interface behaviour, by choosing a 7.5 micron diameter of SiC particles for the interface for a composite containing 16 micron diameter particles. These parameters were just a representative set to describe the interface behaviour. Bruzzi, McHugh, O'Rourke & Linder [122] have used randomly selected values for the cohesive zone representing the interface for simulating the unit cell of metal matrix composites, they also concluded simulations for different aspect ratios for the matrix and the reinforcement, and concluded that aspect ratio of 1 gave the best results. Same results were shown by Chawla, Nikhilesh, and Yu-Lin Shen [123]. For the 2D and 3D unit cell modelling the aspect ratio of the matrix and the reinforcement was set to one.

## CHAPTER 3

### An Empirical Method of Calculating Interfacial Strength in a Second Phase Reinforced Alloy

#### SUMMARY

Particulate-reinforced metal matrix composites (MMCs) are influenced by several factors while considering the fracture at the interface, such as particle size, volume fraction and inter-particle spacing of the reinforcement. A method of calculation has been applied to predict the interfacial fracture toughness in a particulate reinforced composite. The composite used in this study is silicon carbide reinforced with aluminum matrix, in the presence of silicon segregation. The model shows success in making prediction possible of trends in relation to segregation and interfacial fracture strength behaviour in metallic alloys. Small changes in surface energy caused by segregation result in, very large changes in interfacial fracture stress. The interface structure is important in determining the amount of predicted segregation and hence the change of the interfacial energy caused by the segregation. Equations have been developed to forecast the energy change in terms of the coincidence site stress ( $\sigma_a$ ) value describing the interface, and the formation energies of impurities on the interface. The interfacial strength is calculated based on the fracture toughness properties of the interface.

### 3.1 Introduction

In the case of particle-reinforced metals, numerous studies have focused on understanding the influence of crack growth rate [124-126] and the reinforcing particles on the matrix microstructure and the corresponding effect on the fatigue behaviour of the metal matrix composites (MMCs) [127].

In composite materials with ductile matrix and hard-brittle reinforcement, interfaces can be assumed to behave in a similar manner as in the case of grain boundaries of second phase reinforced alloy. In such cases, the crack would propagate through the matrix and the crack tip would meet the interfacial region, where plasticity and/or energy changes. Then, the crack may, (a) continue to propagate through the reinforcement, or (b) be deflected by the matrix-reinforcement interface, as shown in figure 6. It is, therefore, necessary to predict whether the interfacial region has enough fracture strength in order to resist crack growth through the interface or matrix cracking around the reinforcement boundary region. An important factor regulating crack growth behaviour in metal matrix composites is the matrix-reinforcement interface property, which relates to precipitation hardening mechanisms. It takes more energy for a crack to propagate through an interface and this is the ideal situation for a material to resist fracture. Stresses arising by the crack propagation are ideally sustained by the interface strength; therefore, the crack requires more energy in order to propagate. Stress gradients within the matrix/reinforcement interface region can cause varying levels of stress at which the crack becomes separated or trapped due to different levels of crack closure in the wake of the crack tip. The ideal solution is for the crack to be able to propagate through paths with the highest ductility and strength [128].

This model considers the interfacial energy caused by segregation of impurities at the interface and uses Griffith crack-type arguments to forecast the energy change in terms of the coincidence site stress describing the interface and the formation energies of impurities at the interface. Based on Griffith's approach, the fracture toughness of the interface is expressed in terms of interfacial critical strain energy release rate and elastic modulus.

This approach shows success in making prediction possible of trends in relation to segregation and interfacial fracture strength behaviour in SiC particle-reinforced aluminum matrix composites. The proposed model can be used to predict possible trends in relation to segregation and the interfacial fracture strength behaviour in MMCs. Precipitation hardening mechanisms can play an important role in strengthening mechanisms and in tailoring the A359/SiC<sub>p</sub> interface behaviour. The propagation of a crack through the matrix shows good interfacial strength, propagation by cracking the reinforcement indicates higher matrix strength, while propagation through the interface indicates weak interfacial strength.

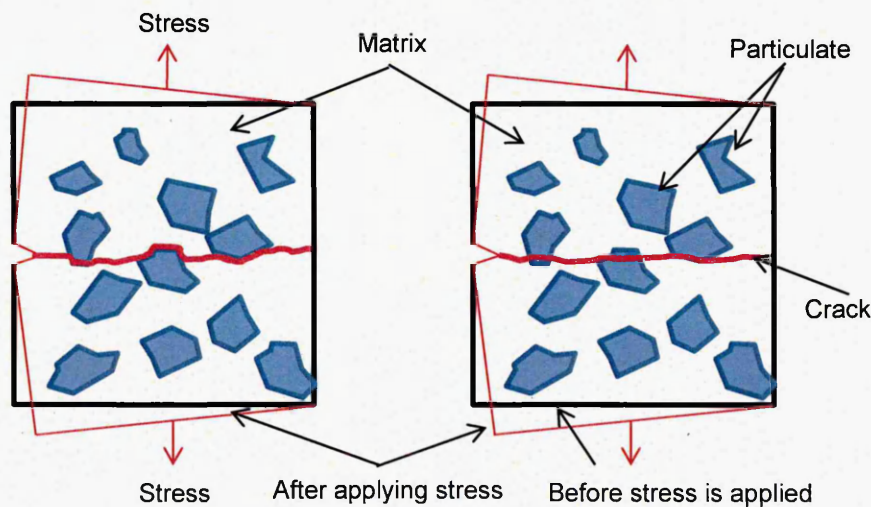


Figure 6: (A) Crack propagating through the interface (B) Crack propagating through the particulate.

## 3.2 Estimation of Interfacial Stress and Strain using Numerical Modelling

### 3.2.1 Interfacial Fracture Strength Model

Griffith [129] was the first who tried to relate the micro-defect fracture strength with the interatomic bond strengths for glass, a perfect brittle material. His model states that crack propagation will occur only if the total energy of the system is decreased. This implies that only if the energy released upon crack growth is sufficient to provide all the energy that is required for crack growth then this crack will propagate. The energy consumed in crack propagation is denoted by  $E_R = \partial w / \partial a$  which is called the crack resistance. Where 'w' is the work done by the fracture and 'a' is the crack area, if  $E_R$  is a constant ( $da = \text{constant}$ ), this means that for the crack to propagate the elastic energy release rate  $G$  must exceed a certain critical value  $G_{IC}$ . For metals,  $E_R$  is mainly the plastic energy; surface energy is so small that it can be neglected. Therefore, the energy criterion for plane stress conditions stipulates that:

$$G_k = \frac{K^2}{E} \quad (2)$$

and for plane strain conditions,

$$G_{IC} = \frac{K_{IC}^2(1-\nu^2)}{E} \quad (3)$$

where,  $K_{IC}$  is the fracture toughness and  $E$  the Young's modulus of the material.

Based on Griffith's approach, the fracture toughness of the interface,  $K_{int}$ , can be expressed in terms of critical strain energy release rate,  $G_{int}$ , of the interface and the Young's modulus of the interface,  $E_{int}$  [130],

$$K_{int} = \sqrt{G_{int} E_{int}} \quad (4)$$

The energy  $\varepsilon_p$  required to create two fracture surfaces is basically related to the work of intergranular fracture,  $G_k$ , which is given, according to Faulkner et al. [131] by:

$$G_k = A\varepsilon_p e^{n \ln\left(\frac{\varepsilon_a}{\varepsilon_o}\right)} \quad (5)$$

Where, A is the dislocation pile-up term describing the effectiveness of dislocations in providing stress concentration at the advancing interfacial crack tip (=100) in ductile materials and n, is the work hardening exponent (= 10 for FCC aluminium)  $\varepsilon_a$  is the new interfacial energy caused by segregation and  $\varepsilon_o$  is the total energy.

Eq. 4 originally developed for intergranular fracture through grain boundaries, also applies to particulate/matrix interfaces. Interphase regions separate into two different phases whereas the grain boundaries separate into new portions of the same phase.

Hence, the grain boundary system has one more degree of freedom than the interface system. Therefore,  $G_k = G_{int}$ , which is the work of interfacial fracture.

Replacing  $G_k$  from Eq. (2) and Eq (5), the following relationship can be obtained:

$$\frac{K_{int}^2}{E_{int}} = 100\varepsilon_p e^{n \ln\left(\frac{\varepsilon_a}{\varepsilon_o}\right)} \quad (6)$$

$\varepsilon_a$ , in Eq. (6), is then the new interfacial energy caused by segregation given by [132]:

$$\varepsilon_a = \varepsilon_o - ZRT \ln(1 - c + Bc) \quad (7)$$

Where:

Z, describes the density of interface sites which are disordered enough to act as segregation sites (=  $d\rho_s$ ), with d the thickness of the interphase, and  $\rho_s$  the density of the interphase, R is the gas constant (=  $8.314472(15) \text{ J}\cdot\text{K}^{-1}\cdot\text{mol}^{-1}$ ), T is the

absolute temperature (= 530 K for T6, = 450 K for HT1) and  $c$ , is the segregate concentration needed to cause embrittlement ( $\approx 0.1$ ).

Substituting the value of  $\varepsilon_a$  from Eq. 7 into Eq. 6 we get,

$$\frac{K_{int}^2}{E_{int}} = 100\varepsilon_p e^{n \ln \left( 1 - \frac{ZRT \ln(1-c+Bc)}{\varepsilon_o} \right)} \quad (8)$$

or

$$\frac{K_{int}^2}{100E_{int}} = \varepsilon_p \left( 1 - \frac{ZRT \ln(1-c+Bc)}{\varepsilon_o} \right)^n \quad (9)$$

From Eq. 9  $\varepsilon_p$  can be estimated if  $K_{int}$  and  $E_{int}$  are known. In the section below the interface fracture toughness  $K_{int}$  is estimated and a model proposed.

$E_{int}$  on the other hand is approximately equal to  $E_m$  [133], A model proposed by McMahon and Vitek [91] predicts the fracture resistance of a ductile material that fails by an intergranular mechanism. Based on this model, an effective work parameter can be developed to predict fracture strength of an interface at a segregated state using Griffith crack-type arguments. The model assumes that small changes in interfacial energy caused by segregation of impurities at the interface will result in a much larger change in the work of fracture. This is due to the fact that the work of fracture must be provided by a dislocation pile-up mechanism around the advancing crack-tip on the interface. This implies that additional work must be provided to deform the material at the crack-tip in addition to the work needed to overcome the interface energy and to replace it with two surfaces.

Hence, from Eq.9 [3] the fracture strength  $\sigma_{int}$  can be determined, which is given by,

$$\sigma_{int} = \sqrt{\frac{100\varepsilon_p E_{int}}{\pi d}} \quad (10)$$

Where: E is Young's modulus, d is the particle thickness, since it is assumed that cracks of the order of the grain size are present when considering crack propagation through the interface and the particulate,

$\varepsilon_p$  is the energy required to create two fracture surfaces =  $2\varepsilon_S - \varepsilon_{gb}$  ( $= \varepsilon_o$ ), with  $\varepsilon_S$  the surface energy, and  $\varepsilon_{gb}$  the grain boundary energy.

The  $100 \varepsilon_p$  component allows for dislocation interaction and movement ahead of the crack-tip in ductile materials. This refers to the work required for a total separation of the lattice planes, which is equal to the area under the force-extension curve.

### 3.2.2 Interfacial Stress / Strain Behaviour of Reinforced Alloy System

To measure the stress transfer to the particle in a particulate reinforced MMC subjected to tensile loading, the stress carrying capability of the particle is defined as the ratio of the normal stress  $\sigma_N$  to the particle in the loading direction to the macroscopic tensile stress,  $\sigma_T$ , defined as the ratio  $L = \sigma_N / \sigma_T$  as the stress transfer from the matrix to the particles in a particulate reinforced MMC is mainly controlled by the misfit of the elastic constants between the two phases [134]. Myriounis-Hasan [133] proposed a micro-mechanics model to determine the fracture strength of the interface in a metal matrix composite, based on thermodynamic principles and given as in Eq.11.

$$K_{1C} = \frac{K_P}{L_P} V'_m + 2 \frac{K_{int}}{L_P + L_m} (V_m - V'_m) + \frac{K_m}{L_m} 2V_m + K_m (1 - 3V_m) \quad (11)$$

Where,  $K_{1C}$  is the fracture toughness of the composite,  $K_P$ ,  $K_m$  and  $K_{int}$  are the fracture toughness of the particle, matrix and the interface respectively.  $L_P$  is the stress carrying capability (ratio of normal and tensile stress as given in Eq 12) of the particle and  $L_m$  is the stress carrying capabilities of the matrix.  $V_m$  is the area fraction for particle cracking and  $(V_m - V'_m)$  is the area fractions for interface failure [9]. Wang and Zhang [136] found the ratio for  $V'_m/(V_m - V'_m)$  about 0.13 in an aluminium silicon carbide composite.

$$L = \frac{\sigma_N}{\sigma_T} \quad (12)$$

Where,  $\sigma_N$  is the normal stress and  $\sigma_T$  is the tensile stress.

By using Eshelby's theory, the stress carrying capability of a spherical inhomogeneity can be written as [137]:

$$L = \frac{9x(2+3x)}{(1+2x)(8+7x)} \quad (13)$$

Where,

$$x = \frac{E_i}{E_m} \quad (14)$$

$E_i$  and  $E_m$  are the young's modulus of the inhomogeneity and the matrix respectively.

According to Cox [138] for a particulate the stress carrying capability can be calculated as,

$$L = 1 + \frac{a}{\sqrt{3}} \quad (15)$$

Where,  $a$  is the aspect ratio of the particle and can be given as a ratio of the average length ( $\bar{h}$ ) and the radius of the particle ( $\bar{r}$ ) as;

$$a = \frac{\bar{h}}{2\bar{r}} \quad (16)$$

Mostly on average, for silicon carbide particles  $L_p = 2$  and for aluminium matrix  $L_m = 2$  [9]. Eq 11 then takes the following form;

$$K_{1C} = \frac{K_p}{2} V'_m + \frac{K_{int}}{2} (V_m - V'_m) + K_m V_m + K_m (1 - 3V_m) \quad (17)$$

The young's modulus of the interface in terms of critical strain energy release rate  $G_{int}$  can be found out using Griffith's approach using Eq.4 [130]. Since interfacial fracture strength  $\sigma_{int}$  is given by Eq.10 it implies that the energy required to create two fracture surfaces  $\epsilon_p$  can be given as;

$$\epsilon_p = \frac{\sqrt{\sigma_{int}}}{100E_{int}} \quad (18)$$

$\epsilon_p$  according to definition is also equal to  $2\epsilon_s - \epsilon_{gb}$  which is the same as  $\epsilon_o$ , where  $\epsilon_s$  and  $\epsilon_{gb}$  are the surface and grain boundary energies.

According to Faulkner et al [131] the work of intergranular fracture  $G_k$  is given by, Eq. 5, since the work of Faulkner et al was based on intergranular fracture we can relate it to interfacial fracture which implies,

$$G_k = G_{int} \quad (19)$$

Substituting  $E_{int} = \sigma_{int} / \epsilon_{int}$  in Eq. 4, we get

$$G_{int} = \frac{\sqrt{K_{int}}}{\sigma_{int}} * \epsilon_{int} \quad (20)$$

Eq.5 then can be written as;

$$\epsilon_{int} = \frac{A \sigma_{int} \epsilon_{int} e^{n \ln(\frac{\epsilon a}{\epsilon_0})}}{\sqrt{K_{int}}} \quad (21)$$

Where  $\epsilon_{int}$  is the interfacial strain caused by segregation and can be given as,

$$\epsilon_{int} = 100 \sigma_{int} \epsilon_p \left[ 1 - \frac{ZRT \ln(1-C-BC)}{\epsilon_p} \right]^n \quad (22)$$

Where,

$\epsilon_{int}$  Strain in the interface

$\sigma_{int}$  Stress on the interface

$\epsilon_p$  Energy required creating two surfaces

Z Density of the interface sites

- R = 8.314472 J/Kmol  
T = 803.15 K and 723.15 K for T6 and HT1 respectively  
C = 0.1 for pure Al (segregate concentration)  
B Adjusted boundary energy taking into account Zuchovitsky equations  
n = 10 for FCC Al (work hardening)

Here a model has been proposed to estimate the effects of particle volume fraction on fracture toughness in a particle-reinforced MMC. This model assumed that SiC particles are uniformly distributed in the matrix and that the pattern of particle distribution is similar to FCC structure in metals. The fracture toughness of the composite can then be written as Eq. 11.

$$K_{1C} = \frac{K_P}{L_P} V'_m + 2 \frac{K_{int}}{L_P + L_m} (V_m - V'_m) + \frac{K_m}{L_m} 2V_m + K_m (1 - 3V_m)$$

### 3.2.3 Constants Calculation

The energy  $\varepsilon_p$  required to create two fracture surfaces is basically related to the work of intergranular fracture,  $G_k$  as described earlier in section 3.2.1. The constant parameter B in Eq. 22, describes the modification of the boundary energy by impurities using the Zuchovitsky equations [3, 141], given by:

$$B = e^{\left(\frac{\varepsilon_1 - \varepsilon_2}{RT}\right)} \cong e^{\left(\frac{0.75\varepsilon_f}{RT}\right)} \quad (23)$$

Where:  $\varepsilon_1 - \varepsilon_2$  is the difference between the formation energy in the impurity in the bulk and the interface region. It is assumed that the values of the surface energy and the impurity formation energy in the bulk are close in value; therefore, the numerator in the exponential term depends on the impurity formation energy in the interface

region, which is assumed to be  $0.75\varepsilon_f$ , where  $\varepsilon_f$  is the formation energy of the impurity in the bulk. Using Faulkner's approach [139] to the derivation of impurity formation energy,

$$\varepsilon_f = \varepsilon_s + \varepsilon_e \quad (24)$$

Where:  $\varepsilon_s$  is the surface energy required forming the impurity atom and  $\varepsilon_e$  is the elastic energy involved with inserting an impurity atom into a matrix lattice site. This is given by:

$$\varepsilon_f = \frac{0.5\varepsilon_s}{1.94} + \frac{8\pi D}{3e} a_m (a_i - a_m)^2 eV \quad (25)$$

Where;

$\varepsilon_s$  is the surface energy (1.02 J m<sup>-2</sup>)

e is the electronic charge (1.60217646 \*10<sup>19</sup> Coulomb)

$a_i$  is the impurity atomic radius (0.118 nm for Si)

$a_m$  is the matrix atomic radius (0.143 nm for aluminum)

G is the shear modulus (26 GPa for aluminum)

By performing the calculations the impurity formation energy,  $\varepsilon_f$ , for aluminium alloy can be determined and then substituted in Eq. 23 to calculate  $B$  (Zuchovitsky).

Hence, as calculated from Eq 23,  $B$  for Al-SiCp, 31% Vol fraction at different heat treatments is as follows,

T6 1.000029539

HT1 1.000032807

T1 1.000079082

The range of the value of the boundary energy by impurities (B) is between  $0.2^{-4}$  –  $0.7^{-4}$  and hence can be averaged to 1.

The values of  $\varepsilon_f$  further calculated for T1, HT1 and T6 are 0.263. Which is compared to the value of 0.303 as calculated by Myriounis et al [9] and 4% improvement recorded to original estimates.

### **3.3 Interfacial Strengthening Behaviour of Reinforced Alloy System**

#### **3.3.1 Strengthening Behaviour in MMCs**

The strengthening mechanisms observed in MMCs may be divided into two categories, direct and indirect strengthening. Direct strengthening in particulate reinforced metals is an extension of the classical composite strengthening mechanisms used to describe the behaviour of continuous fibre reinforced composites [140-142]. Under an applied load, the load is transferred from the weaker matrix, across the matrix/reinforcement interface, to the typically higher stiffness reinforcement. In this manner, strengthening takes place by the reinforcement carrying much of the applied load. Due to the lower aspect ratio of particulate materials, load transfer is not as efficient as in the case of continuous fiber reinforcement, but is still significant in providing strengthening [143-145].

In metal matrix composites, where a high stiffness ceramic reinforcement is embedded in a metallic alloy, the thermal mismatch between the high expansion metallic matrix and the low expansion ceramic is typically quite high. Thus, upon cooling, dislocations form at the reinforcement/matrix interface due to the thermal

mismatch. In this manner, thermally induced dislocation punching results in indirect strengthening of the matrix [146-149]. In age harden-able matrix materials, the thermally-induced dislocations (formed upon quenching from the solution treatment) serve as heterogeneous nucleation sites for precipitate formation during the aging treatment [150]. Not only is there a preferential distribution of precipitates in the particle/matrix interface region, but the higher density of dislocations also causes an acceleration in the time to peak-aging compared to the unreinforced alloy of a similar composition. An increase in reinforcement volume fraction or a decrease in particle size increases the amount of indirect strengthening, since a larger amount of interfacial area exists for dislocation punching to take place.

The extent of indirect strengthening is more difficult to quantify than the contribution from direct strengthening. Krajewski et al [151] used a thermo-mechanical treatment, consisting of solution treating, rolling, followed by aging to provide a homogeneous distribution of dislocations (and subsequently precipitates) in both the matrix of the composite and the unreinforced alloy. In this manner, the difference in strengthening between unreinforced and composite could be attributed primarily to load transfer to the reinforcement. Chawla et al [145], compared experimental data on composites with a simple modified shear lag analysis proposed by Nardone and Prewo [143], and obtained extremely good correlation. It was shown that in peak-aged materials only (without rolling), the strengthening in the composite could be partitioned into direct and indirect strengthening components.

## **CHAPTER 4**

### **Finite Element Analysis of a Unit Cell Using ANSYS**

#### **SUMMARY**

There are numerous different software's available in the market to model and perform structural analysis of different composites like Abaqus, ADINA, Altair HyperWorks, COMSOL Multiphysics, Femap, Siemens PLM Software, HyperSizer, LS-DYNA, MSC Marc, Nastran, Radioss, STRAND7, TSV etc., out of which ANSYS mechanical software suite was chosen, which is trusted by organizations around the world to rapidly solve complex structural problems with ease. Finite element analysis was performed on a unit cell of Al/SiC with 20% and 31% volume fraction of the particulate and the stress/strain results compared with the experimental results focusing on the interfacial region of the matrix and the reinforcement.

#### **4.1 Introduction**

Structural analysis solutions from ANSYS provide the ability to simulate every structural aspect of a product, including linear static analysis that provides stresses or deformations, modal analysis that determines vibration characteristics, through to advanced transient nonlinear phenomena involving dynamic effects and complex behaviours.

All users, from designers to advanced experts, can benefit from ANSYS structural analysis solutions. The fidelity of the results is achieved through the wide variety of

material models available, the quality of the elements library, the robustness of the solution algorithms, and the ability to model every product — from single parts to very complex assemblies with hundreds of components interacting through contacts or relative motions.

ANSYS structural analysis solutions also offer unparalleled ease of use to help product developers focus on the most important part of the simulation process: understanding the results and the impact of design variations on the model.

To start off with ANSYS software basic simulations were made to understand the depth of the software. A few of the experimental simulations are listed in Appendix A.

## **4.2 Analysis Using ANSYS**

### **4.2.1 Unit Cell Concept**

The unit cell was designed in ANSYS which represented a small part of the composite which has aluminium matrix and silicon carbide as reinforcement. The top and bottom edges were fixed and loads were varied from 77MPa to 310MPa, and were applied on the X-axis if the unit cell is viewed from the front on the positive and negative X-axis as shown in chapter 2, figure 5. In this study bulk properties have been used and hence the scale of the unit cell does not have any effect on stress and material properties.

The mechanical properties of aluminium and silicon carbide for the ANSYS simulations are as shown in table 1. The can be seen in figure 7. In this study the polynomial (p-method) for meshing in ANSYS is used. The meshing around the

reinforcement is mapped and further in the matrix is free. The free meshing in the matrix area was chosen to save time while calculating the solution. Refinement has also been put to meshing near the interface. Another consideration was to put mapped meshing on the edge of the unit cell to see the effect of deformation when the loading was applied. The matrix and the reinforcement can clearly be seen in figure 7, which also depicts the coordinate system which is used in the simulations. The red ring around the reinforcement is the interface between the matrix and the reinforcement which are glued together frictionless.

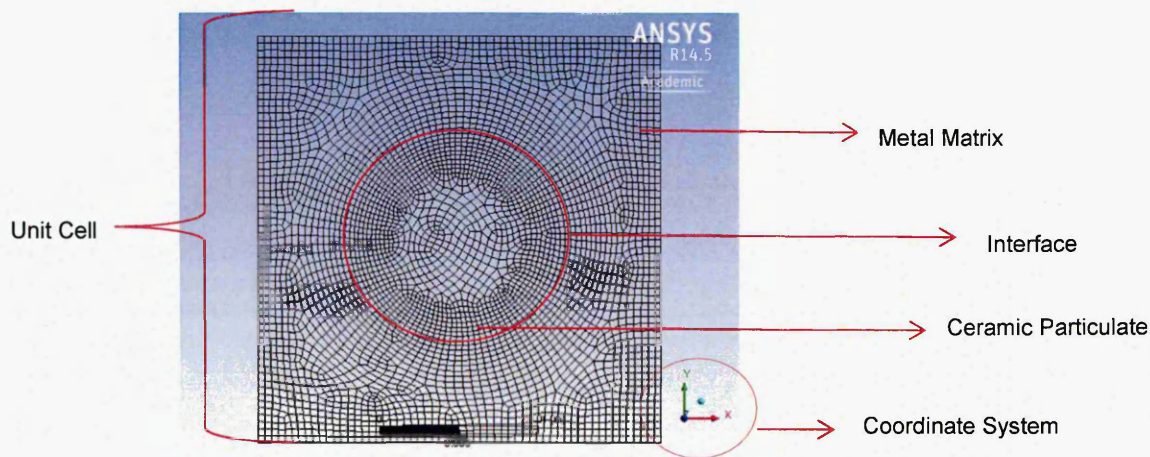


Figure 7: The grid pattern showing the Meshing used in this model.

The same simulations were tested upon a tetrahedral mesh with an element size of 0.1 but there were no differences in the results. The only difference was that it took a lot longer for the solution and the files being generated were very big because of the more number of elements, figure 8 shows the tetrahedral mesh, another reason was that since ANSYS treated both the materials i.e. the metal matrix and the ceramic reinforcement as different materials, and upon applying infiltration convergence was an issue. As the mesh in figure 8 shows the coarseness in the rest of the matrix other than the interface which is our main area of focus, infiltration is done very

smoothly and the convergence is very good at the interface of the matrix and the reinforcement. Some examples of non-convergence of the mesh can be seen in appendix B.

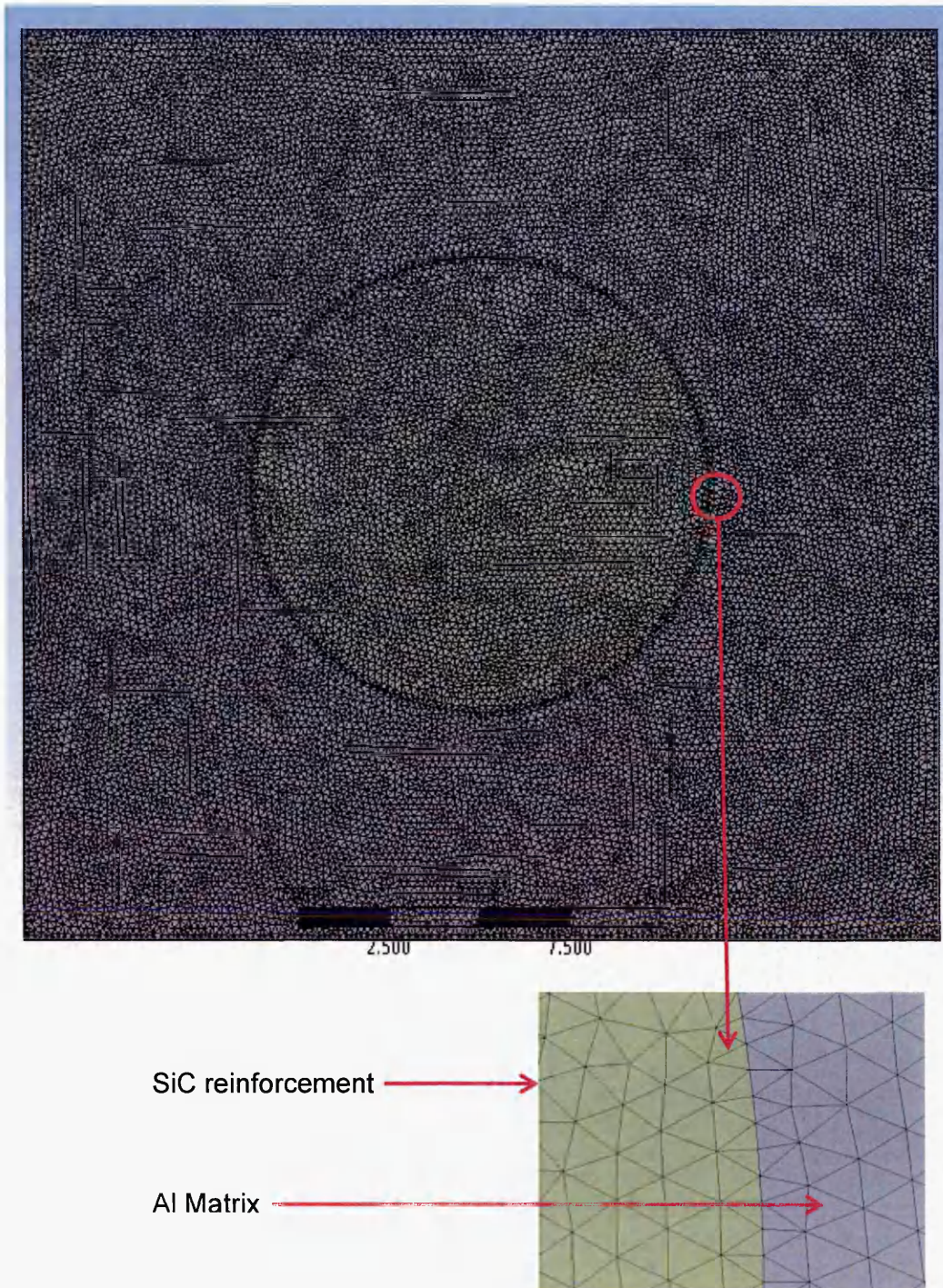


Figure 8: (A) The grid pattern showing the tetrahedral meshing (B) Magnified mesh at the interface

	Symbol	Units	SiC	Al
Density	$\rho$	g/cm <sup>3</sup>	3.2	2.7
Youngs Modulus	E	GPa	427	71.7
Poissons Ratio	$\gamma$	--	0.17	0.33
Yeild Stress	$\sigma_o$	MPa	1000	503
Ultimate Strength	$\sigma_{UTS}$	MPa	--	527
Elongation at Break	$e_f$	%	2.34	11.0
Coefficient of thermal expansion	CTE	$\times 10^6$ °C	4.3	23.6

Table 1: Mechanical properties of Al and SiC

#### 4.2.2 Finite Element Analysis of Interfacial Characteristics of Al/SiC Metal Matrix Composite

A Unit Cell is the simplest repeating unit in a crystal. The unit cell is designed using ANSYS which has a 1 X 1 square with a circle of diameter 0.5 inch, with an Aspect Ratio of 1. The Element type taken is Solid 8 Node 183, both the materials are taken as Structural - Linear - Elastic and Isotropic. The square part is Aluminium (Al) with the following properties,

$$EX = 71.7\text{GPa}$$

$$\text{Poissons Ratio PRXY} = 0.33$$

The circle part is Silicon Carbide (SiC) with

$$EX = 427\text{GPa}$$

$$\text{PRXY} = 0.17$$

The matrix and the reinforcement were glued together, and then Meshed (a finer mesh on the interface was done as that is the region of interest). The two top and bottom sides are given initial conditions of zero displacement for fixed supports and forces applied on the right and left (stretching the cell).

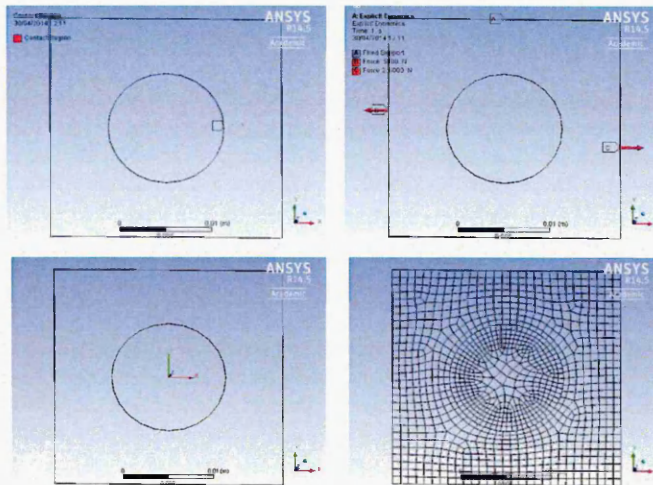


Figure 9: (A) The contact plane between aluminium matrix and SiCp reinforcement (B) The fixed supports and the forces been applied (5000N is just an example of the magnitude) (C) The coordinate system (D) Meshing of the model used.

The full set of results for the stress and the strain are shown in the following grid patterns, the stresses were applied with the following forces applied to the 0 degrees and 180 degrees of the unit cell perpendicular to the fixed supports which are applied on 90 degrees and 270 degrees. All the degrees are stated when looking at the unit cell as shown in figure 9 (C). The strains were recorded at the following different stresses (values in MPa) 77, 147, 149, 151, 155, 193, 232, 310 as seen in figure 10, and the corresponding stresses are shown in figure 11.

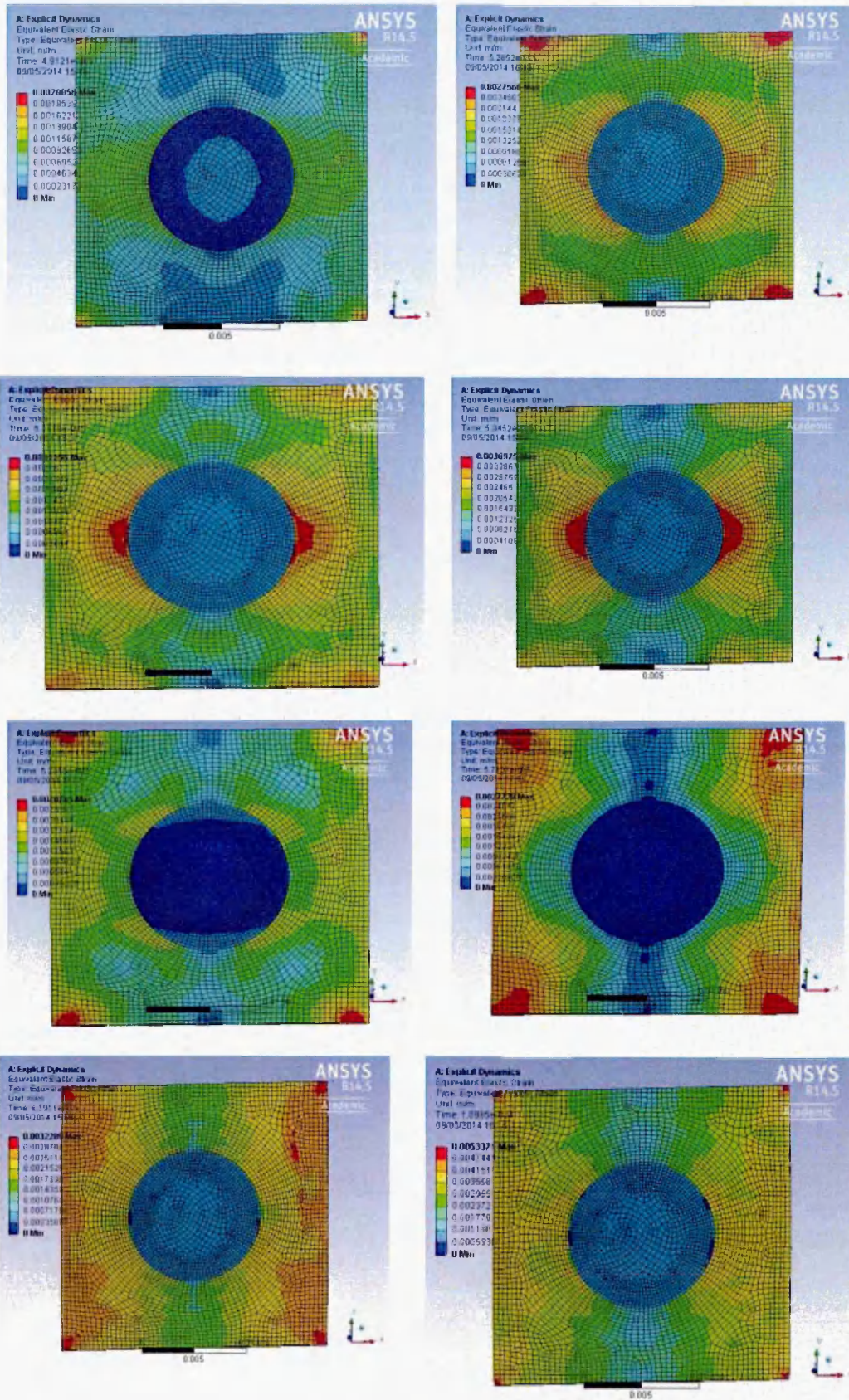


Figure 10: The girder patterns showing strains recorded at 77, 147, 149, 151, 155, 193, 232, 310 MPa

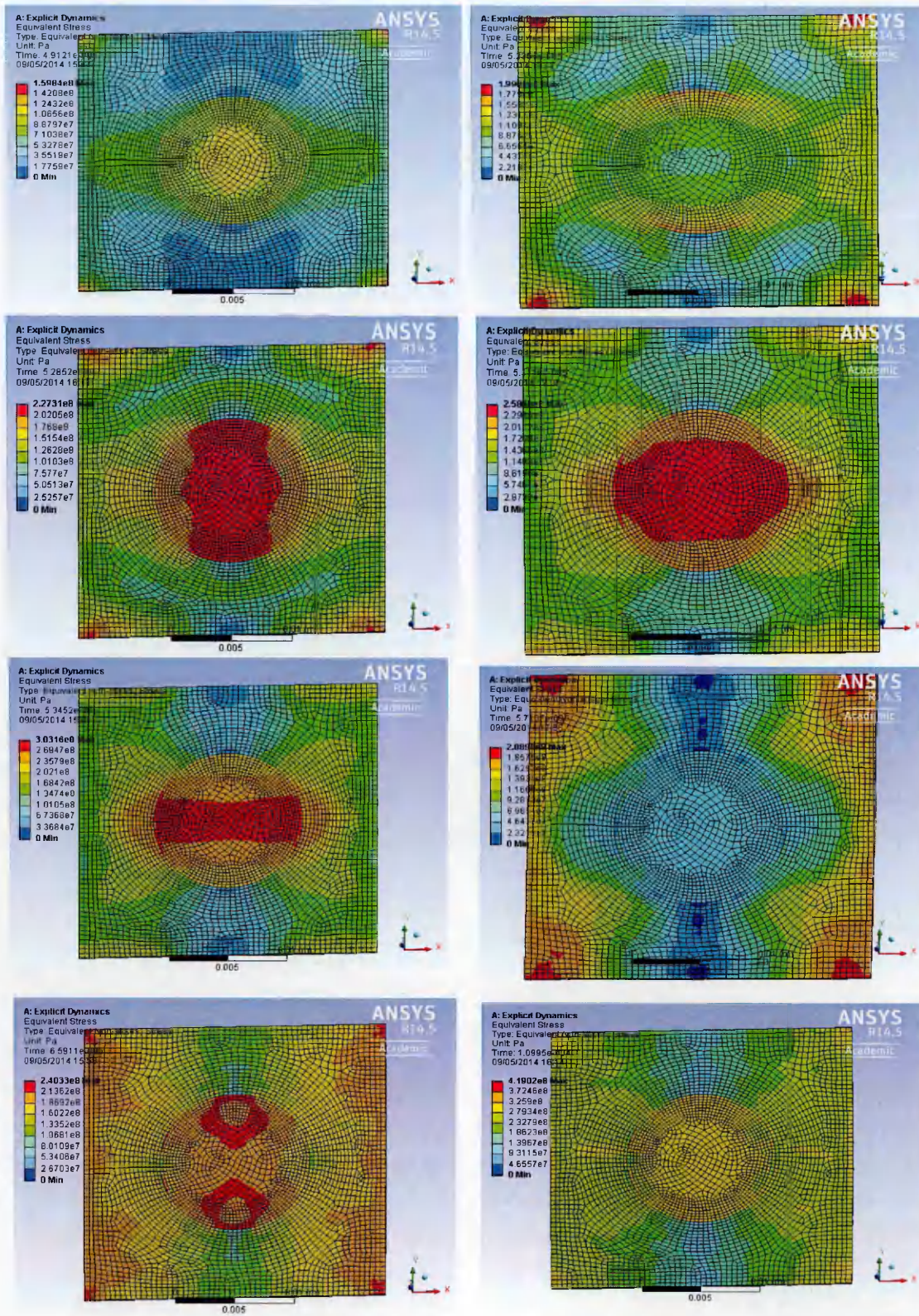


Figure 11: The gird patterns showing stresses recorded at 77, 147, 149, 151, 155, 193, 232, 310 MPa

### 4.3 Al/SiC Stress Strain Simulations using ANSYS

The pressure was varied from 8MPa to 310MPa. The interface between the matrix and the reinforcement was bonded frictionless and the meshing done in a way that the meshed blocks on the interface met each other to simulate the actual bonding in an actual composite. This gives a much realistic scenario in simulation of the actual composite. Figure 9-D, shows the meshing performed on the unit cell. Figure 11 shows the output when loads of 77, 147, 149, 151, 155, 193, 232, 310 MPa and 310 MPa respectively were applied to the composite. The strain levels can be seen changing in the figure 12, especially on the interface where the stress levels start very small and then gradually get to a point where they are at the peak level and then start decreasing again which shows the failure of the material. Looking at figure 12 it can be seen that the strain on the interface starts increasing, reaches to a peak and then starts decreasing which shows the failure of the material as tensile forces are increased on both sides of the unit cell.

Figure 12 shows a comparison of the stress/strain values at the centre of the unit cell, at the interface of the unit cell and the edge of the unit cell. All values were taken at the horizontal axis in the centre of the unit cell. The edge in at the extreme right of the unit cell. The graph in figure 12 clearly shows that after reaching the peak strain value the material fails at the interface first.

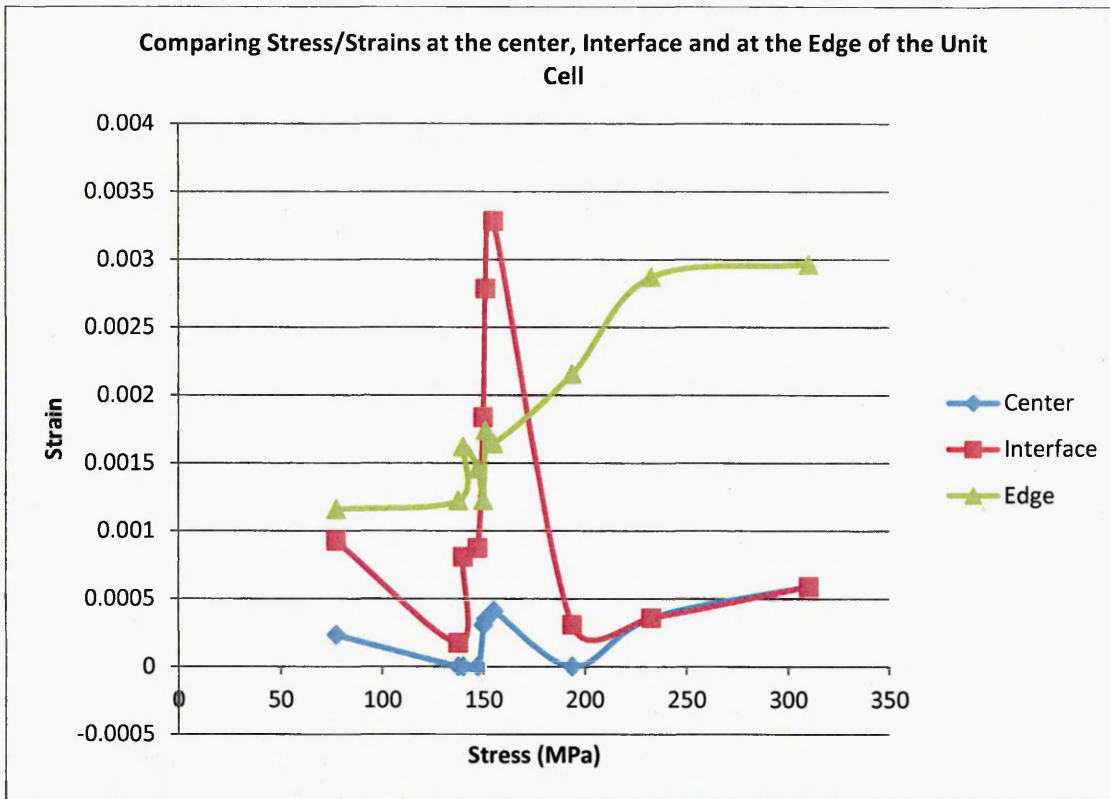


Figure 12: Comparison of the stress/strain values at the center, interface and the edge of the unit cell.

The strain levels are plotted on 5 positions at 0, 30, 45, 60 and 90 degrees of the applied load from the centre of the interface, an average of two values one from the silicon carbide and the other from aluminium was taken to predict the strain patterns at the interface. Best fit data plotted at 0, 30, 45, 60 and 90 degrees of the applied load are given by Eq's 26, 27, 28, 29 and 30 respectively and shown in figure 13,

$$\sigma_{int_0} = 41.8 \ln(\varepsilon_{int}) + 416. \quad (26)$$

$$\sigma_{int_{30}} = 26.3 \ln(\varepsilon_{int}) + 300. \quad (27)$$

$$\sigma_{int_{45}} = 40.1 \ln(\varepsilon_{int}) + 404. \quad (28)$$

$$\sigma_{int_{60}} = 45.5 \ln(\varepsilon_{int}) + 442. \quad (29)$$

$$\sigma_{int_{90}} = 46.6 \ln(\varepsilon_{int}) + 484. \quad (30)$$

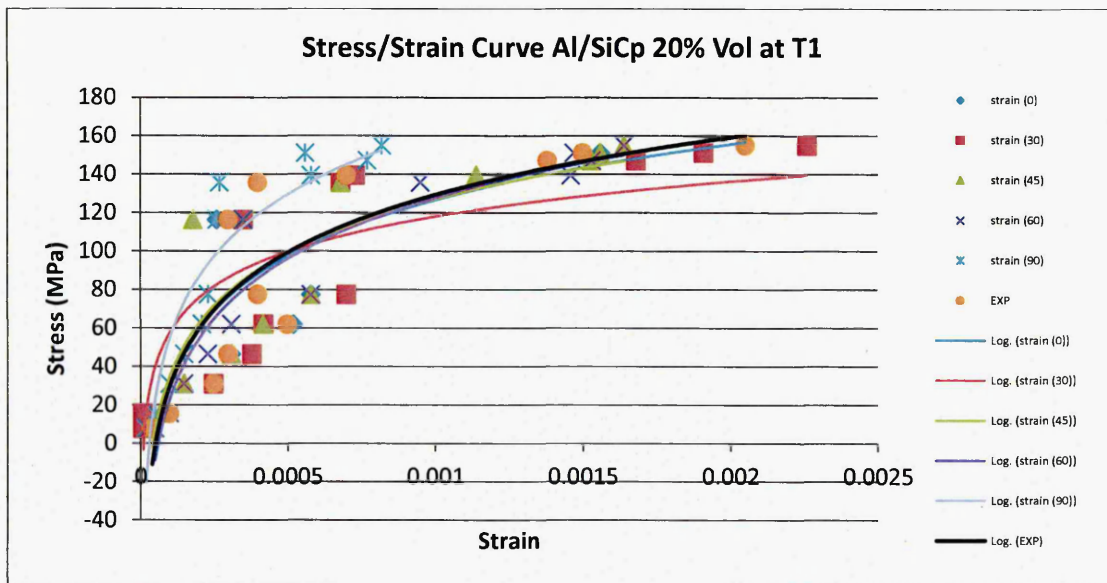


Figure 13: Comparison of Interfacial Stress / Strain curves of Al/SiC composite unit cell and the Empirical results.

In this study the numerical results were compared with the empirical results and as shown in figure 13, interfacial stresses and interfacial strains of Al/SiC composite unit cell were plotted at  $0^\circ$ ,  $30^\circ$ ,  $45^\circ$ ,  $60^\circ$  and  $90^\circ$  of the applied load from the unit cell approach taking into consideration that at the interface a frictionless bond has been made versus the experimental data, It can be seen that the strain at  $0^\circ$  was recorded higher than that at  $90^\circ$  at the same point of reference for particular stress value. When compared to the real world problem the results are comparable to the

empirical data with that of the  $0^\circ$ , as compared to the  $90^\circ$  which is perpendicular to the loading condition performed at  $0^\circ$ . Hence practically the  $0^\circ$  is more near to reality and will be considered throughout this study, as can be shown in figure 14.

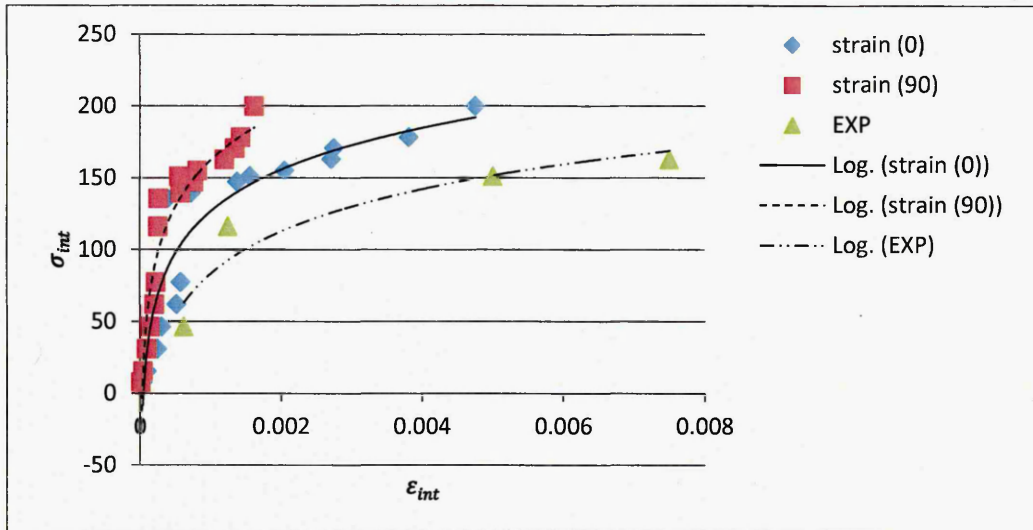


Figure 14: Comparison of Interfacial Stress / Strain curves of Al/SiC composite unit cell at  $0^\circ$  and  $90^\circ$  of the applied load and the empirical results.

It is observed that for the initial loads of up to 75MPa of load the correlation is very good and both the results are in harmony i.e. the experimental and simulated. As the stress reaches 110 MPa the strain as shown in figure 14, increases and then the gap between the trend lines for the empirical and simulated data become constant. In this study the numerical simulations are carried out taking stresses on  $0^\circ$ , as the results from figure 14 it is evident that when stresses are applied at  $0^\circ$  from the axis of the unit cell and strains recorded the results correspond to the experimental results pretty well specially for lower strains. The deviation is about 3% between the two results which is due to the interfacial segregation and precipitation; it can be concluded that if more data sets are plotted of the empirical data the trend line would match that of the simulated data.

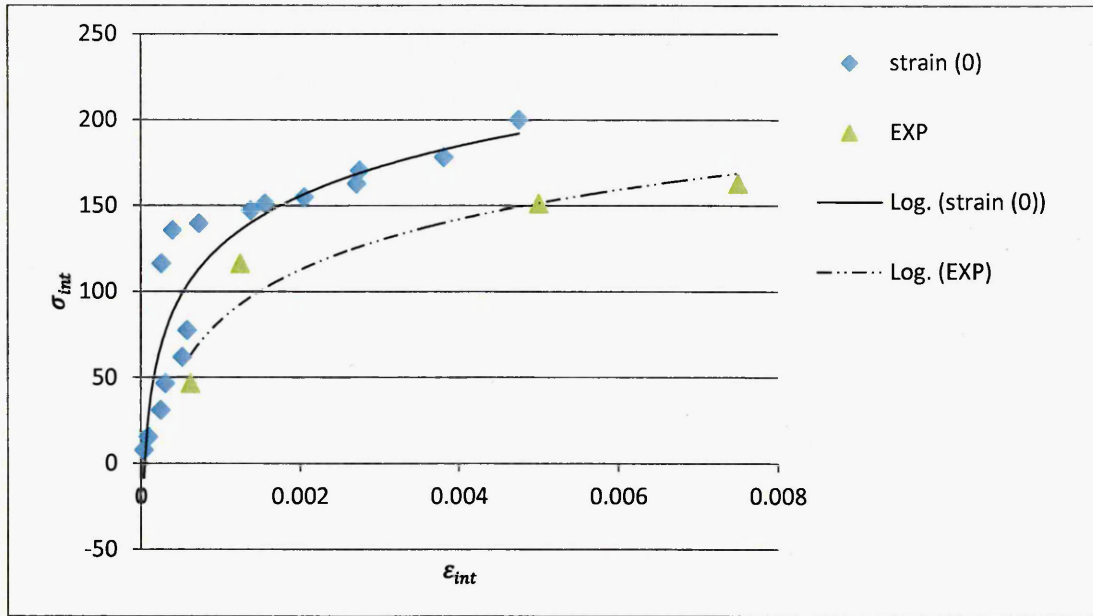


Figure 15: Comparison of Interfacial Stress / Strain curves of AL/SiC composite unit cell and the Empirical results.

#### 4.4 Empirical Model of a Unit Cell: Young's Modulus at the Interface

The spherical particle in the unit cell is converted to a cubic particle as shown in figure 16. The diameter of the particle  $d$ , thickness of interphase region  $d_i$ , volume fraction of the particles including the interface  $v'_f$ , the equivalent dimension of the particle is  $d_e$  and the overall dimension of the cubic unit cell  $s$ , are given by [152],

$$\frac{\pi(d+d_i)^3}{6} = v'_f s^3 = (d_e + d_i)^3 \quad (31)$$

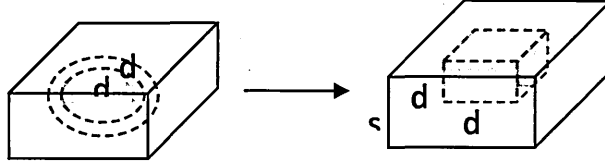


Figure 16: Conversion of a spherical particle to a cubic particle [153]

The volume fraction of the particles including the interface region is therefore,

$$v'_f = \left(\frac{d_e + d_i}{s}\right)^3 \quad (32)$$

And the volume fraction of the particles is

$$v_f = \left(\frac{d_e}{s}\right)^3 \quad (33)$$

Consider the unit cell is subjected to a uniaxial load in the longitudinal direction. The total load on the unit cell is defined from force equilibrium:

$$p_c = p_p + p_m + p_i \quad (34)$$

In an average sense if  $A_{uc}$  is the area of the unit cell,

$$\sigma_c A_{uc} = \sigma_p A_p + \sigma_m A_m + \sigma_i A_i \quad (35)$$

Dividing Eq. 35 by  $A_{uc} = s^3$  and substituting the actual areas, one obtains:

$$\sigma_c = \sigma_p \frac{d_e^2 s}{s^3} + \sigma_m \frac{(s^2 - (d_e + d_i)^2) s}{s^3} + \sigma_i \frac{((d_e + d_i)^2 - d_e^2) s}{s^3} \quad (36)$$

or,

$$\sigma_c = \sigma_p V_f^{2/3} + \sigma_m \left(1 - V_f'^{2/3}\right) + \sigma_i \left(V_f'^{2/3} - V_f^{2/3}\right) \quad (37)$$

Compatibility of longitudinal displacement requires that strain in the composite and each constituent be the same (i.e.  $\varepsilon_c = \varepsilon_m = \varepsilon_p = \varepsilon_i$ ), so the Eq. 37 reduces to:

$$E_c = E_p V_f^{2/3} + E_m \left(1 - V_f'^{2/3}\right) + E_i \left(V_f'^{2/3} - V_f^{2/3}\right) \quad (38)$$

So, the Young's modulus of a particulate composite  $E_c$  is given as a function of the moduli of the particles  $E_p$ , matrix  $E_m$ , and interface  $E_i$ .

Due to the fact that the difference  $V_f' - V_f$  is very small, a good approximation is to consider that the Young's modulus of the interface is close to that of the matrix;

$$E_i \cong E_m \quad (39)$$

#### 4.5 Correlation with Empirical Model

As explained in section 4.4, the Young's modulus of a particulate composite  $E_c$  is given as a function of the moduli of the particles  $E_p$ , matrix  $E_m$ , and interphase  $E_i$ . Due to the fact that the difference  $(V_f' - V_f)$  is very small, a good approximation is to consider that the Young's modulus of the interface is close to that of the matrix and given by Eq. 39, when subjected to numerical simulation and tested upon our model in ANSYS, following results were obtained in which the stresses and strains are compared on the interface with the matrix.

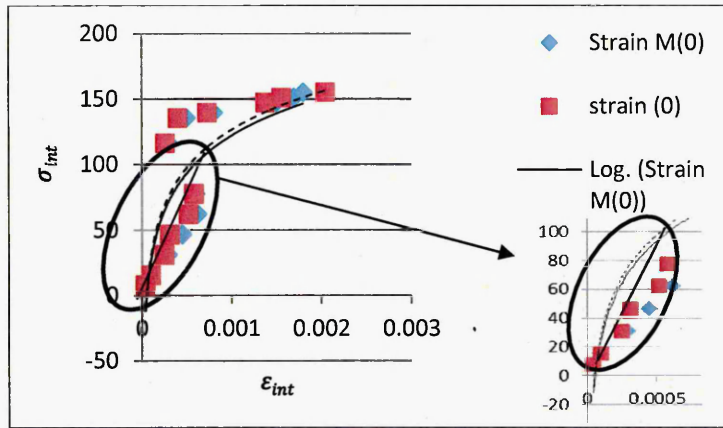


Figure 17: Interfacial Stress Strain Curves of Al/SiC unit cell at 0°

Stress Strain Curves of Al/SiC unit cell at 0 degrees of the loading where strain M(0) is stress and strain on the Matrix side of the unit cell at 0 degrees and strain (0) is strain at 0 degrees on the reinforcement.

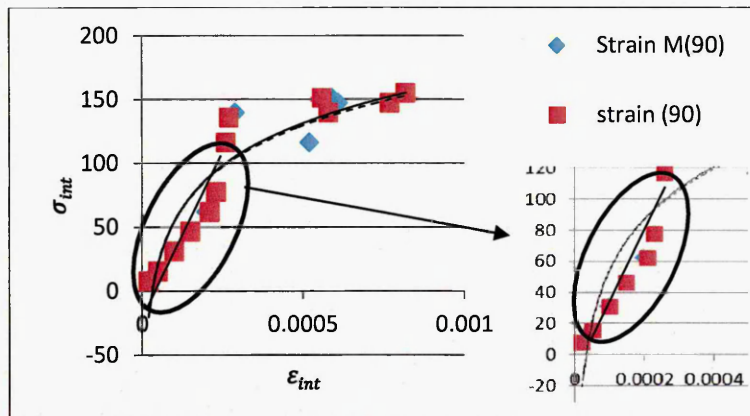


Figure 18: Stress Strain Curves of Al/SiC unit cell at 90°

It can be concluded from figure 17 and figure 18, that when the young's modulus is considered the young's modulus of the interface is nearly equal to the young's modulus of the matrix which proves the empirical hypothesis as explained by Eq. 39 given as follows for the young's modulus of interface and the matrix  $E_i \cong E_m$ .

## **4.6 Modelling and Analysis of Cohesive Zone Element at Matrix-Reinforcement Interface**

The cohesive zone is a layer with independent properties between the matrix and the reinforcement; it was assumed to be the interface. The unit cell model was made in ANSYS using APDL coding. Figure 19 (A) shows the outline of the model of the unit cell produced indicating the matrix and the reinforcement along with the cohesive zone element in between them. Figure 19 (B and C) show the nodes represented in this analysis in 3D and 2D respectively. Figure 19 (D) is a snap shot of the complete 3D unit cell showing the strains produced at a random point in time when stresses were applied to the unit cell.

Figure 19 (E and F) are a close up of the interface region of the unit cell; they show the matrix, reinforcement and the interface between them. Figure 19 (E) was taken from the initial analysis when the properties of matrix and the interface were kept same. Figure 19 (F) on the other hand depicts the changed properties of the interface which were taken from the experimental work of Myriounis [9].

The properties of Aluminium and silicon carbide were taken same as defined in table 1, chapter 4. Whereas for the properties of the interface an assumption was made that the poisson's ratio of the interface was equal to the poisons ratio of the reinforcement. The young's modulus of the interface was taken from the experimental results of Myriounis [9] as explained further in table 3, chapter 5.

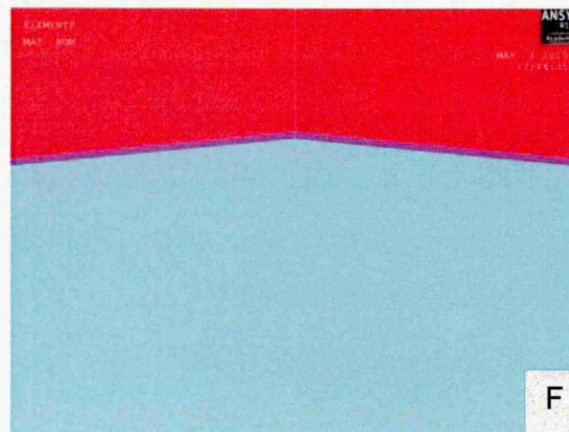
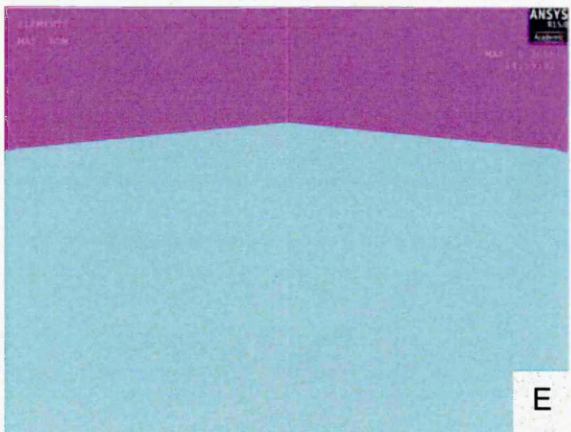
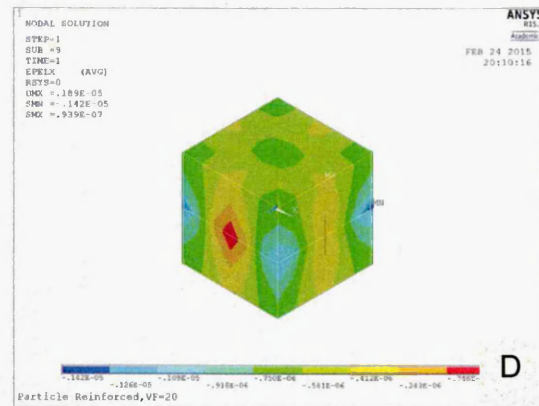
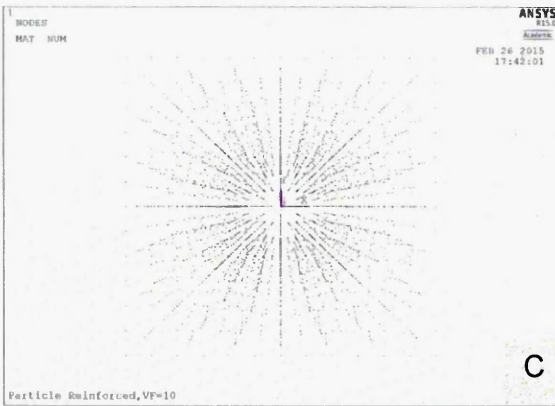
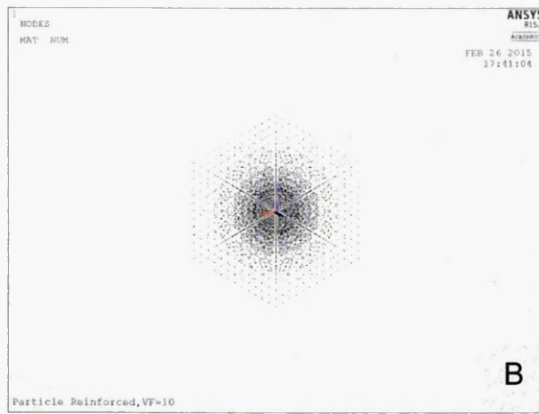
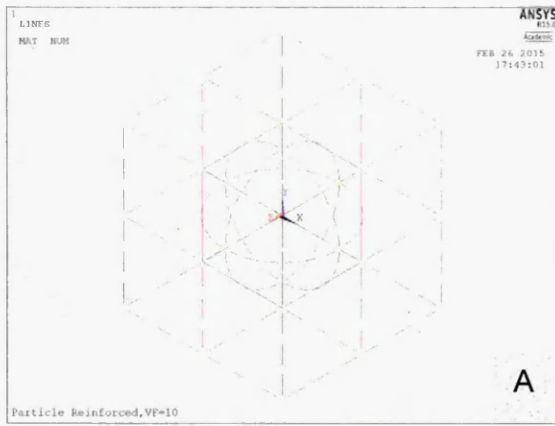


Figure 19: (A) 3D-Unit Cell Lines, (B) Nodes 3D, (C) Nodes 2D, (D) 3D-complete Unit Cell, (E) Interface with same properties as the Matrix, (F) Interface with different properties.

Figure 20 (A) shows the cohesive zone element alone without the matrix and the reinforcement, it is extended on the x-axis but this is just a depiction of ANSYS as it by default shows a plane along with the cohesive zone element, as can be clarified by the section view of the half cut unit cell in figure 20 (B) which shows the completely rounded interface between the matrix and the reinforcement.

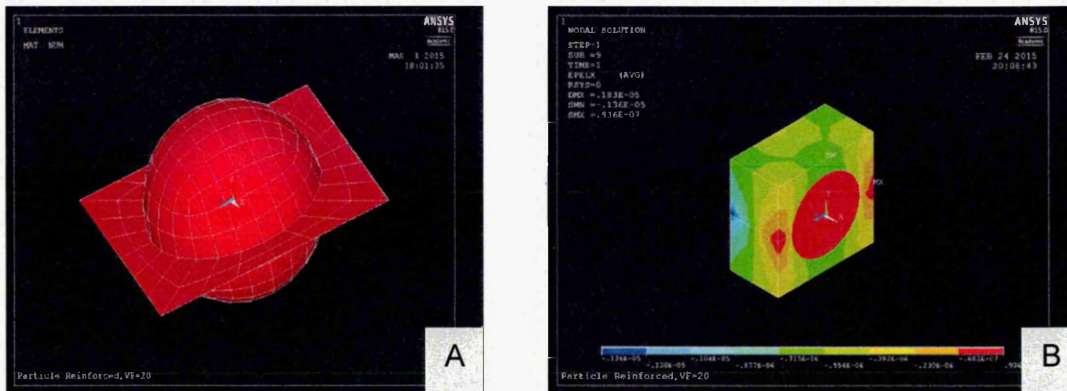


Figure 20: (A) CZE (B) Half Section Unit Cell with CZE

The properties of matrix and reinforcement were kept the same as shown in table 1, chapter 4, and values of the young's modulus for the interface were kept as shown in table 3, chapter 5. For the interface the poissons ratio was kept same as that of silicon carbide reinforcement on the basis that the interface is stronger than the matrix.

The stress/ strain values were observed for T1, T6 and HT1 heat treatments, for Al-SiC with 20% and 31% volume fraction of SiC, as shown in figures 21 and 22.

#### 4.7 Observations from the CZE Analysis

From the graphs presented in figure 21 and 22 it can be observed that the strain values remain almost the same for the corresponding stress for the same volume fraction of particulates of reinforcement.

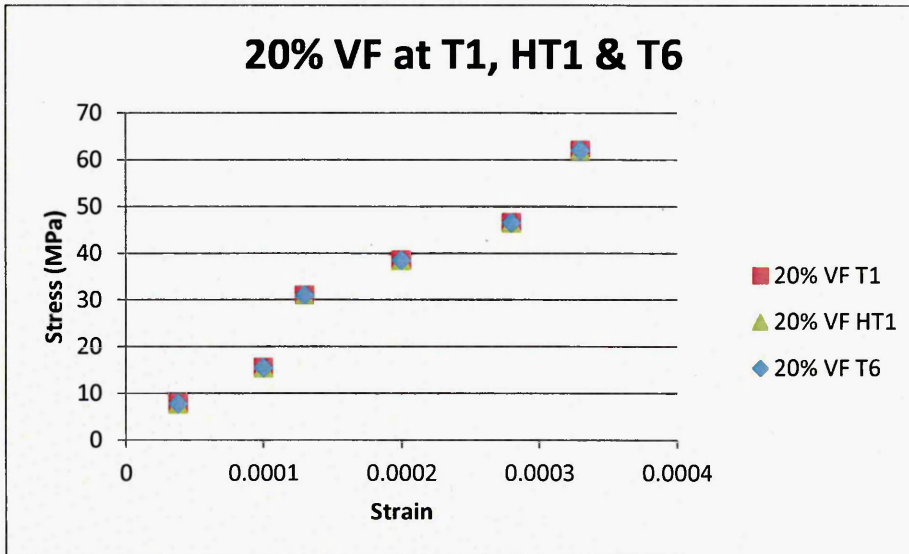


Figure 21: Stress/Strains at the CZE for 20% Vol fraction SiC at T1, HT1 and T6

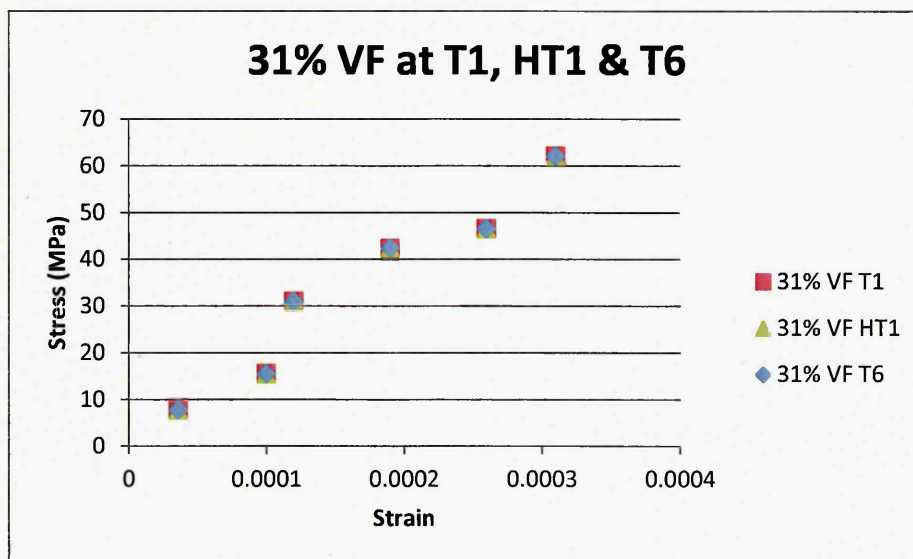


Figure 22: Stress/Strains at the CZE for 31% Vol fraction SiC at T1, HT1 and T6

The difference is quite evident when the volume fraction of the reinforcement is changed from 20% to 31%.

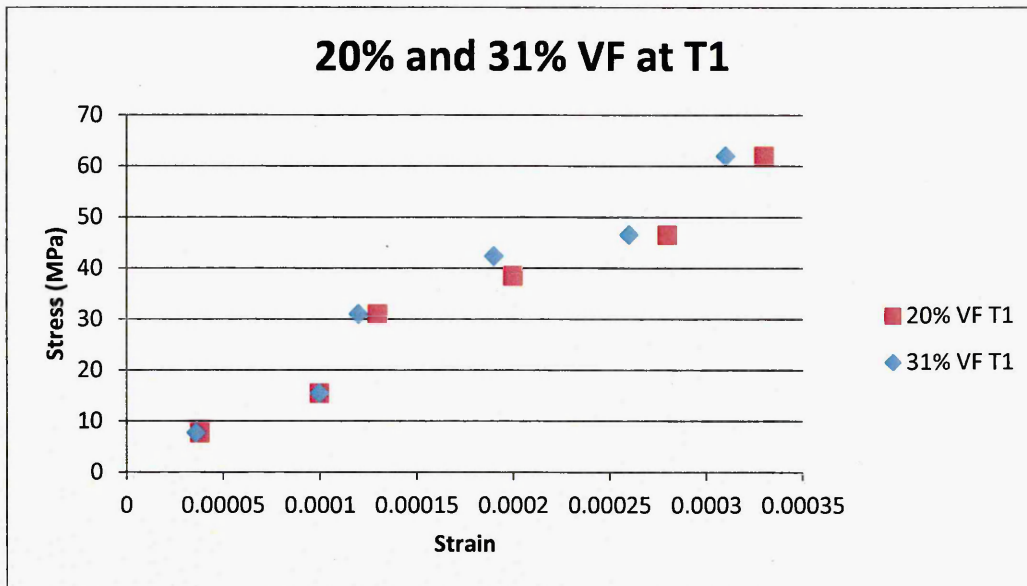


Figure 23: Stress/Strains at the CZE for 20% and 31% Volume fraction SiC at T1

The cohesive zone element (CZE) when introduced for the 20% volume fraction and the 31% volume fraction of SiC in an aluminium matrix, the stresses and strains were measured at the CZE and it is evident from figures 21 and 22 that the heat treatment did not have any effect on the CZE (this was the reason that only T1 heat treatment is further compare in figure 24) but the volume fraction of the reinforcement play's a significant role and as expected when the volume fraction of SiC was raised from 20% to 31% because of the CZE becoming tougher. The stress/strains as shown in figure 23 at any point of strain high stress was observed to be endured for the 31% volume fraction of SiC as compared with the 20% volume fraction of SiC in aluminium matrix.

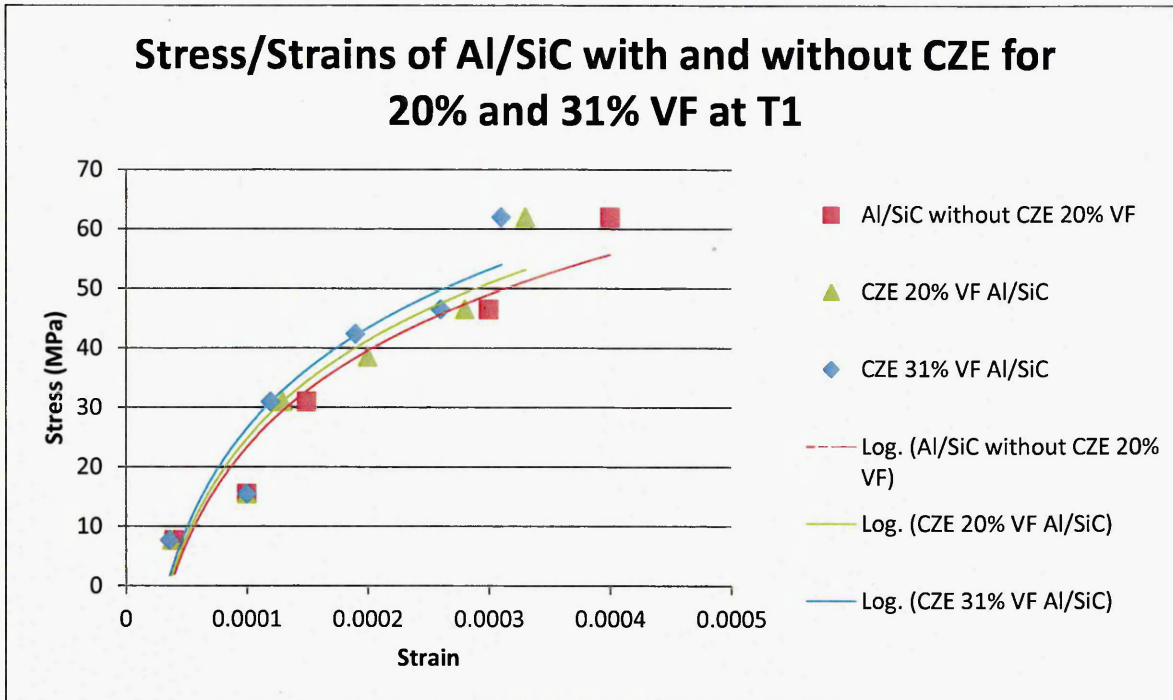


Figure 24: Stress/Strains at the CZE for 20% and 31% Volume fraction SiC at T1 compared with stress/strains at the interface without the CZE for 20% volume fraction SiC at T1.

Another comparison was made with the unit cell with a CZE, the results of which are described in figure 21 and 22, with the model discussed earlier in section 4.2.2 in which the matrix and the reinforcement are glued together frictionless. The stresses and strains were measured at the interface. As shown in figure 24 it is shown that when the matrix and the reinforcement are bonded frictionless without a CZE present the stress strain values at a certain point in time are lower as compared to the values recorded with a CZE.

## 4.7 Conclusion

It can be concluded that the stress strain curves are best observed in simulation of a unit cell when the forces are acting axially at  $0^\circ$  from the centre of the unit cell. It is also observed from the results that the degradation is more pronounced in the interfacial elements near the axis of symmetry where the stresses are high resulting in more degradation in these zones. The interfacial shear stress changes with change in SiC content. From these results, it is observed that the higher the volume fraction of SiC the more interfacial shear stress. The maximum interfacial shear stress occurs just inside the model at some distance from the free end of the unit cell. It can be concluded that the young's modulus of the matrix is equal to the young's modulus of the interface as verified empirically and through FE simulation.

It can also be concluded that the interface does play a very important role in the strengthening of the metal matrix composite as it is evident from the results shown in figure 24.

## **CHAPTER 5**

### **Strengthening Behaviour with T6 and HT1 Heat Treatments**

#### **SUMMARY**

This chapter focuses at the strengthening behaviour of the aluminium silicon carbide metal matrix composite with different volume fractions of SiC, along with different heat treatments, finite element analysis is used for comparing the different heat treated Al-SiC MMCs, material properties of whom were taken from previous studies. Both scenarios were simulated i.e. keeping the same volume fraction with different heat treatments along with keeping same heat treatment for different volume fractions.

#### **5.1 Introduction**

The thermal conditions for the reaction between the matrix and the reinforcement depends on the composition of the MMC and its processing method. A good bond can be formed by proper and adequate interaction between the reinforcement and the matrix. Inadequate interaction results in lack of proper bonding, whereas excessive interaction leads to the loss of the desired properties and inferior performance of the MMC. The important factors affecting the heat treatment process are the temperature, the cooling rate, the concentration of solute atoms and the binding energy between solute atoms and vacancies. Temperature control is extremely important during the fabrication process. If the melt temperature of

SiC<sub>p</sub>/Al composite materials rises above a critical value, Al<sub>4</sub>C<sub>3</sub> is formed [145], increasing the viscosity of the molten material, which can result in severe loss of corrosion resistance and degradation of mechanical properties.

Heat treatment of composites though has another aspect to consider, which is the particles introduced that may alter the alloy's surface characteristics and increase the surface energies. The process variables affecting the dispersion of the particulate is very important, including temperature and type of heat treatment of the particles size and shape, melt temperature, feed rate of the particulate and volume percent of the dispersion [135].

One of the most used heat treatments for the Al A359/SiC<sub>p</sub> composite is the T6 heat treatment. It is known that molten aluminium does not wet silicon carbide readily, which is one of the major concerns which needs to be overcome to prevent silicon carbide particles being displaced from molten aluminium and to ensure Al/SiC<sub>p</sub> bonding. MC-21 Inc. patented melt stirring, a method of satisfying these requirements and producing high quality composites. SiC particulates are added to Al-Si casting alloys, where Si in the alloy slows down the formation of Al<sub>4</sub>C<sub>3</sub>. The process yields material with a uniform distribution of particles in a 95-98% dense aluminium matrix. The rapid solidification, inherent in the process, ensures minimal reaction between reinforcing material and the matrix [146].

The two heat treatments T6 and HT1 have been considered since due to heat treatments the precipitates and segregates at the interface are more pronounced, and to validate our simulated results a complete set of experimental results were present from the work of Myriounis [9].

## 5.2 T6 Heat Treatment

The T6 Heat treatment consists of quenching and age hardening. In the solution heat treatment, the alloy is heated to a temperature just below the initial melting point of the alloy, where all the solute atoms are allowed to dissolve to form a single phase solid solution. The alloy is then quenched to room temperature at a rate sufficient to inhibit the formation of Mg-Si precipitates, resulting in a non-equilibrium solid solution which is supersaturated. In age hardening, the alloy is heated to an intermediate temperature where nucleation and growth of the Mg-Si precipitates can occur. The precipitate phase nucleates within grains and at grain boundaries, as uniformly dispersed particles. The holding time plays the key role in promoting precipitation and growth which results in higher mechanical deformation response of the composite. The material is then cooled to room temperature, where it may receive further processing [136].

The T6 heat treatment process used for the samples used by Myriounis [9] for the experimental results which are compared with the simulated results in this work, consisted of the following steps: solution heat treatment, quench and age hardening. In the solution heat treatment, the alloys have been heated to a temperature just below the initial melting point of the alloy for 2 hours at  $530\pm 5$  °C where all the solute atoms are allowed to dissolve to form a single-phase solid solution then quenched in water. Next, the composites were heated to a temperature of 155 °C for 5 hours then cooled in air.

### **5.3 HT1 Heat Treatment**

The second heat treatment process is the HT1 heat treatment, where the alloys in the solution treatment are heated to a temperature lower than the T6 heat treatment, at  $450\pm 5$  °C for 1 hour, and then quenched in water. Subsequently, the alloys are heated to an intermediate temperature of 170 °C for 24 hours in the age hardened stage and then cooled in air.

The T6 heat treatment has been selected according to the literature studied, where it is proposed as the ideal treatment for these kind of composites, whereas the HT1 heat treatment cycle was determined throughout a trial and error procedure by Myriounis.

### **5.4 Materials Considered for Simulations**

The materials used by Myriounis for his experiments were supplied by MC-21, Inc located in Carson City, NV, USA [154], which developed, patented, and demonstrated at a commercial scale a proprietary process improvement that achieves much greater efficiency in the mixing operation. This increased efficiency allows SiC particles to be mixed into molten aluminium much more rapidly. Aluminium alloys A359 are important materials in many industrial applications, including aerospace and automotive applications.

For the investigation data for the following two types of materials were used:

- 1) Hot rolled as received A359/31 vol.% SiC<sub>p</sub> with an average particle size of  $17\pm 1$  micron

- 2) Hot rolled as received A359/20 vol.% SiC<sub>p</sub> with an average particle size of 17±1 micron.

The above mentioned materials were thermally modified by the two heat treatments T6 and HT1 by the manufacturer and Table 2, contains the details of the chemical composition of the matrix alloy as well as the amount of silicon carbide particles in the metal matrix composites provided by manufacturer [154] MC-21 inc. The benefits of the rapid mixing process developed by MC-21, Inc. include its demonstrated ability to produce a much wider range of reinforcement size and volume fraction combinations. For example, materials with twice the stiffness of aluminium at comparable density greatly reduced thermal expansion coefficient and orders of magnitude improvement in wear resistance are achievable in the higher reinforcement volume fraction composites. The material properties taken for our simulation inputs were from the study of Myriounis work.

<b>TYPES</b>	<b>Si</b>	<b>Mg</b>	<b>Mn</b>	<b>Cu</b>	<b>Fe</b>	<b>Zn</b>	<b>SiC<sub>p</sub></b>
INGOT A359	9.5	0.5	0.1	0.2	0.2	0.1	<b>40</b>
INGOT A359	9.5	0.5	0.1	0.2	0.2	0.1	<b>25</b>
CAST A359	9.5	0.5	0.1	0.2	0.2	0.1	<b>30</b>
ROLLED A359	9.5	0.5	0.1	0.2	0.2	0.1	<b>31</b>
ROLLED A359	9.5	0.5	0.1	0.2	0.2	0.1	<b>20</b>

Table 2: The chemical composition of the matrix alloy and the amount of SiC<sub>p</sub> [9]

## **5.5 Microstructure of Al/SiCp**

The microstructure of composite materials consists of a major phase which in our case is the aluminium, silicon carbide is the reinforcement and the eutectic mixture of these two elements is at the interface. In this system, each element plays a role in the material's overall behaviour. In particular, Si improves the fluidity of Al and also Si particles are hard and improve the wear resistance of Al. By adding Mg, Al-Si alloys become age hardened through the precipitation of  $Mg_2Si$ .

## **5.6 Unit Cell - FEA Analysis**

To validate the effects of heat treatments on the strengthening behaviour of Al A359/SiCp, two different volume fractions were used 20 % Vol SiCp and 31 % Vol SiCp. Three different simulations were performed on both of the volume fractions at T6, HT1 and for comparison purposes simulated results were calculated on as received composite.

### **5.6.1 Modelling the Unit Cell from the Interface**

To look at the behaviour at the interface of Al A359/SiCp the model used was a 1 x 1 x1 unit block as shown and described in chapter 4. This block/unit cell represents a very small unit on the interface of Al A359/SiCp as shown in figure 25. For the initial simulations the properties of aluminium and silicon carbide only were studied with a frictionless bond between them. The interface properties were then studied by taking an average value from the matrix and the reinforcement on the meshing blocks

touching the boundary of aluminium and silicon carbide respectively. The stress/strain results from taking a unit cell from the interface region were found to be very close to the results which Myriounis [9] got in his experiments. The results obtained were compared with the numerical simulations and predictions made as discussed further in this chapter.

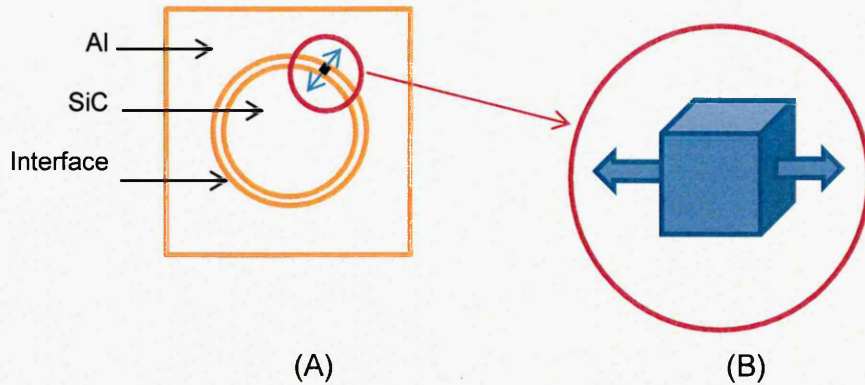


Figure 25: A blown up unit cell showing the interface as a ring with one unit on the interface which is further blown up in (B)

The structure was designed in ANSYS with the following Young's modulus (E) as can be seen in table 3 and the Poisson's ratio was considered same as that of Al as proved by Eq. 39.

Material	Condition	Young Modulus (E)
Rolled Al A359-SiCp-20p	As Received	100
	T6	112
	HT1	102
Rolled Al A359-SiCp-31p	As Received	108
	T6	116
	HT1	110

Table 3: Youngs Modulus of Al A359-SiCp-20p and 31p at different heat treatments [9].

## **5.6.2 Comparing Different Heat Treatments with Same Volume Percent of SiCp**

For the Al A359/SiC 20% Volume fraction and A359/SiC with 31% volume fraction of SiC three comparisons each were carried out, the first was to compare the as received condition with the HT1, the stress and strain's were recorded in ANSYS and were compared with the experimental results. Similarly simulations were carried out between the as received condition and T6 and the third set of simulations, was to compare the HT1 and T6 heat treatments and the results are compared and analysed in figure 26 for A359/SiC with 20% volume fraction of SiC and in figure 27 for A359/SiC with 31% volume fraction of SiC.

From the stress strain graphs shown in figure 26 and 27 it is clear that the simulation results corresponded very much like the experimental results in the linear region but as the non-linearity is reached the experimental results show much lower strains as compared to the simulated strains, this could mainly be attributed to the experimental conditions when the experiments were performed. Other than that a very good correlation between the experimental and simulated results for both Al A359/SiC 20% volume fraction and A359/SiC with 31% volume fraction of SiC is observed, at all the three heat treatments T6, T1 and HT1.

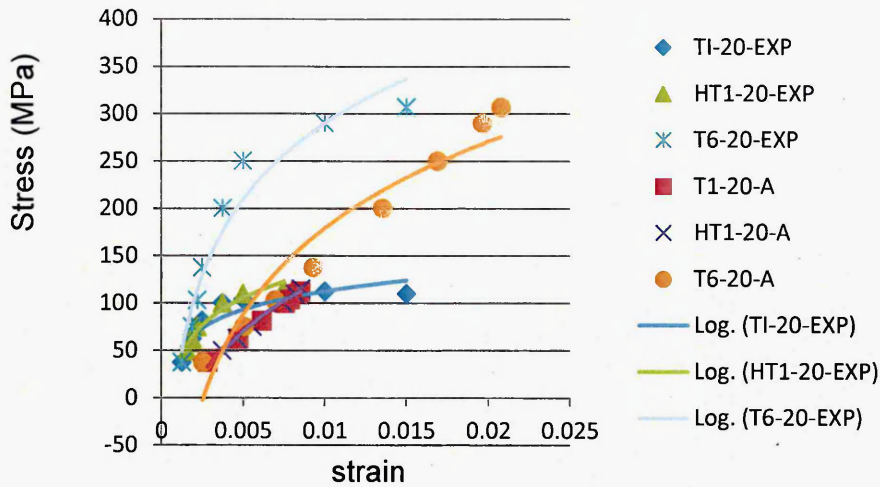


Figure 26: Comparing stress vs strain of the experimental results vs ANSYS FEA simulation results for Al A359/SiCp, 20% vol for T6 heat treatment, HT1 heat treatment and the as received sample.

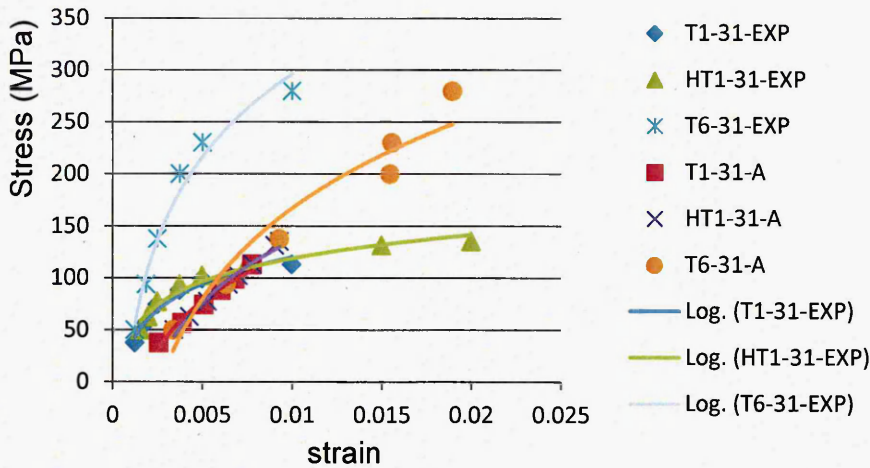


Figure 27: Comparing stress vs strain of the experimental results vs ANSYS FEA simulation results for Al A359/SiCp, 31% Vol for T6 heat treatment, HT1 heat treatment and the as received sample.

Also from the results in figure 20 and 21, it can be clearly seen that heat treatment does have an impact on the strengthening behaviour at the interface of the composite Al A359/SiCp 20% Volume fraction and A359/SiC with 31% volume

fraction of SiC. The most profound effect was found to be with the T6 heat treatment, followed by the HT1 heat treatment.

### **5.6.3 Varying the Volume Percent of SiCp: Keeping the same Heat Treatment**

To validate the effects of volume percentages while keeping the same heat treatments on the strengthening behaviour of Al A359/SiCp, was studied with two different volume fractions again with 20 % Volume fraction of SiCp and 31 % Volume fraction of SiCp. Three different sets of simulations were performed on both of the volume fractions at T6, HT1 and for comparison purposes experimental results were calculated on as received composite.

For as received conditions of Al A359/SiC 20% Vol and Al A359/SiC 31% Vol, experimental and simulated stress strain values were compared as shown in figure 28 for t1 heat treatment condition, figure 29 for T6 heat treatment condition and figure 30 for HT1 heat treatment condition . It is evident that experimentally lower strains are observed when compared to the simulated conditions, from the results there exists a factor difference of two between the experimental and the simulated results. Other than that a very good correlation between the experimental and simulated results for both Al A359/SiC 20% Volume fraction and A359/SiC with 31% volume fraction of SiC was observed, at all the three heat treatments T6, T1 and HT1.

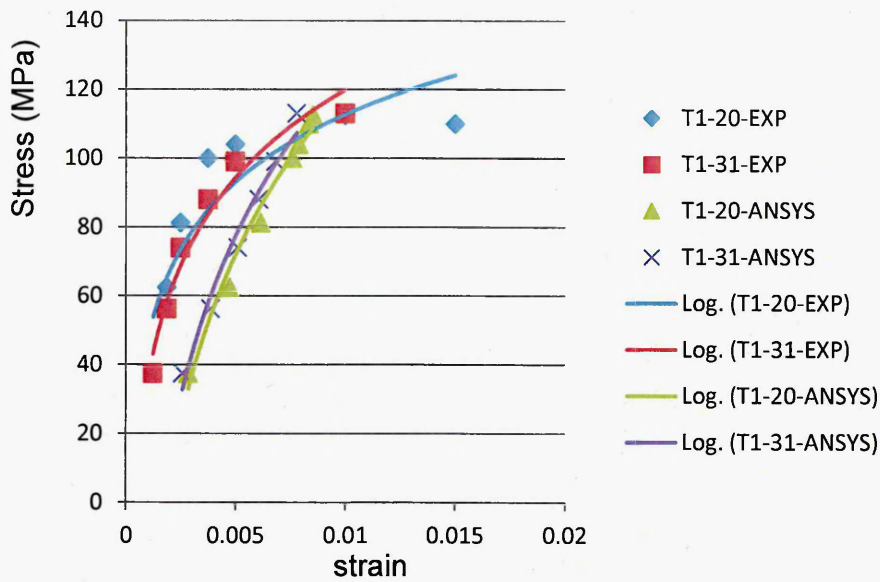


Figure 28: Comparing Experimental results vs ANSYS FEA simulation results for Al A359/SiCp, 20% vol at T1 Vs 31% vol SiC at T1.

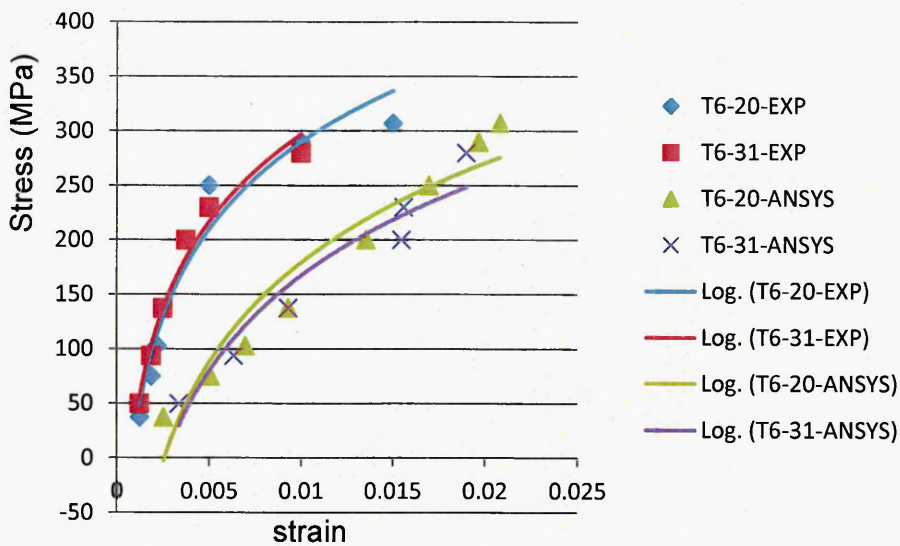


Figure 29: Comparing Experimental results vs ANSYS FEA simulation results for Al A359/SiCp, 20% vol at T1 Vs 31% vol SiC at T6.

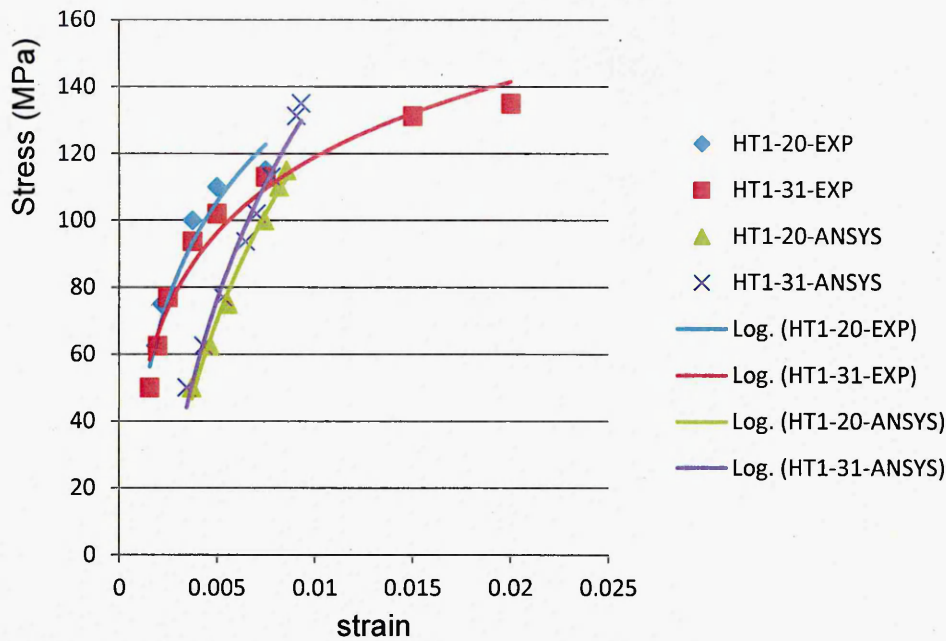


Figure 30: Comparing Experimental results vs Ansys FEA simulation results for Al A359/SiCp, 20% vol at T1 Vs 31% vol SiC at HT1.

Comparing figure 28, figure 29 and figure 30 for all three heat treatments which are as received (T1), T6 and HT1 it is evident that the T6 heat treatment irrespective of the volume fraction of SiCp has a very profound effect on the strengthening behavior of the composite as compared with the T6 and the HT1 heat treatment conditions.

#### 5.6.4 Effects of Dislocation Pile Up upon Strengthening in A359/SiCp

After analyzing the data it can be predicted that the differences in the stress/strain results, were because of the dislocation pile ups and the Bauschinger effect.

The Bauschinger effect refers to a property of materials where the material's stress/strain characteristics change as a result of the microscopic stress distribution of the material. For example, an increase in tensile yield strength occurs at the

expense of compressive yield strength. The effect is named after German engineer Johann Bauschinger [155].

The Bauschinger effect is normally associated with conditions where the yield strength of a metal decreases when the direction of strain is changed. It is a general phenomenon found in most polycrystalline metals. The basic mechanism for the Bauschinger effect is related to the dislocation structure in the cold worked metal. As deformation occurs, the dislocations will accumulate at barriers and produce dislocation pile-ups and tangles.

### **5.6.5 Predictions and Correlations**

To check the model as explained in section 5.6.1, the same model which was made in ANSYS was used with the addition of MISO (Multilinear Isotropic Hardening model). For the analysis in ANSYS which uses the von Mises yield criteria coupled with an isotropic work hardening assumption which in our case was the heat treatment and simulations were used to define the stress strain curves.

As shown in figure 31 there is a factor difference between the experimental results and the simulated results for the stress and strains, for both 20% and 31% volume fraction of SiC, the difference of these results is in the region of  $10^{-3}$  which is very small but the reason for this is basically because when the reinforcement is put into the matrix, the matrix is displaced, producing strain, to accommodate the volume fraction of the composite. This is the mis-fit parameter which is responsible for under predicting the stress/strain values in the simulations, as compared to the experimental values.

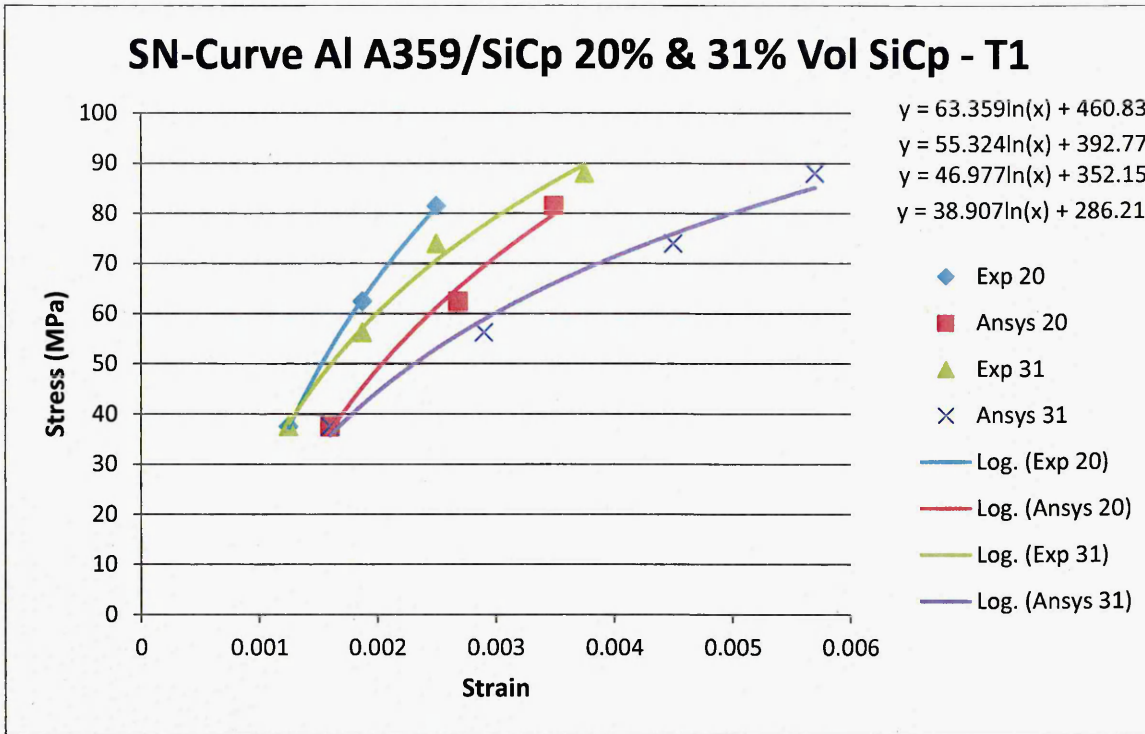


Figure 31: Comparing Experimental results vs ANSYS FEA simulation stress/strain results for Al A359/SiCp, 20% vol and 31% vol at T1.

The exact values are listed in table 4 for Al A359/SiCp 20% vol and table 5 for Al A359/SiCp 31% vol .

Stress (MPa)	EXP	ANSYS	% Diff
37.5	0.0012	0.0016	33
62.5	0.0018	0.0026	44
81.5	0.0025	0.0034	36

Table 4: Values of Stress and Strain as measured in the simulations and experimentally with their difference for Al A359/SiCp 20% vol .

Stress (MPa)	EXP	ANSYS	% Diff
37.5	0.00125	0.0016	28
56.25	0.001875	0.0029	54
88	0.00375	0.0057	52

Table 5: Values of Stress and Strain as measured in the simulations and experimentally with their difference for Al A359/SiCp 31% vol .

Plotting the stress-strain curve enables us to understand of what occurs during a loading and reverse loading cycle. This proposed method was also tested for non-proportional loading for plastic strain controlled cyclic tests with a combined axial force for particulate metal matrix composite unit cell of Al/SiC. The results obtained for aluminium silicon carbide with 20% volume fraction varied between 33-44%, where as in case of aluminium silicon carbide with 31% volume fraction varied between 28-54%, at high stresses the deviation of strains is more when compared with the experimental results obtained by the work of Myriounis et al. [9], which is mainly due to the more energy required to overcome the particulate shearing when new surfaces are formed and dislocation pile up occurs at the particles interface as shown in figure 32.



Figure 32: Particulate Shearing, forming new surfaces.

Heat treatment considerably improved the fracture toughness of the composites. In particular, the specimens simulated under the T6 condition exhibited enhanced fracture toughness compared to the other two conditions. This behaviour can be attributed to a mechanism related to alterations in the microstructure at the vicinity of the interface induced by the heat treatment. This mechanism was associated with precipitates accumulated at the interfacial region resulting in material hardening.

As it can be clearly seen in figures 28, 29 and 30, the HT1 heat treatment has improved both the strength and strain to failure in comparison with the untreated composites for both volume fractions. Furthermore, the failure strain for this temper is considerably higher than the one for the T6 heat treatment; this may be attributed to the annealing which acts competitively to the precipitation leading to the toughening of the composite. However, the T6 heat treatment exhibits the highest strength followed by the HT1 and the T1 state. Finally, as it was expected, the T1 composites behaviour in tension deteriorates with increasing filler concentration.

## **CHAPTER 6**

### **Simulating Linear Response of SiC Reinforced Aluminium Alloy (VAMUCH)**

#### **Summary**

The complexity of composite analysis requires the use of an accurate model for calculating the properties of various composite patterns. Confidence in the model requires analytical studies that are comparable to accepted published results [136]. The mechanical properties of MMCs are the main characteristic which drives its uses in many fields as the properties of MMCs can be tailored by selecting the matrix and reinforcements for a specific application. Like, it is possible to specify coefficient of expansion in one direction and strength and stiffness in another, and so forth. This is not possible with monolithic materials as they tend to be isotropic.

Particulate-reinforced MMCs, tend to be isotropic as monolithic metals. The brittle reinforcements and metal oxides present in such composites reduce their overall ductility and fracture toughness, whereas the modulus and strength of metal matrices are significant when compared to the reinforcing agents.

In this section of the study an attempt has been made to simulate a hard particulate reinforced Al alloy system using, Variational Asymptotical Method for Unit Cell Homogenization (VAMUCH) [156], which is a finite element-based code used in conjunction with ANSYS to homogenize anisotropic and heterogeneous material properties, using a unit cell approach [157]. VAMUCH works by calculating the effective material properties of the whole composite first and then recovers the

localized field based on the macroscopic analysis of the effective medium [158]. The results indicate an increasing trend of hardness and impact strength with increase in percentage of SiC. Since the linear part of the stress strain data forms the basis of maximum design load for structural data, the linear part of the stress strain curve has been studied in depth and verifications of the results have been made on three different heat treated Al-SiC metal matrix composites, using 20% and 31% volume fraction of SiC in Al.

### **6.1 VAMUCH Simulation of Al/SiC**

In this study simulations are based on a unit cell. A unit cell is the simplest repeating unit consisting of all the constituents of the composite in a crystal. Each unit cell is defined in terms of lattice points which are points in space about which the particles are free to vibrate in a crystal.

A cubic unit cell with 8 nodes on its corners has been chosen for this study described in section 4.2.1 and as shown in figure 7, showing the Schematic of the model Unit cell showing where the forces were acting and the fixed supports. The material properties used for our simulations are listed in table 1. The experimental results which are compared are taken from the work of Myriounis et al [9].

To date no attempt has been made, to introduce total volume fraction of the reinforcement into strength predictions rather than area of the interface. Hence, an opportunity to validate/refine the above hypothesis to model matrix-reinforcement interfaces in 3D for volume fraction calculation rather area of the interface has been attempted. Hence, more accurate predictions.

VAMUCH in ANSYS was used to simulate a unit cell of Al-SiCp with 20% and 31% volume fraction in 3D, representing a small part of the composite which has aluminium as the base material with a hard reinforcement of Silicon Carbide (SiC) in the centre. It is assumed to be in symmetry and the aspect ratio was kept 1. Loads of equivalent to 40% of the UTS of the composite were applied on the positive and negative X-axis, whereas at the perpendicular Y-axis positive and negative were acting as fixed supports as shown and explained in chapter 4, section 4.2.1, figure 7. The interface between the matrix and the reinforcement was bonded frictionless and the meshing done in a way that the meshed blocks on the interface met each other to simulate the actual bonding in an actual composite. This gives a much realistic impact in simulation of the actual composite.

The Stress / Strains were taken at 3 different heat treatments for both 20% and 31% volume fraction of Al-SiC. T1 is the as received state where the absolute temperature was 300<sup>0</sup> K, HT1 was at 800<sup>0</sup> K, and T6 at 723.9<sup>0</sup> K. The experimental data is listed in table 4, and the plotted experimental results can be seen in figure 33.

## 6.2 Inputs to VAMUCH code

Firstly the length of side of the cubic unit cell was calculated with respect to the volume fraction of silicon carbide present in the composite. The diameter was considered to be 17 microns and the lengths were multiplied by 100 to enlarge the unit cell for easier analysis and the final lengths were,

$$L_{20\% \text{ vol frac}} = 2.343\text{mm}$$

$$L_{31\% \text{ vol frac}} = 2.025\text{mm}$$

The experimental results which were compared with the VAMUCH simulation results were taken from the work of Myriounous [9]. The experimental stress/strain results were averaged out using,

$$\bar{\sigma} = E_{eff} * \overline{\varepsilon_{xy}} \quad (40)$$

Where,  $E_{eff}$  is the effective properties of the composite.

For the effective properties of the composite the input in VAMUCH was as follows,

$$\begin{array}{|c|c|c|} \hline u & v & w \\ \hline \varepsilon_{11} & \varepsilon_{12} & \varepsilon_{13} \\ \varepsilon_{21} & \varepsilon_{22} & \varepsilon_{23} \\ \varepsilon_{31} & \varepsilon_{32} & \varepsilon_{33} \\ \hline \end{array} \quad (41)$$

where,

$\varepsilon_{11}$  = strain value

The non-diagonal  $\varepsilon$  values i.e.  $\varepsilon_{12}, \varepsilon_{13}, \varepsilon_{23}, \varepsilon_{21}, \varepsilon_{31}$  &  $\varepsilon_{32}$  are kept zero which are representing shear strain.

$$\varepsilon_{11} = \frac{u}{l_0} \quad (42)$$

This implies,

$$u = \varepsilon_{11} * l_0 \quad (43)$$

Where,  $l_0$  is the length of the cube according to the volume fraction of silicon carbide.

The effective properties for Aluminium silicon carbide with 20% and 31% volume fraction of silicon carbide are listed in table 5 for three different heat treatments at as received condition T1, HT1 and T6.  $\nu_{12}$  values as listed in table 6 were taken from VAMUCH.

Volume Fraction	T1 (GPa)	HT1 (GPa)	T6 (GPa)
20%	101.17457	101.17819	101.19441
31%	127.07547	127.08229	127.10142

Table 6: Values of E1 for different heat treatments for different volume fractions from VAMUCH

Volume Fraction	T1	HT1	T6
20%	0.30054405	0.30054281	0.30053725
31%	0.27699202	0.2769896	0.27698284

Table 7: Values of  $\nu_{12}$  for different heat treatments for different volume fractions from VAMUCH

$$\text{Now, } \nu_{12} = \frac{-\varepsilon_{22}}{\varepsilon_{11}} \quad (44)$$

$$\varepsilon_{22} = -\nu_{12} * \varepsilon_{11} \quad (45)$$

Since the unit cell is in symmetry as it is a cube,  $\varepsilon_{22} = \varepsilon_{33}$ ,

Hence,

$$\varepsilon_{33} = -\nu_{12} * \varepsilon_{11} \quad (46)$$

$$\text{Now since } \Delta w = w_o = -\nu_{12} \varepsilon_{11} l_o \quad (47)$$

Putting the value of  $\varepsilon_{33}$  from Eq. 46 in Eq. 47, implies,

$$\varepsilon_{33} = \frac{\Delta w}{l_o} \quad (48)$$

Which implies,

$$\Delta w = \varepsilon_{33} * l_o \quad (49)$$

and,

$$v_{13} = \frac{-\varepsilon_{33}}{\varepsilon_{11}} \quad (50)$$

$$\varepsilon_{33} = -v_{13} * \varepsilon_{11} = -v_{12} * \varepsilon_{11} \quad (51)$$

$$\Delta w = w = -v_{12} * \varepsilon_{11} * l_o \quad (52)$$

The value of 'u' remains same as that expressed in Eq.43, for each case of different volume fraction of silicon carbide.

$$-\varepsilon_{22} = \frac{v}{l_o}$$

$$v = -\varepsilon_{22} * l_o \quad (53)$$

Since,

$$v_{12} = \frac{-\varepsilon_{22}}{\varepsilon_{11}} \quad (54)$$

$$v = -v_{12} * \varepsilon_{11} * l_o \quad (55)$$

$$\text{Hence, } v = w \quad (56)$$

Also,  $\varepsilon_{22} = \varepsilon_{33}$  as  $v_{12} = v_{13}$  from the effective properties, as the unit cell that was considered was a cube and is symmetrical.

### 6.3 VAMUCH Outputs

The stress / strain values plotted with the results from VAMUCH for the heat treatments T1, T6 and HT1 are given in table 8, the values from VAMUCH are engineering stresses and strains which have been normalized to engineering stress/strain values to compare the experimental results to plot against the experimental values to see the difference. The lengths of the unit cell because of the constraints of ANSYS were set to 100% increase due to the small size meshing was giving infinitesimal small error and hence the difference between the experimental and simulated values on average were recorded to be around 1.6% difference. This difference can be attributed to a number of reasons like work hardening while manufacturing the composite under heat treatments which was not incorporated in the simulated results, in which case the experimental strains are lower than the simulated strains. At present in literature heat treatment improves the fracture properties of the composite and this is related to a precipitation hardening mechanism caused by the accumulation of precipitates at the interfacial region.

The engineering stress/strain values were converted to true stress/strain by first getting the effective properties from VAMUCH and then multiplying the effective strain with the effective properties of the composite to get the stress at that particular point, this was in Pascals and then converting it to MPa (T1 (N), T6 (N) and HT1 (N)) to plot the stress / strain curves.

The results obtained from VAMUCH were plotted for every different heat treatment with 20 and 31 percent of silicon carbide individually and can be shown in the graphs in figure 34 to figure 39; the experimental values which were compared are given in

table 8. Figure 27 has a red marking which shows the linear region which is being studied.

Strain	VAMUCH RESULTS (STRESSES MPa)			NORMALISED STRESSES (MPa)		
	T1	HT1	T6	T1 (N)	HT1 (N)	T6 (N)
-						
0.000313	31.61705	31.6181	31.62325	31.61705	39.71322	31.62325
0.000625	63.23411	63.23636	63.2465	63.23411	79.42643	63.24651
0.00125	126.4682	126.4727	126.493	126.4682	158.8529	126.493
0.001875	-	-	189.7	189.7023	238.2793	189.7395
0.0025	252.9364	252.9455	252.986	252.9364	317.7057	252.986
0.00375	-	-	379.4	379.4046	476.5586	379.479
0.005	-	-	505.872	505.8729	635.4115	505.9721
0.0075	-	-	758.8	758.8093	953.1172	758.9581

Table 8: VAMUCH values to be plotted

Strain	STRESSES (MPa)					
	T1-20	T1-31	HT1-20	HT1-31	T6-20	T6-31
-						
0.000156	6.25	6.25	6.25	6.25	6.25	6.25
0.000313	23	23	23	23	23	23
0.000625	40	40	40	40	40	40
0.000938	62.5	62.5	62.5	62.5	62.5	62.5
0.00125	87.5	87.5	87.5	87.5	87.5	87.5
0.001563	100	100	100	100	112.5	112.5
0.001875	110	110	112	112	135	135
0.002188	125	120	125	120	162.5	162.5
0.0025	131.25	125	131.25	128.125	181.25	181.25
0.00375	150	140	150	143.75	252	252
0.004844	155	148	157	151	285	280
0.005	157	151	159	153	290	285
0.0068	160	157	166	163	320	310
0.0072	160.5	158	167	165	314	313
0.0075	161	159	168.75	166	330	320
0.01	163	165	-	174	348	331
0.0125	163	-	-	180	350	-
0.015	160	-	-	182	352	-
0.0175	-	-	-	184	353	-
0.02	-	-	-	185	351	-

Table 9: Experimental results for stress / stains for Al SiC for 20% and 31 % vol fraction at temperatures T1, HT1 and T6.

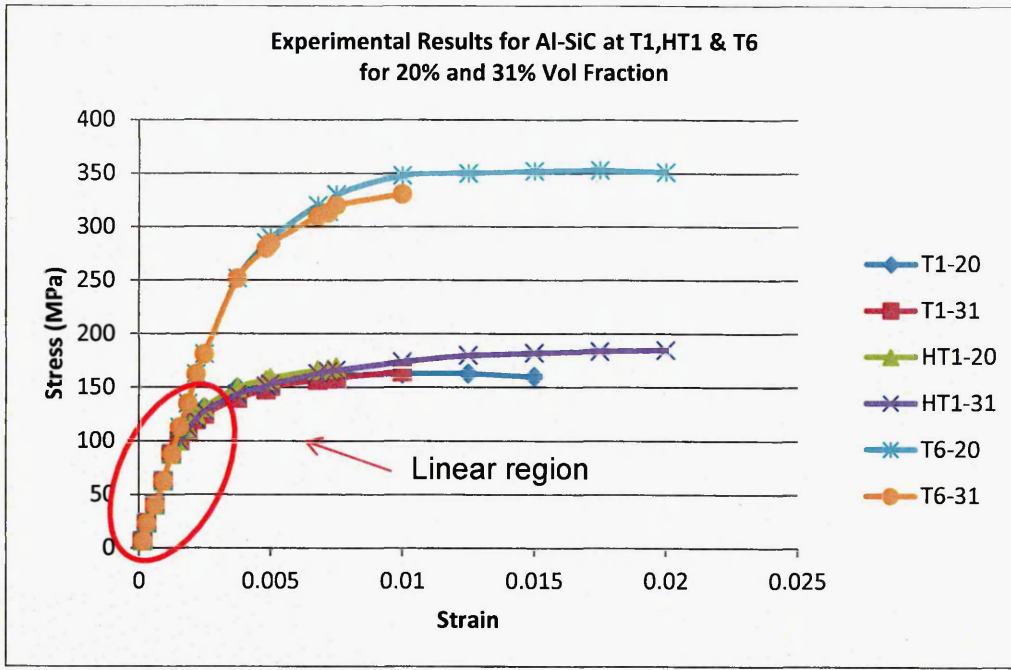


Figure 33: Experimental results plotted for stress / strains for Al SiC for 20% and 31 % vol fraction at temperatures T1, HT1 and T6 [9].

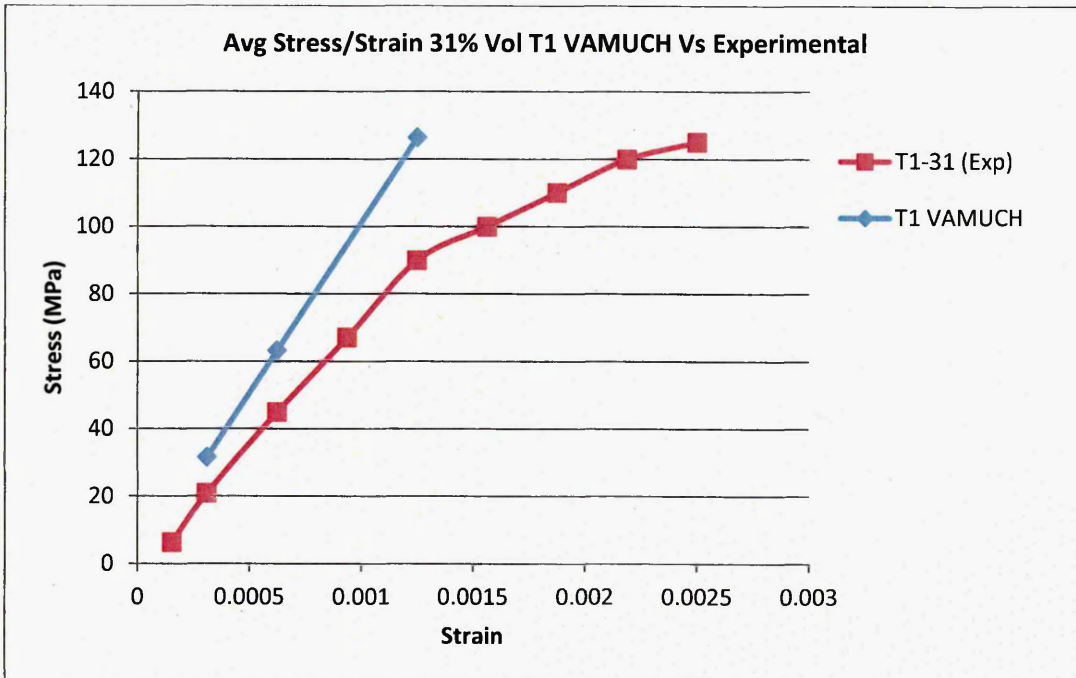


Figure 34: Comparison of Exp (section of fig 27) and VAMUCH linear results for Al/SiC 31% at T1

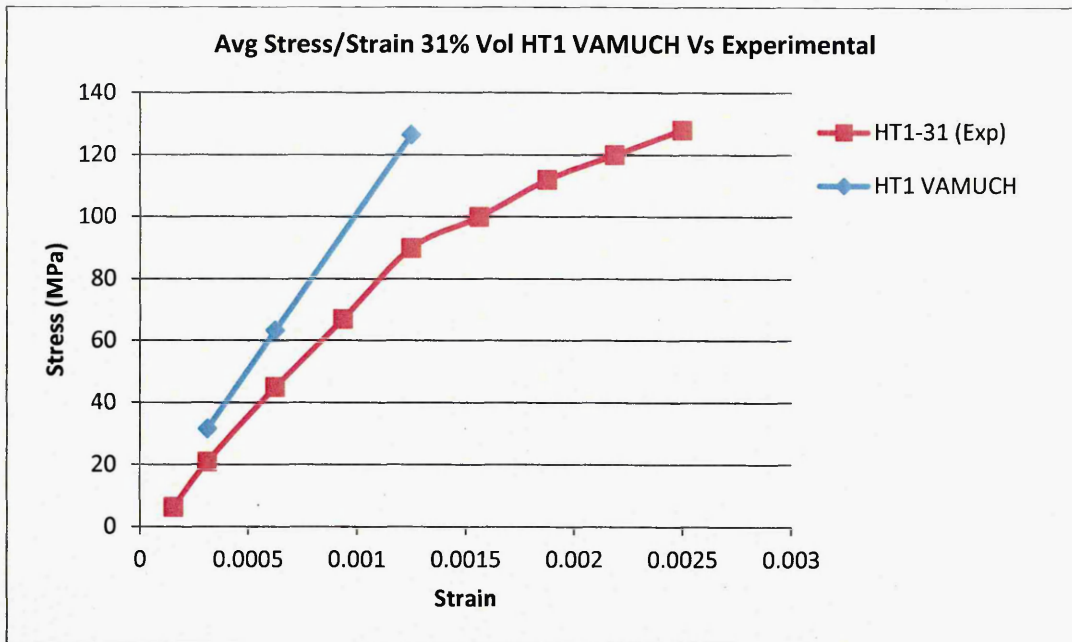


Figure 35: Comparison of Exp (section of fig 27) and VAMUCH linear results for Al/SiC 31% at HT1

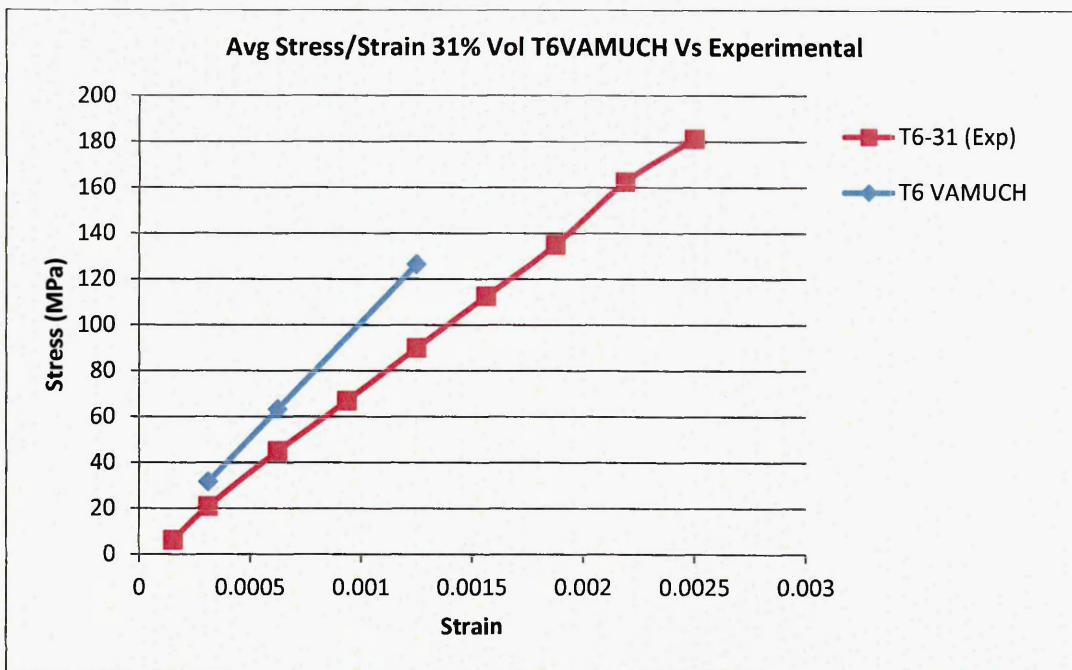


Figure 36: Comparison of Exp (section of fig 27) and VAMUCH linear results for Al/SiC 31% at T6

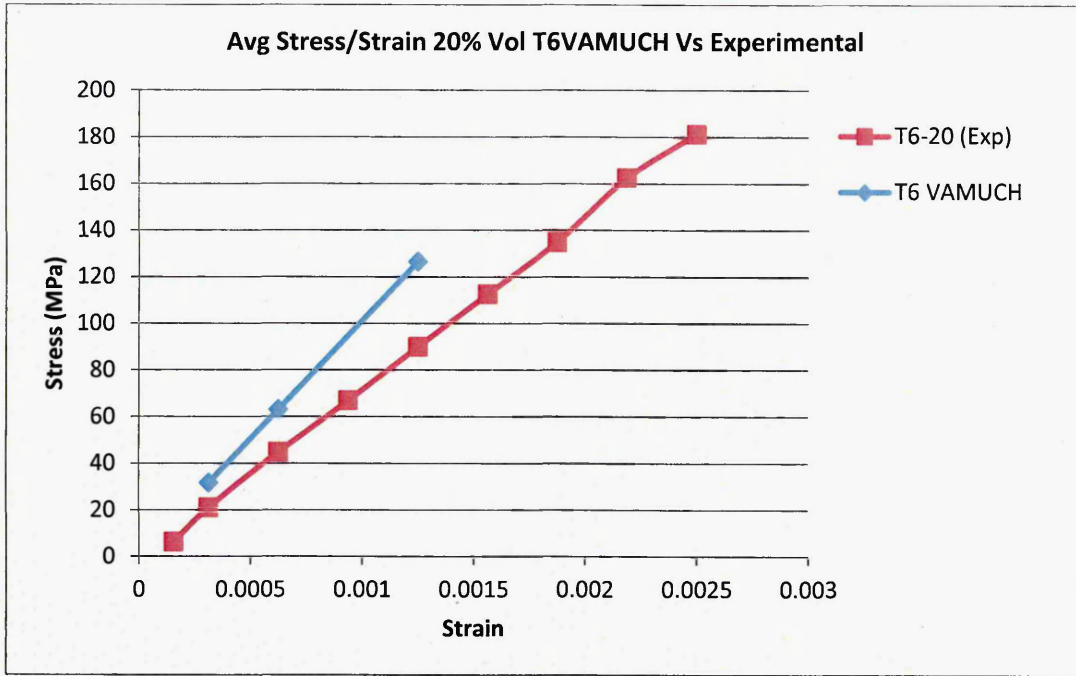


Figure 37: Comparison of Exp (section of fig 27) and VAMUCH linear results for Al/SiC 20% at T6

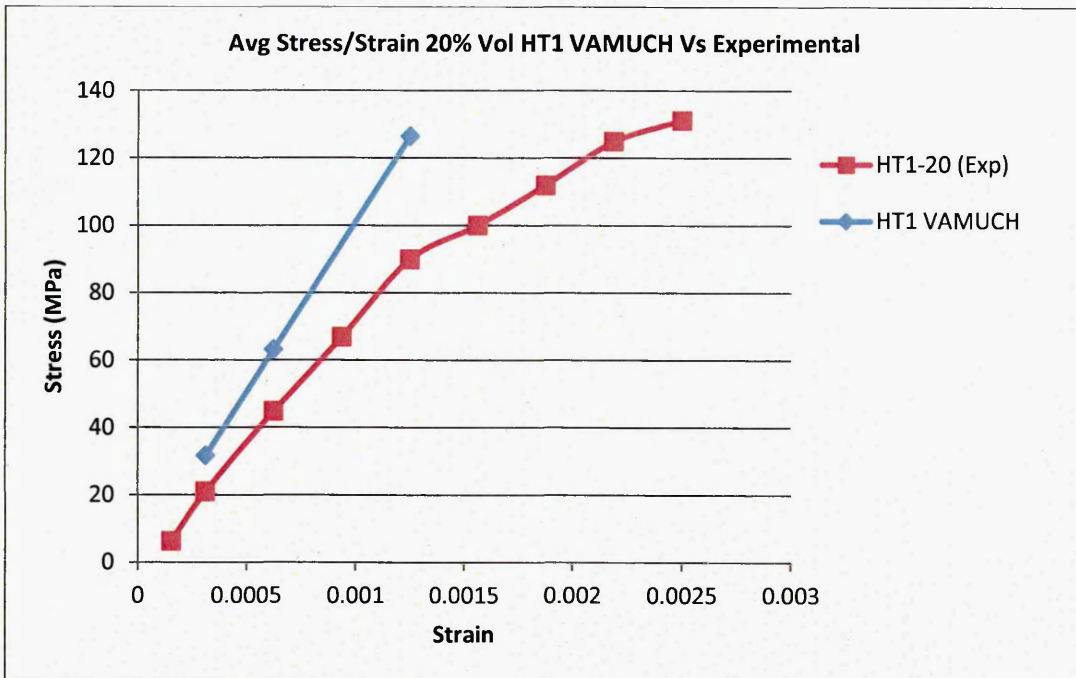


Figure 38: Comparison of Exp (section of fig 27) and VAMUCH linear results for Al/SiC 20% at HT1

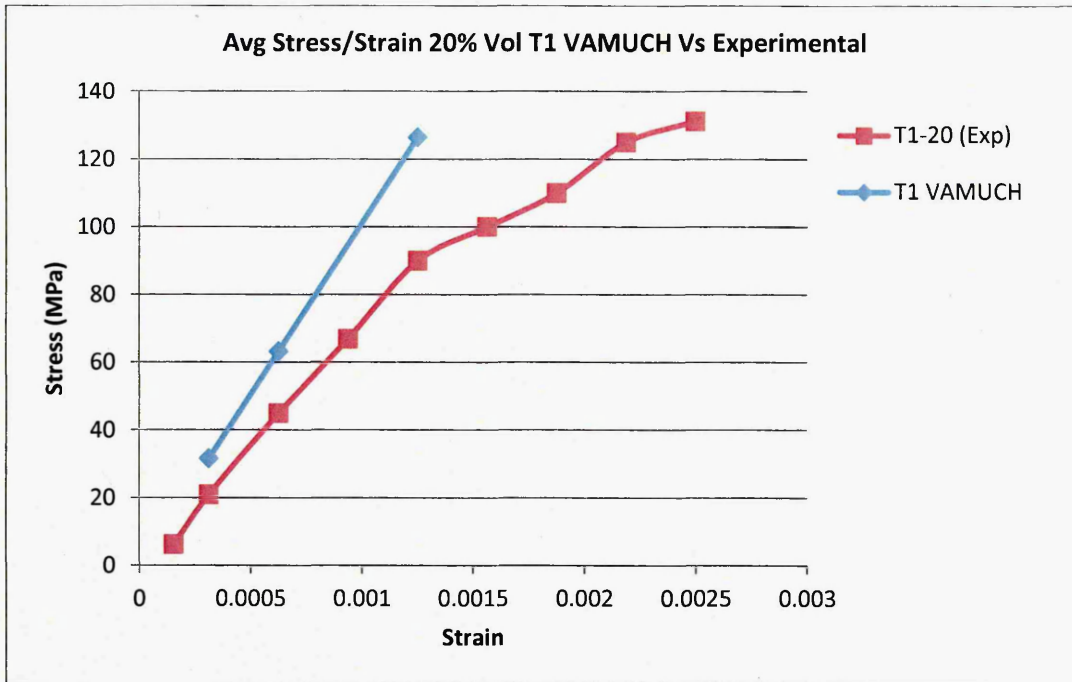


Figure 39: Comparison of Exp (section of fig 27) and VAMUCH linear results for Al/SiC 20% at T1

The experiments by Myriouns [9] showed a very interesting fact that the increasing percentage of the reinforcement i.e. silicon carbide led to a change in the yield and the ultimate tensile strengths of the aluminium silicon carbide composites. As the percentage of silicon carbide was increased from 20% to 31% stress concentrations were created in the composite and thus the ductility of aluminium was reduced due to the induced embrittlement, thus reducing the failure strain of the composite.

#### 6.4 Predictions and Correlations

The strain levels are plotted as shown in figure 40 and figure 41 for correlation from the data given in table 8 and table 9, of which individual comparison graphs are plotted in figure 34-39, from Variational Asymptotical Method for Unit Cell Homogenization and compared with the experimental results.

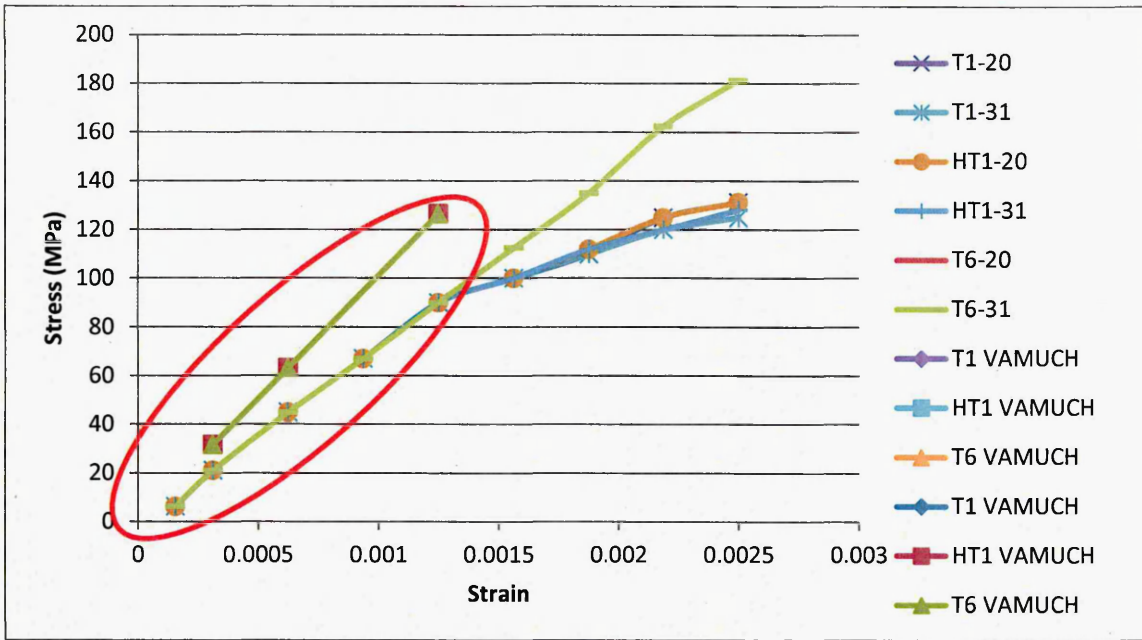


Figure 40: Experimental results and VAMUCH results plotted for stress / strains for Al SiC for 20% and 31 % vol fraction at temperatures T1, HT1 and T6 along with the T6

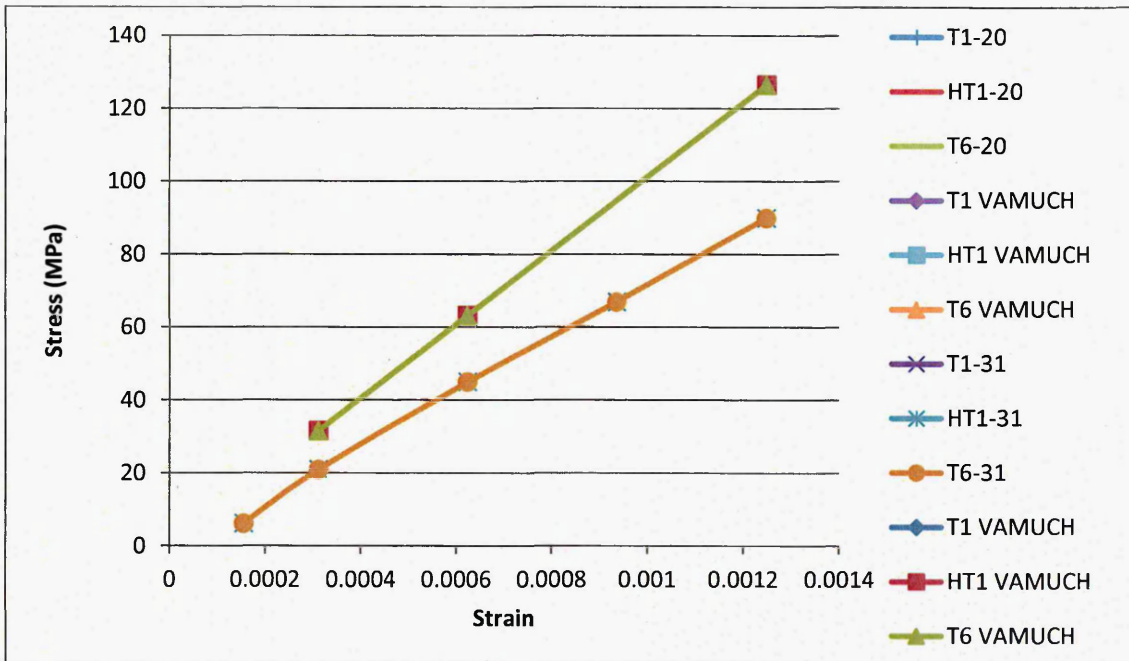


Figure 41: Linear section (section marked red in fig 34) of the experimental results and VAMUCH results plotted for stress / strains for Al SiC for 20% and 31 % vol fraction at temperatures T1, HT1 and T6.

According to the proposed hypothesis above the values were also calculated and the difference was about 2% from the experimental values.

In this study the numerical results were compared with the empirical results and as shown in figure 40 and figure 41, interfacial stresses and interfacial strains of Al/SiC composite unit cell were plotted at 0° of the applied load from the unit cell approach versus the numerical data, it can be observed that for the initial loads up to 75MPa of load the correlation is very good and both the results are in harmony. As the stress goes higher than 110 MPa the strain increases and the gap between the values for the empirical and simulated data become constant. The deviation on average is about 1.5-3% between the two results which is due to the interfacial segregation and precipitation; it can also be concluded that if more data sets are plotted of the empirical data the trend line would match that of the simulated data.

## **6.5 Conclusions**

In this study a hard particulate reinforced Al alloy system was simulated and a numerical model proposed using finite element method, to predict the interfacial strain values of aluminium, in the presence of silicon. This model reflects the interfacial energy at the matrix-reinforcement interface caused by segregation and precipitation of impurities to forecast the formation of energies by taking into account the Griffith's crack type arguments. VAMUCH in ANSYS was also used to verify the experimental results which were then verified by the numerical model proposed. This model can also be found useful to predict the trends in relation to the interfacial fracture strength of a particulate reinforced aluminium alloy system. The numerical

model proposed made good predictions in relation to the interfacial stress / strain behaviour in aluminium silicon carbide metal matrix composites.

The simulations showed that for the same range of conditions tested, the yield and the ultimate tensile strengths of the SiC<sub>p</sub>/Al composites were mainly controlled by the percentage of reinforcement as well as by the intrinsic yield/tensile strengths of the matrix alloys. The addition of the SiC<sub>p</sub> reinforcement created stress concentrations in the composite, and thus the aluminium alloy could not achieve its ductility due to the induced embrittlement. As a result, it was seen that with the increasing reinforcement content, the failure strain of the composites was reduced and that the heat treated composites clearly have improved fracture properties. This can be related to a precipitation hardening mechanism caused by the accumulation of precipitates at the interfacial region.

## **CHAPTER 7**

### **Modelling Non-Linear Response of SiC Reinforced Aluminum Alloy**

#### **SUMMARY**

This chapter reports a finite element study of non-linear response effect of load on silicon carbide (SiC) reinforced aluminium alloys interfacial stress/strain characteristics. The non-linear behaviour of the composite is simulated by using ANSYS finite element package, using a unit cell model and applying appropriate boundary conditions. An attempt is made to study the influence of different volume fractions of the reinforcement on the stress transfer from matrix to particle analysis, it is found that the volume fraction of the particulate plays an important role in the ductility and overall fracture toughness of the composite, also the results show that de-bonding is more pronounced in the interfacial element near the axis of symmetry.

#### **7.1 Introduction**

MMCs exhibits plasticity and damage due to their microstructural heterogeneity under mechanical loading, whereas its plasticity is related to metal matrix behaviour, the damage mechanism is generally due to particle breaking and interfacial de-bonding between the matrix and the particle. To achieve good mechanical properties for processing structural materials from MMCs it is vital to have good bonding between metallic matrices and ceramic reinforcements.

To a large extent the performance of the composite is controlled by the stability of the interface between the matrix and the particulate, and this interface is

fundamentally important in determining the mechanical properties of MMCs as it controls the stress transfer between the matrix and the particulate.

It is known qualitatively the poor matrix-particle adhesion produces composite materials with poor properties. Numerical analysis illustrated that matrix-particle adhesion has a strong effect on the composites transverse properties which only change slightly. Generally composite materials with weak interfaces have relatively low strength, whereas materials with strong interfaces have high strength and stiffness but are somewhat brittle [159].

A number of theoretical and numerical modelling has been done on MMCs along with experimental investigations. Macroscopic properties of the composites are determined by the experimental observations; however, the inclusion of an interface region in to these analyses has been neglected in many cases.

The objective of the present work is to understand the non-linear response of SiC reinforced Al alloy system, focusing on the interface behaviour of metal matrix composite during the tensile loading with the effect of different volume fraction of reinforcements.

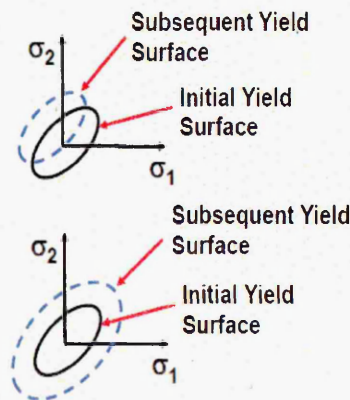


Figure 42: (A) Kinematic Hardening (B) Isotropic Hardening [162]

The different existing kinematic hardening models, along with their advantages and shortcomings are described below. Basically the hardening rule describes how the yield surface changes (size, centre and shape) as the result of plastic deformation. It determines when the material will yield again if the loading is continued or reversed. This is in contrast to elastic-perfectly-plastic materials which exhibit no hardening i.e., the yield surface remains fixed.

There are two basic hardening rules to prescribe the modification of the yield surface, Kinematic hardening and Isotropic hardening as shown in figure 42. In Kinematic hardening the yield surface remains constant, whereas in isotropic hardening the yield surface expands subsequently and uniformly in all directions with plastic flow. Most metals exhibit kinematic hardening behaviour for small strain cyclic loading. The stress-strain behaviour for linear kinematic hardening is when subsequent yield in compression is decreased by the amount that the yield stress in tension increased, so that a  $2\sigma_y$  difference between the yields is always maintained as shown in figure 43. (Also known as Bauschinger effect). An initially isotropic material is no longer isotropic after it yields and experiences kinematic hardening. For very large strain simulations, the linear kinematic hardening model can become inappropriate because of the Bauschinger effect.

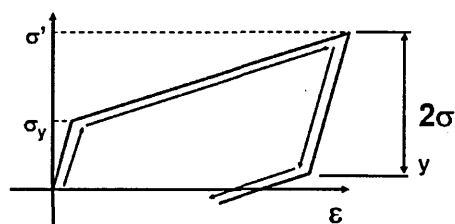


Figure 43: Bauschinger Effect [160]

Kinematic hardening is generally used for small strain, cyclic loading applications. Isotropic hardening states that the yield surface expands uniformly during plastic flow. The term isotropic refers to the uniform dilation of the yield surface and is different from an isotropic yield criterion (i.e. material orientation)

Plotting the stress-strain curve enables an understanding of what occurs during a loading and reverse loading cycle, the subsequent yield in compression is equal to the highest stress attained during the tensile phase as shown in figure 43. Isotropic hardening is often used for large strain or proportional loading simulations. It is usually not applicable for cyclic loading.

### **7.1.1 Different Hardening models**

Prager [161], describes the translation of the yield surface in his model. According to this model, the simulation of plastic response of materials is linearly related with the plastic strain.

Armstrong and Frederick [162], simulated the multiaxial Bauschinger effect (movement of the yield surface in the stress space). When compared to the previously existing models, this one predicts Bauschinger effect where intuitively one would be expected. This model also proposed some advancement in terms of simplicity for computer programs. Although the subroutine for calculating strain increments from stress were more complex than the ones for Prager Model, however, there was improvement in results and better correlation with experiments. Armstrong and Frederick model [162] was based on the assumption that the most recent part of the strain history of a material dictates the mechanical behaviour.

Wang and Ohno [163], proposed a model based on the non-linear kinematic hardening rule of Armstrong and Frederick [162]. It demonstrates the effect of two terms, temperature rate and relative translation, on two forms of non-linear kinematic hardening, multi-surface and multicomponent. The study shows that in the case of multi-surface form, the omission of the temperature rate terms leads to unstable deformation. This unstable deformation occurs due to intersection of the surfaces.

The omission of the temperature rate term results in shifting of the hysteresis loop along the stress axis in both the forms. The omission of the relative translation term has little or no influence on the two forms.

In this work, the kinematic hardening variables are decomposed into components to examine the relation for the ratcheting behaviour. Each component is assumed to have a critical state, after which its dynamic recovery is fully activated. Chaboche kinematic hardening is chosen, which was proposed by Chaboche and his co-workers [163 - 164], this model is based on a decomposition of non-linear kinematic hardening rule proposed by Armstrong and Frederick.

To improve the ratcheting prediction in the hysteresis loop, Chaboche et al. [163], initially proposed three decompositions of the kinematic hardening rule. In the same work, Chaboche [166] analysed three models to describe kinematic hardening behaviour. The first model that was studied used independent multi-yield surfaces as proposed by Mroz [165]. This model is useful in generalizing the linear kinematic hardening rule. It also enables the description of:

- The nonlinearity of stress-strain loops, under cyclically stable conditions,
- The Bauschinger effect, and

- The cyclic hardening and softening of materials with asymptotic plastic shakedown.

The shortcoming of this model is its inability to describe ratcheting under asymmetric loading conditions, but this does not affect the simulations done in this study as symmetric behaviour for the unit cell is used throughout this study, also it shows the following differences against the Mroz [167] model:

- It uses two surfaces whereas Mroz uses a large number of surfaces
- In terms of the general transition rule for the yield surface, the Mroz formulation had an advantage over this model
- This model gives a function to describe a continuous variation of the plastic models, thus enabling description of a smooth elastic-plastic transition.

In the Mroz model, the number of variables needed for the description of ratcheting is very high and for cyclic stabilized conditions no ratcheting occurs. In the two-surface model, the updating procedure to describe a smooth elastic-plastic transition and simulate ratcheting effects leads to inconsistencies under complex loading conditions.

In the case of the Dafalias and Popov [168] model, it was done by continuously varying the hardening modulus, from which the translation rule of the yield surface is deduced. It was later found that this model tends to greatly over-predict ratcheting in the case of normal monotonic and reverse cyclic conditions.

To overcome these pitfalls, Chaboche [169] introduced a fourth decomposition of the kinematic hardening rule based on a threshold. This fourth rule simulates a constant linear hardening within a threshold value and becomes nonlinear beyond this value. With the use of this fourth decomposition, the over-prediction of ratcheting is reduced and there is an improvement in the hysteresis curve. This is because, with in the threshold, the recall term is ignored and linear hardening occurs as it did without the fourth rule. Beyond the threshold the recall term makes the hardening non-linear again and reduces the ratcheting at a higher rate to avoid over-prediction.

## 7.2 Modelling of the Composite

Three dimensional elastic finite element analysis calculations are used to find the global and local stress and strain status of the MMC to focus on its non-linear behaviour.

The actual composite is normally replaced by a regularly spaced array of parallel spherical particles of reinforcement in a homogeneous matrix material of infinite dimensions. The regular inclusion array is then reduced to the smallest, fully informative, repeating segment as shown in figure 44. This repeating segment is called unit cell or representative volume element [170].

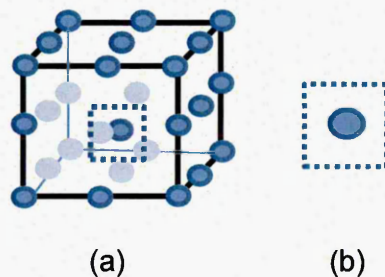


Figure 44: Unit cell model. (a) Square array arrangement of particles; (b) unit cell

For the analysis of MMCs, many researchers have suggested this unit cell concept. An assemblage of elements subsequently re-replaces this segment. The periodicity of the problem is then taken in to account by the boundary conditions prescribed to an isometric unit cell as described in section 4.2.1 and shown in figure 7. The unit cell aspect ratio is taken equal to one in this analysis and the various volume fractions of SiC are considered for the analysis. Periodical boundary conditions of the unit cell are imposed by the necessity that the unit cell has to remain straight during the deformation. The unit cell method is very much useful to analyse the effects of volume fraction, shape, particle distribution, matrix and inclusion stress/strain status and damage such as particle cracking or interface de-bonding. This method gives an accurate estimate of global mechanical properties behaviour with an indication of the micro mechanical stress/strain distributions around the particle.

### **7.2.1 Finite Element Modelling**

Finite element modelling is used in this study to generate detailed distributions of stress and strain in the unit cell (matrix, particle and the interface between them), which are essential for understanding the mechanical behaviour of the composites.

The three dimensional model of a unit cell as shown in figure 44 was created in ANSYS 14.5 for different volume fraction of SiC. Simulations were done on 5, 10, 15, 20, 25, 30, 35, 40, 45 and 50% volume fraction of SiC for the analysis. The models were created with the assumption that the SiC particles deform elastically and the matrix deforms elasto-plastically depending on the local effective stress level.

Typical damage in a unidirectional metal matrix composite includes interface de-bonding. The method used for modelling the matrix-reinforcement interface is the

spring stiffness layer method. In the spring layer model, the predefined layer is replaced by negligible thickness interface. So, interface in this case represents the border separating distinct phases such as particle and matrix. The interface between particle and matrix is assumed to be very strong and frictionless so that any stress and strain level can be transferred.

The pairs of nodes on matrix-reinforcement interface area are coupled. Under the tensile loading the node pairs will be released when the combination of normal and shear stresses at the nodes reaches a predefined criterion.

### **7.2.2 Boundary Conditions**

The boundary conditions applied to the model must accurately enforce the periodicity of the geometry and the stress/strain distributions. The model illustrated in the figure 5 is bounded by six surfaces. The nodes on the top and bottom surfaces of symmetry were constrained such that they could not move, hence, the surface remained flat and on its original plane. The nodes on the boundary surfaces were constrained only such that each node on the surface had an identical displacement in the direction normal to the surface. Therefore, no surface rotation or warping could occur [171]. These constraints force the corners of the unit cell to remain at right angles throughout the analyses.

The SiC inclusion was treated as an isotropic perfectly elastic material following the generalised Hooke's law. The material properties were based on commonly accepted values, as shown in chapter 4, section 4.2.1, Table 1. Convergence is performed during the solution processor in ANSYS, using the Newton-Raphson (N-R) method, which involves an iterative procedure, the local time scale factor was set to

4 as recommended by ANSYS for non-linear structural problems and the numbers of subsets defined are 400.

### **7.3 Methodology**

In a particulate metal matrix composite the crack can propagate in two ways as described in chapter 3, section 3.1. This propagation of the crack in turn depends upon the ductility of the interface. Simulations were done using finite element analysis and a 3d multiple particle unit cell was used in ANSYS, to look closer at the non-linearity at the interface, a code in ANSYS APDL was written incorporating the Chaboche kinematic hardening (Appendix C).

#### **7.3.1 3D Unit Cell**

A 3D unit cell was designed in ANSYS, representing a small part of the composite which has aluminium as the base material with a hard reinforcement of Silicon Carbide (SiC) in the centre. The percentage of SiC was adjustable and simulations were made on 10%, 20% and 31% of SiC in Al matrix. The aspect ratio was kept 1. Loads of 50N to 1000N equivalent to 40% of the UTS of the composite were applied on the positive and negative X-axis, whereas at the perpendicular Y-axis positive and negative were acting as fixed supports.

The interface between the matrix and the reinforcement was bonded frictionless and the meshing done in a way that the meshed blocks on the interface met each other to simulate the actual bonding in an actual composite. This gives a much realistic impact in simulation of the actual composite. The two grid patterns in figure 45 and

46 show a cross section cut from a unit cell to visually see the silicon carbide particles used in the simulation.

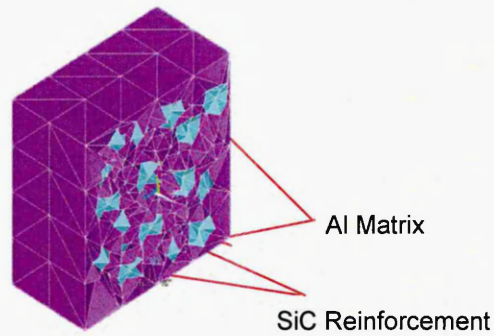


Figure 45: A cross section cut from a unit cell to visually see the silicon carbide particles

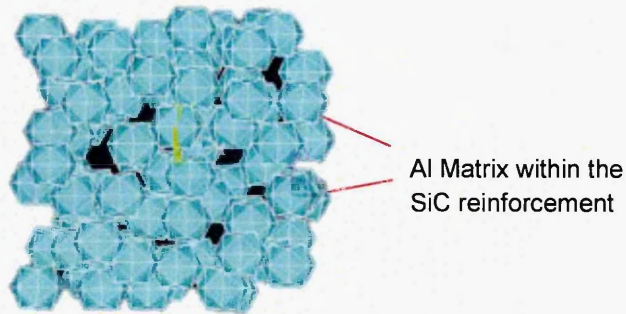


Figure 46: Silicon carbide particles in 20% volume fraction instance without the matrix block.

The problem with multiple particles was that the results were not conclusive because of the overlapping interfaces and the proximity of the particles, hence a single particle in 3D out of all the multiple particles was considered as shown in figure 47, the grid of the single particle can be seen. The simulations on the ceramic-metal interface considering Chaboche kinetic hardening model.

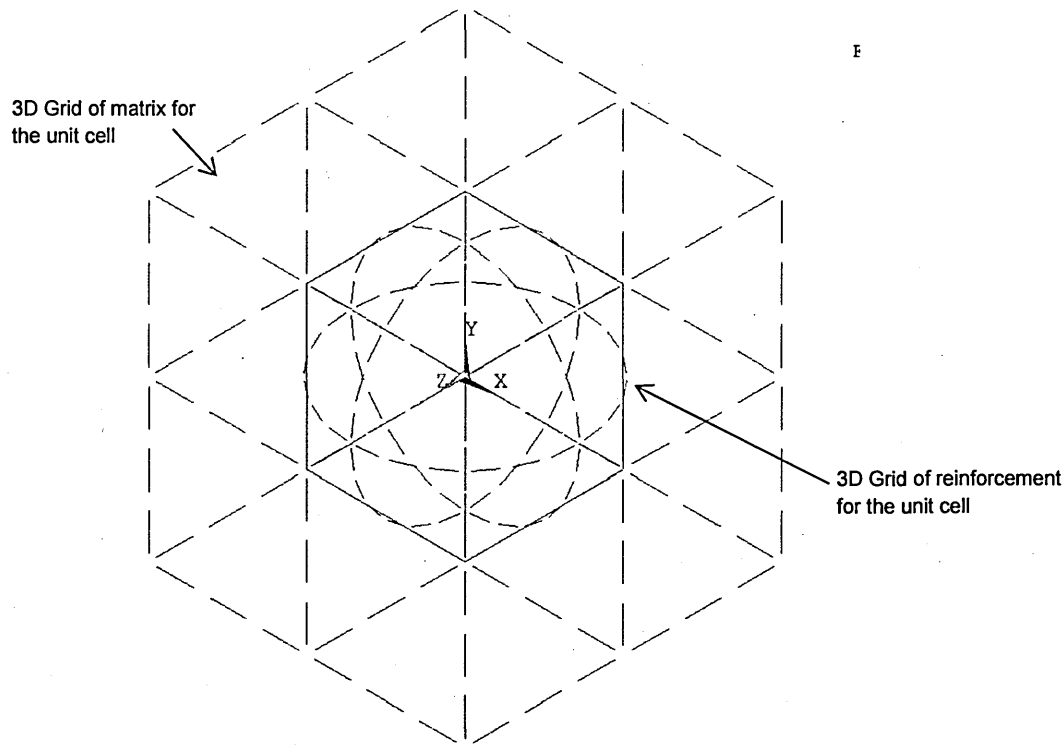


Figure 47: Grid of the single 3D unit cell showing the reinforcement and the matrix

### 7.3.2 Chaboche Kinematic Hardening Model

The hardening rule describes how the yield surface changes the size, centre and shape of the material as a result of plastic deformation; it determines when the material will yield again if the loading is continued or reversed. In this study kinematic hardening is focused as illustrated in figure 48. In kinematic hardening subsequent yield in compression is decreased by the amount that the yield stress in tension increased, so that a  $2\sigma_y$  difference between the yields is always maintained. (This is known as Baushinger effect)

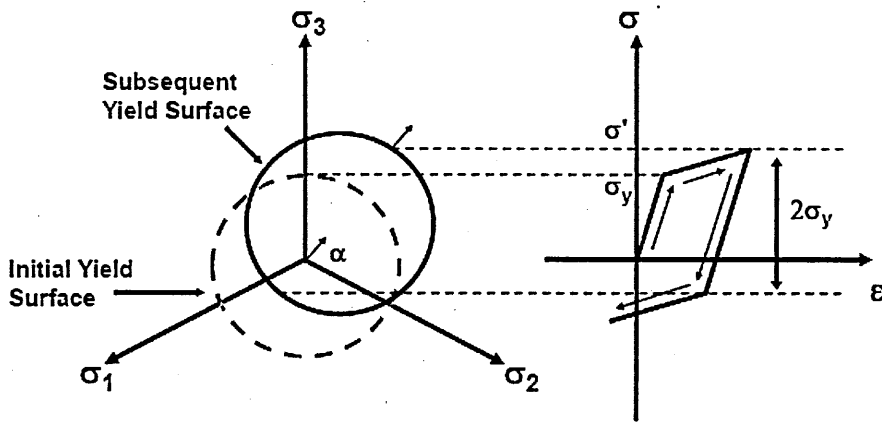


Figure 48: Stress-strain behaviour for linear kinematic hardening illustrated

An initially isotropic material is no longer isotropic after it yields and experiences kinematic hardening. For very large strain simulations, the linear kinematic hardening model can become inappropriate because of the Bauschinger effect. Hence kinematic hardening is generally used for small strain, cyclic loading applications.

In this study Chaboche non-linear kinematic hardening rule is applied to improve the ratcheting prediction in the hysteresis loop. This model is also useful in generalizing the linear kinematic hardening rule, enabling the nonlinearity of stress-strain loops, under cyclically stable conditions and the Bauschinger effect

The nonlinear kinematic hardening rule is an intermediate approach of the models that uses differential equations that govern the kinematic variables. Beyond the threshold the recall term makes the hardening non-linear again and reduces the ratcheting at a higher rate to avoid over-prediction.

Chaboche theorem [172] was incorporated which is based on a decomposition of non-linear kinematic hardening rule. This decomposition is mainly significant in better describing the three critical segments of a stable hysteresis curve which includes the

initial modulus when yielding starts, the nonlinear transition of the hysteresis curve after yielding starts until the curve becomes linear again and the linear segment of the curve in the range of higher strain.

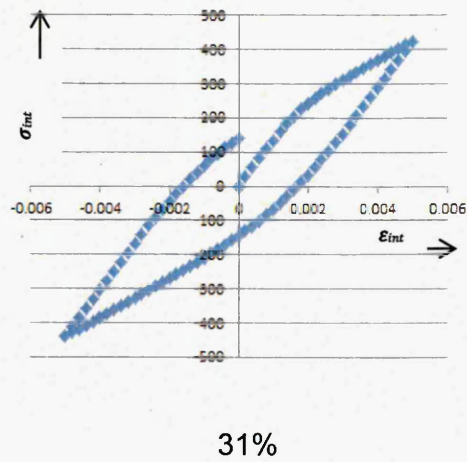
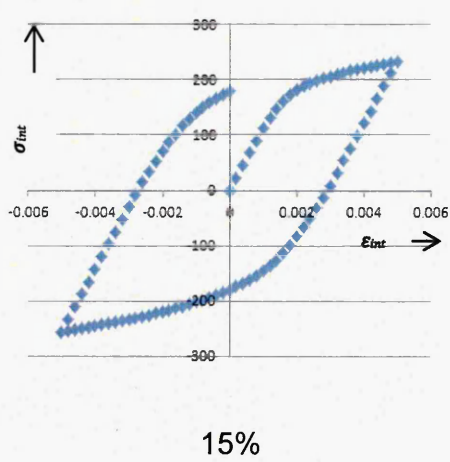
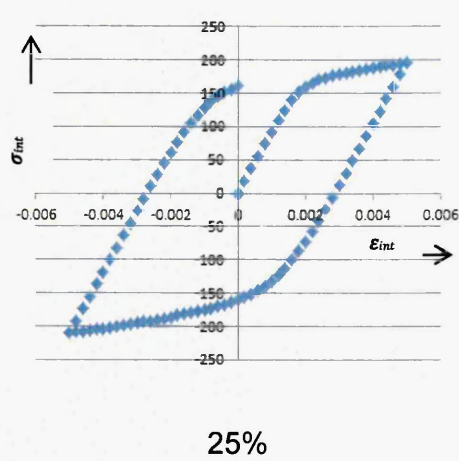
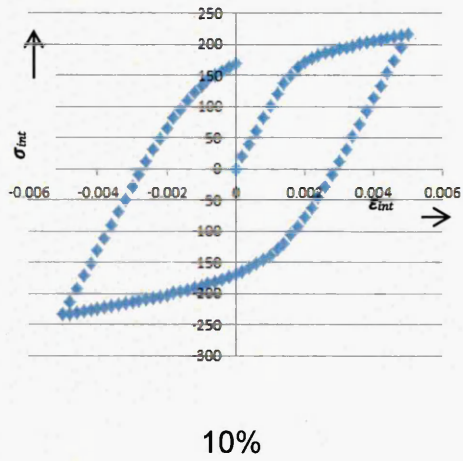
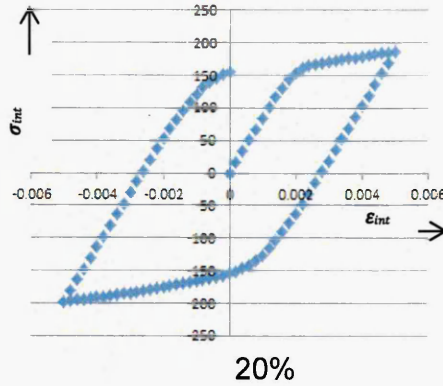
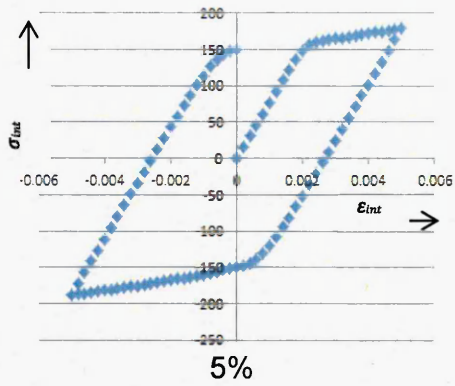
## 7.4 Results and Discussion

The effect of stress and strain history on the micro-mechanisms is likely to be of greatest importance to the segregation and precipitation phenomena and in turn on interfacial strengthening behaviour of particulate reinforced metallic alloy system. The methods of incorporating stress into the description of the segregation process are based on Rauh-Bullough theory. The tensile behaviour of the metal matrix composite is simulated in ANSYS 14.5. The Micro-mechanics model, based on thermodynamics principles developed by Myriounis and Hasan [133], is used to simulate the fracture strength  $K_{1C}$  at the interface at segregated state in MMC which is explained in chapter 3, section 3.2.2 equation 11. The interfacial characteristics of MMCs gave stress/strains close to the experimental results when loaded at  $0^\circ$  in the radial interface and interface along particle direction for tensile loading condition.

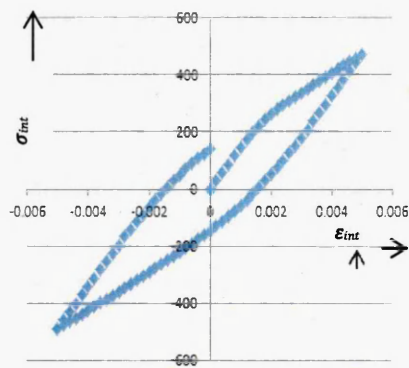
Simulations using finite element analyses were conducted using the unit cell concept as explained in detail in chapter 4, section 4.2.1. To look closer at the non-linearity at the interface, a code in ANSYS APDL was written in collaboration with Dr.Hue's team at Purdue University, USA, incorporating the Chaboche kinematic hardening (Appendix C).

An ANSYS APDL code was written to incorporate all the above mentioned scenarios and to include Chaboche kinematic hardening model to get hysteresis loops for

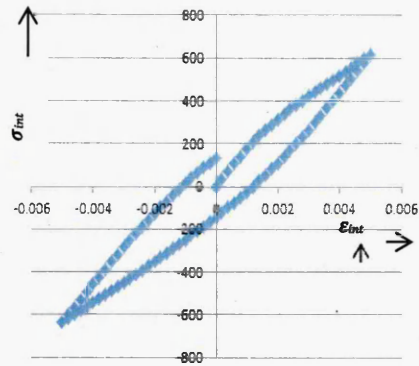
different volume fractions of silicon carbide in Aluminium matrix. The results for volume fraction from 5% to 50% with 5% increments are shown in figure 49.



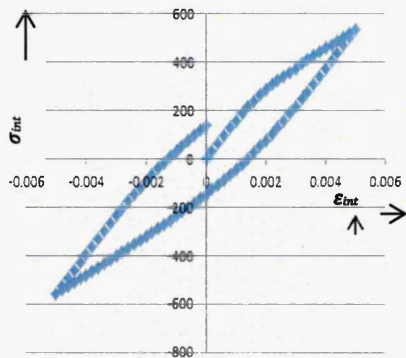
Part of Figure 49 continued on the next page



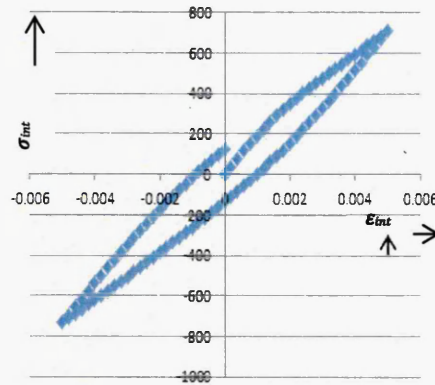
35%



45%



40%



50%

Figure 49: Hysteresis loop for 5-50% Volume fraction SiC in Al matrix (400 sub steps)

The simulations on the ceramic-metal interface considering Chaboche kinetic hardening model, for T6 heat condition at 20% and 31% volume fraction of SiC in Al produced hysteresis loops as shown in figures 50 and 51 respectively. Figure 52 is a comparison of the two different volume fraction with the same heat treatment i.e. T6. It is evident that as the volume fraction of the SiC increases the ductility of the composite decrease.

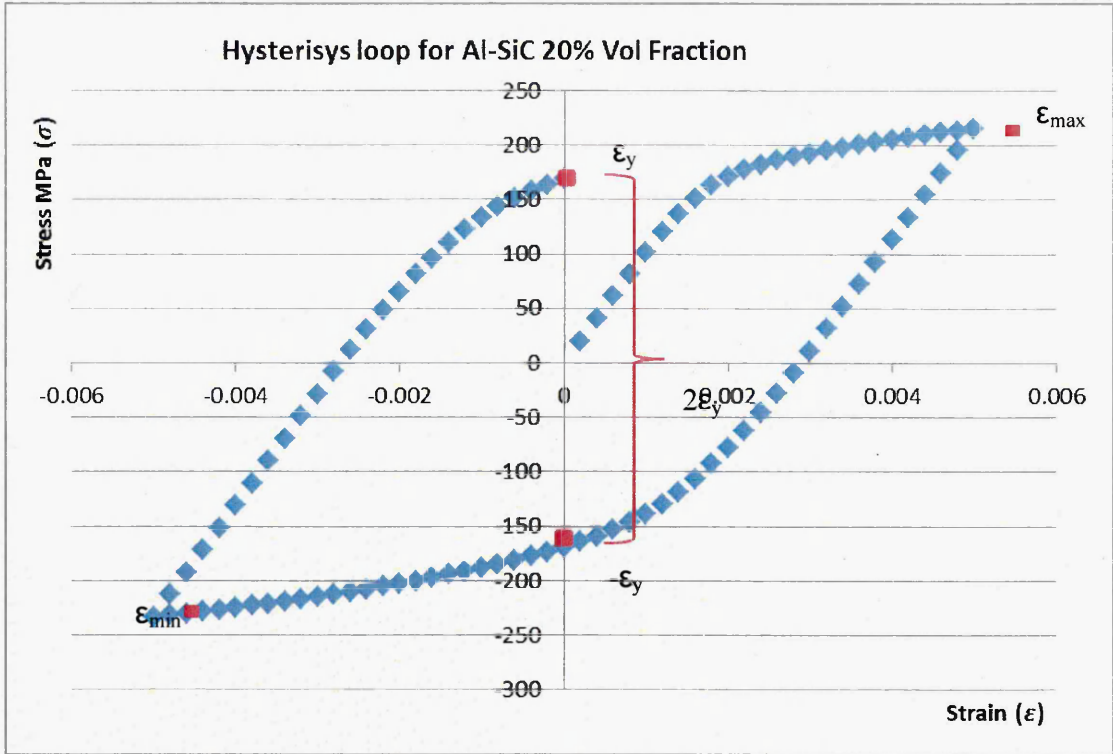


Figure 50: Hysteresis loop for Al-SiC 20% Vol Fraction

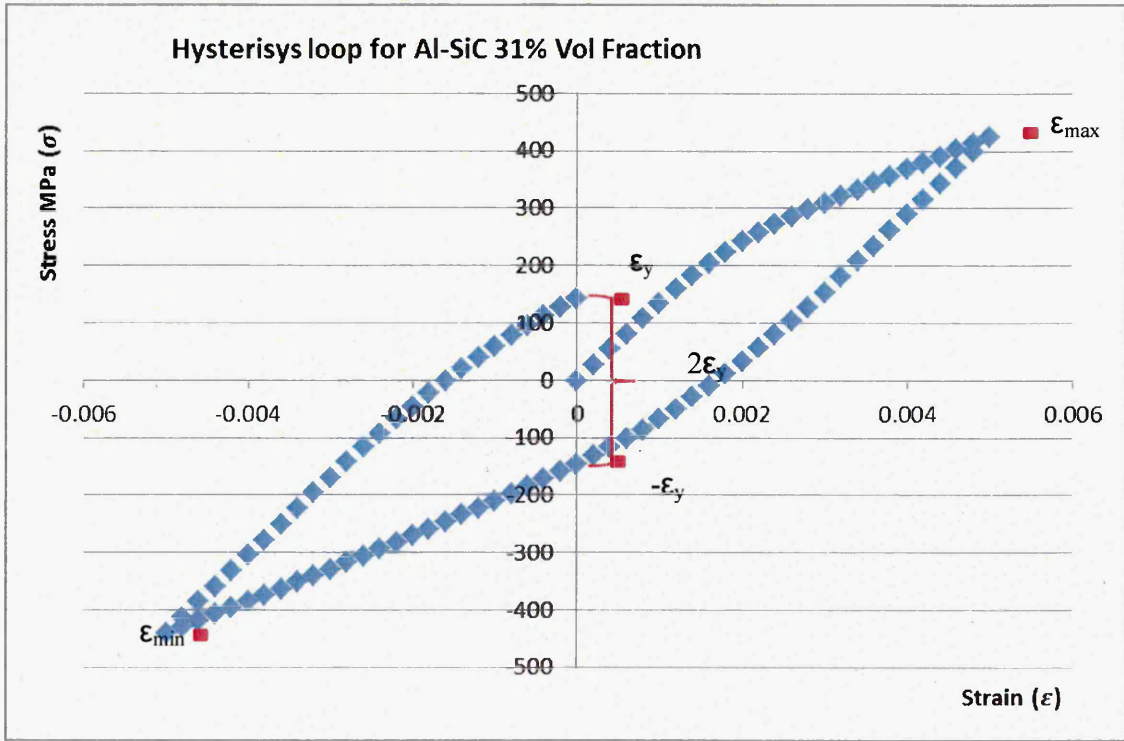


Figure 51: Hysteresis loop for Al-SiC 31% Vol Fraction

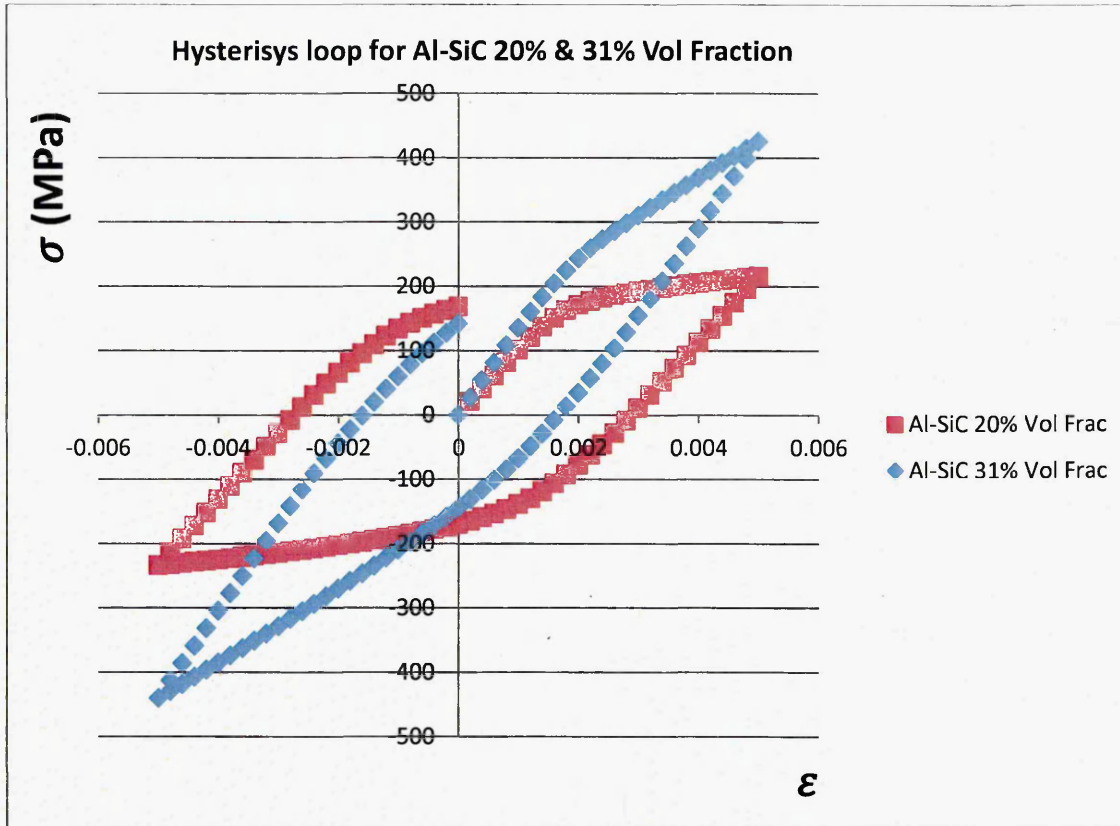


Figure 52: Hysteresis loop for Al-SiC 20% and 31% Vol Fraction

The strain rate is a concept of materials science and continuum mechanics that plays an essential role in deformable solids. It is the rate of change in strain (deformation) of a material with respect to time. The strain rate at some point within the material measures the rate at which the distances of adjacent particles of the material change with time in the neighbourhood of that point. It comprises both the rate at which the material is expanding or shrinking (expansion rate), and also the rate at which it is being deformed by progressive shearing without changing its volume (shear rate). It is zero if these distances do not change, as happens when all particles in some region are moving with the same velocity (same speed and direction) and/or rotating with the same angular velocity, as if that part of the medium were a rigid body. It is defined as given in Eq.57

$$\varepsilon(t) = \frac{L(t) - L_0}{L_0} \quad (57)$$

where  $L_0$  is the original length and  $L(t)$  its length at each time  $t$ . Then the strain rate will be,

$$\dot{\varepsilon}(t) = \frac{d\varepsilon}{dt} = \frac{d}{dt} \left( \frac{L(t) - L_0}{L_0} \right) = \frac{1}{L_0} \frac{dL}{dt}(t) = \frac{v(t)}{L_0} \quad (58)$$

Where,  $v(t)$  is the speed at which the ends are moving away from each other.

The Elastic - Plastic solution Model states,

$$\sigma = E\varepsilon \quad (59)$$

$$\sigma = k(\varepsilon)^n \quad (60)$$

The hysteresis loops in figure 50 and 51 can be identified by 5 different cases which can be given as case A to E described below.

CASE A            If  $-\varepsilon_y \leq \varepsilon_{max} \leq \varepsilon_y$   
                          &  $-\varepsilon_y \geq \varepsilon_{min} \geq \varepsilon_y$

$$\sigma_{max} = E\varepsilon_{max} \quad (61)$$

$$\sigma_{min} = E\varepsilon_{min} \quad (62)$$

CASE B            If  $\varepsilon_{max} > \varepsilon_y$   
                          &  $(\varepsilon_{max} - \varepsilon_{min}) \leq 2\varepsilon_y$

$$\sigma_{max} = k(\varepsilon_{max})^n \quad (63)$$

$$\sigma_{min} = \sigma_{max} - E(\varepsilon_{max} - \varepsilon_{min}) \quad (64)$$

CASE C            If  $\varepsilon_{min} > \varepsilon_y$   
                       &  $(\varepsilon_{max} - \varepsilon_{min}) > 2\varepsilon_y$

$$\sigma_{max} = k(\varepsilon_{max})^n \quad (65)$$

$$\sigma_{min} = \sigma_{max} - 2k\left(\frac{\varepsilon_{max} - \varepsilon_{min}}{2}\right)^n \quad (66)$$

CASE D            If  $\varepsilon_{max} < -\varepsilon_y$   
                       &  $(\varepsilon_{min} - \varepsilon_{max}) \leq 2\varepsilon_y$

$$\sigma_{max} = -k(-\varepsilon_{max})^n \quad (67)$$

$$\sigma_{min} = \sigma_{max} + E(\varepsilon_{min} - \varepsilon_{max}) \quad (68)$$

CASE E            If  $\varepsilon_{max} < -\varepsilon_y$   
                       &  $(\varepsilon_{min} - \varepsilon_{max}) > 2\varepsilon_y$

$$\sigma_{max} = -k(-\varepsilon_{max})^n \quad (69)$$

$$\sigma_{min} = \sigma_{max} + 2k\left(\frac{\varepsilon_{min} - \varepsilon_{max}}{2}\right)^n \quad (70)$$

In this work, the kinematic hardening variables are breakdown into components to examine the relation for the ratcheting behaviour. Each component is assumed to have a critical state, after which its dynamic recovery is fully activated.

The grid patterns in figure 52 do show the differences in ductility but the differences are very small and hard to distinguish especially with a 5% step size. The graph in figure 53 shows the same stress and strain for all the percentages of volume fractions under study (5 - 50%), in a different manner to show the differences visually.

From the grid patterns in figure 49 it can be observed that the volume percentage of the reinforcement (SiC) for the same level of strain change, much higher levels of stresses can be endured, also the ductility of the material keeps on decreasing as the volume percentage of the SiC is increased.

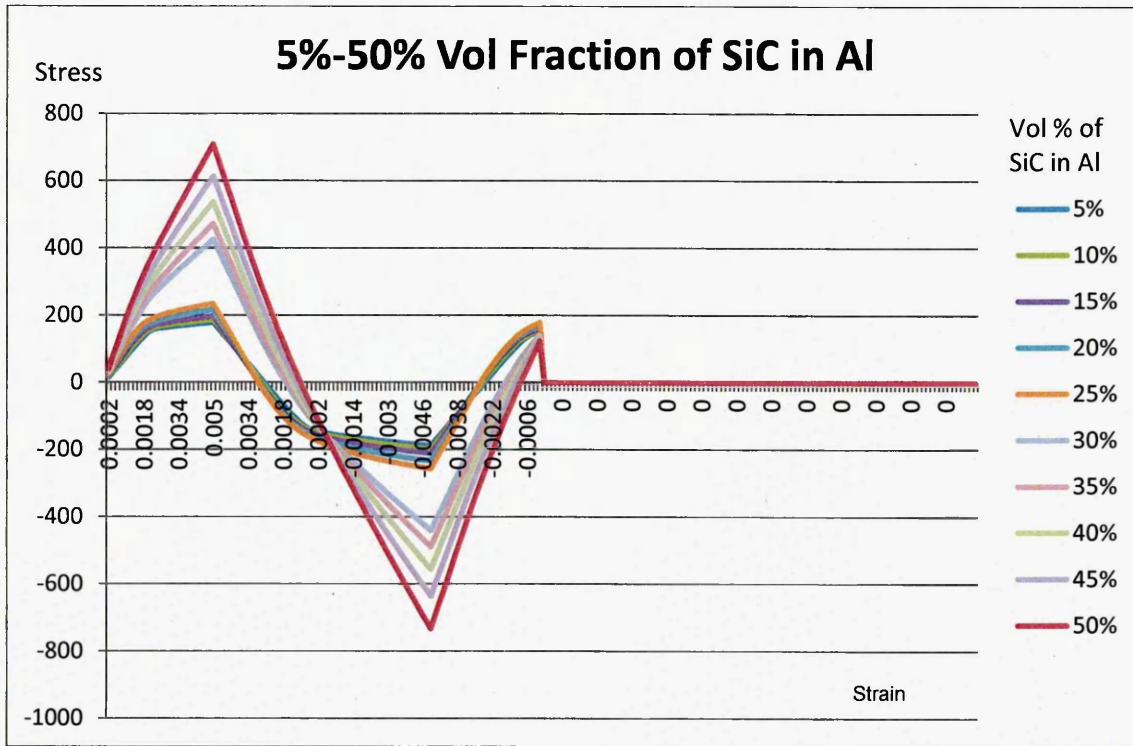


Figure 53: Hysteresis loop defining the ductility differences for 5-50% volume fraction SiC in Al Matrix. (Each result consisting of 400 subsets per one cycle)

## 7.5 Conclusions

This research applies the numerical simulation of hard particulate reinforced Al alloy system using ANSYS. The stress-strain history is predicted at micro-level and fracture toughness behaviour correlated with numerical simulation. Taking advantages of finite element analysis, the current study analysed interface characteristics of Al/SiC metal matrix composites with varying volume fractions of reinforcement from 5% to 50%.

The grid patterns in figure 52 do show the differences in ductility but the differences are very small and hard to distinguish especially with a 5% step size. The graph in figure 53 shows the same stress and strain for all the percentages of volume fractions under study (5 - 50%), in a different manner to show the differences visually. It can be observed from the graph in figure 46 that the volume percentage of the reinforcement (SiC) for the same level of strain change, much higher levels of stresses can be endured, also the ductility of the material keeps on decreasing as the volume percentage of the SiC is increased.

In this work, the kinematic hardening variables are decomposed into components to examine the relation for the ratcheting behaviour. Each component is assumed to have a critical state, after which its dynamic recovery is fully activated.

Plotting the stress-strain curve enables to understand of what occurs during a loading and reverse loading cycle. The subsequent yield in compression is equal to the highest stress attained during the tensile phase.

The hysteresis loops produced as shown in figures 44 and 45 fulfil the failure criteria of the elastic-plastic models and all the different cases defined with respect to strain.

## CHAPTER 8

### Conclusions and Future Works

#### 8.1 Conclusions

The performance of MMC's depend critically on the quality of the matrix-reinforcement interface. The nature of the interface depends on the processing of the MMC component. At the micro-level the development of local stress concentration gradients around the ceramic reinforcement (as the metal matrix attempts to deform during processing), can be very different to the nominal conditions and play a crucial role in important microstructural events such as segregation and precipitation at the matrix-reinforcement interface. These events dominate the cohesive strength and subsequent mechanical properties of the interface. At present the relationship between the strength properties of metal matrix composites and effects at the interface of the matrix and reinforcement is not well understood.

An attempt has been made to simulate atomic movement, at or near matrix-reinforcement interface. A hard and stiff particle in a soft aluminium matrix is simulated and the deformation of soft matrix (aluminium) under applied load is recorded. The forces are acting axially at  $0^\circ$  from the center of the unit cell. It shows that the degradation is more pronounced at the interfacial elements near the axis of symmetry where the stresses are highest, resulting in more degradation near the interfacial zone. The interfacial shear stress changes with varying SiC content. It shows that the higher the volume fraction of SiC the more interfacial shear stress, as more area of the composite is with the higher strength of the reinforcement. The deformation characteristics in terms of localized stress and strains at or near matrix-

reinforcement interface recorded and compared with experimental data generated by Myriounis [9]. The results are in agreement with measured values and suggest an increased strength and improved hardness due to the presence of hard particulates in the soft matrix.

It was observed that varying the volume percent of SiC and keeping the same heat treatment, T6 heat treatment irrespective of the volume fraction of SiCp has a very profound effect on the strengthening behavior of the composite as compared with the T1 and the HT1 heat treatment conditions. Adding multilinear isotropic hardening model, which uses the von Mises yield criteria coupled with isotropic work hardening, using different values of Young's modulus and Poisson's ratio derived from different heat treatments, improved the difference between the experimental and simulated stress/strains, for both 20% and 31% volume fractions of SiC. The results obtained for aluminium silicon carbide with 20% volume fraction varied between 33-44%, where as in case of aluminium silicon carbide with 31% volume fraction varied between 28-54%, at high stresses the deviation of strains is more when compared with the experimental results obtained by the work of Myriounis et al. [9], which is mainly due to the more energy required to overcome the particulate shearing when new surfaces are when dislocation pile up occurs in the particles formed and hence more energy is required to achieve the same level of strain as seen in the experimental conditions which in turn gives slightly less strain levels, when measured at the same points of reference of the unit cell.

To understand the linear response of metal matrix composites, VAMUCH in ANSYS was used to verify the experimental results which were then verified by the numerical model proposed above. The difference in the stress/strain between the simulated

and the experimental stress/strain values was around 2%, this difference was because of the work hardening function which has not been included in VAMUCH. According to the proposed hypothesis the values were also calculated to predict the trends in relation to the interfacial fracture strength of a particulate reinforced aluminium alloy system, although at high stresses the strains did deviate from the experimental results which was due to the work hardening effect and the formation of new surfaces when dislocation pile up occurs at the matrix-particulate interface; it can also be concluded that if more data sets are plotted of the empirical data the trend line would match that of the simulated data as the experimental conditions resulted in low strains in the reinforcement region.

Kinematic hardening was introduced for the matrix with its elastic-plastic behaviour taken from the experimental stress-strain behaviour of the unreinforced Al alloy. Von Mises stresses were observed for this purpose for cancelling out the multi-axial stress correction factors, the stresses were then compared with the number of cycles and as expected, as the stresses increase, the number of cycles to failure reduce.

The Non-Linear response of SiC reinforced Al alloy was also studied incorporating Chaboche kinematic hardening model to draw hysteresis loops for different volume fractions of SiC in Al matrix. It was observed that the volume percentage of the reinforcement (SiC) for the same level of strain change, much higher levels of stresses can be endured, also, the ductility of the material keeps on decreasing as the volume percentage of the SiC is increased. The hysteresis loops produced, fulfil the failure criteria of the elastic-plastic models and all the different cases defined with respect to strain.

This research will help and proves that, it is feasible to conduct virtual experiments at a computer workstation to check the strengthening behavior of the composites instead of the actual experiments, thus reducing the cost of experiments dramatically. The stress-strain response at matrix reinforcement interface will form the basis of correlating empirical to numerical results. The method of analysis proposed will help the design engineers to incorporate advanced MMC's in real life applications to identify the key parameters controlling the fracture at matrix-reinforcement interface.

The results obtained from this work conclude that the role of precipitation and segregation on the mechanical properties of Al/SiC composites is crucial, affecting the overall mechanical behaviour.

## **8.2 Key Contributions to Knowledge**

- Proposed and applied the various micro-scale modelling techniques to the aluminium alloy matrix composite, strengthened with varying amounts of silicon carbide particulate to develop a composition model to predict the interfacial strengthening behaviour of particulate reinforced alloy.
- Successfully completed the numerical modelling of particulate reinforced metal matrix composites and a strain based relationship has been proposed for the strengthening behaviour of the MMC at the interface rather than stress based.
- Predict and correlate the interfacial strengthening behaviour of ceramic particle reinforced metallic alloy.
- Developed an algorithm to model a hard ceramic particle in a soft matrix with a clear distinct interface.

- Successfully made stress/strain predictions
- Numerically verified the SN data
- Effect of reinforcement on Hysteresis

To achieve the above mentioned objectives of the project the following conditions were studied to model matrix-reinforcement interface.

- Effect of heat treatment on particulate metal matrix composites
- Deforming characteristics around the reinforcement
- Cohesive and Non-cohesive region at/and around the reinforcement
- Numerical simulation of reinforced alloy deformation under a point load.
- Numerical analysis for non-linear deformation
- Predict the composition variation at matrix reinforcement interface.

### **8.3 Future Work**

The effect of stress and strain history on the micro-modelled mechanisms is likely to be of greatest importance to the segregation and precipitation phenomena and thus indirectly affect cohesive strength. Stress-strain response at matrix reinforcement interface under cyclic loading conditions can help to estimate the stiffness of the metal matrix composites. Furthermore, the performance of MMCs could be modified further by altering the microstructural behaviour of the composites throughout by modelling new heat treatment cycles to influence segregation and precipitation mechanisms operating at matrix-reinforcement interface in turn improving the interfacial properties of the composite.

Improvements could also be made by selecting a different heat treatment cycle or selecting a composite with a higher or lower percentage of reinforcement. As upto

now it has been observed that Al-SiC MMC with T6 heat treatment has enhanced strength and the fracture toughness properties, due to the precipitation hardening mechanisms. There is much more work that can be done by changing the latter parameters, which will affect directly the mechanical properties of the composite. The models that are present for determining the interfacial fracture strength can also be improved by reducing the number of parameters involved such as Young's modulus and Poison's ratio.

Finally, to accurately predict the interfacial strength of matrix reinforcement interface further precise method of analysis are required, like introducing a crack like imperfection in the unit cell to accurately estimate the interfacial strength of matrix reinforcement interface. The dynamic response of the crack propagation at the interface in turn will determine the strength of the system and a complete picture of the effect of strain on precipitate growth is also possible.

## REFERENCES

- [1] Aaron, H.B., Aaronson, H.I., "Growth of grain boundary precipitates in Al-4% Cu by interfacial diffusion", *Acta Met* 16, (1968), 789.
- [2] Aaron, H.B., Fainstein, D., Kotler, G.R., "Diffusion-Limited Phase Transformations: A Comparison and Critical Evaluation of the Mathematical Approximations", *Journal of Applied Physics* 41(11), (1970), p. 4404-4410.
- [3] Hasan, S.T., Beynon, J.H. Faulkner, R.G., "Role of segregation and precipitates on interfacial strengthening mechanisms in SiC<sub>p</sub> reinforced aluminium alloy when subjected to thermomechanical processing", *Journal of Materials Processing Technology* 153-154, (2004), p.757-763.
- [4] Shercliff, H.R., Ashby, M.F., "A process model for age hardening of aluminium alloys. The model", *Acta Met* 38, (1990), p.1789-1802.
- [5] Carolan, R.A., Faulkner, R.G., "Grain boundary precipitation of M<sub>23</sub>C<sub>6</sub> in an austenitic steel", *Acta Met* 36, (1988), p.257-266.
- [6] Lim, L. C., and T. Watanabe. "Fracture toughness and brittle-ductile transition controlled by grain boundary character distribution (GBCD) in polycrystals", *Acta metallurgica et materialia* 38(12) (1990), 2507-2516.
- [7] Rauh, H., and R. Bullough., "The stress-driven migration of point defects to a crack." *Proceedings of the Royal Society of London, a mathematical, physical and engineering sciences*, (1985), Vol. 397, No. 1812, the royal society.
- [8] Carolan, R.A., Faulkner, R.G., "Grain boundary precipitation of M<sub>23</sub>C<sub>6</sub> in an austenitic steel", *Acta Met* 36, (1988), p.257-266.

- [9] Dimitrios Myriounis, "Role of segregation and precipitates on interfacial strengthening mechanisms in Metal Matrix Composites when subjected to thermo-mechanical processing." PhD Thesis Sheffield Hallam University, UK, July 2009.
- [10] Sinclair, J. E., and R. Fletcher. "A new method of saddle-point location for the calculation of defect migration energies." *Journal of Physics C: Solid State Physics* 7.5 (1974), 864.
- [11] Lloyd, D. J. "Particle reinforced aluminium and magnesium matrix composites", *International Materials Reviews* 39(1) (1994), 1-23.
- [12] Chawla N., Andres C., Jones J. W., Allison J. E., "Effect of SiC volume fraction and particle size on the fatigue resistance of a 2080 Al/SiCP composite", *Metall Mater Trans A* 29, (1998), 2843–54.
- [13] Voituriez C., Hall I. W., "Strengthening mechanisms in whisker-reinforced aluminum composites", *J Mater Sci* 26, (1991), 4241–9.
- [14] Wu, Y., and E. J. Lavernia., "Strengthening behaviour of particulate reinforced MMCs", *Scripta metallurgica et materialia* 27(2), (1992), 173-178.
- [15] Shao, J. C., et al. "An enhanced FEM model for particle size dependent flow strengthening and interface damage in particle reinforced metal matrix composites." *Composites Science and Technology* 71(1), (2011): 39-45.
- [16] Campbell F.C., "Structural Composite Materials", ASM International, Chapter 1, (2010), Publication ID : 05287G.
- [17] Chou T. W., Kelly A., and Okura A., "Fibre-reinforced metal-matrix composites", *Composites* 16(3), (1985): 187-206.

- [18] Matthews, F. L., Rawlings, R. D., "Composite materials: engineering and science", (1999), p.8.
- [19] Tjong S. C. and Ma Z. Y., "Microstructural and mechanical characteristics of in situ metal matrix composites." *Materials Science and Engineering, Reports* 29(3), (2000), 49-113.
- [20] Flom, Y., and R. J. Arsenault. "Deformation of SiC/Al Composites." *Journal of the Minerals, Metals and Materials Society* 38(7), (1986), 31-34.
- [21] Flom, Y., and R. J. Arsenault. "Interfacial bond strength in an aluminium alloy 6061—SiC composite." *Materials Science and Engineering* 77 (1986), 191-197.
- [22] Mortensen A., Gugor M. N., Cornie J. A., Flemings M. C., "Alloy microstructures in cast metal matrix composites." *JOM* 38(3), (1986), 30-35.
- [23] Mortensen A., James A. C. and Merton C. F., "Solidification processing of metal-matrix composites." *JOM* 40(2), (1988), 12-19.
- [24] Nardone V. C., and Prewo K. M., "On the strength of discontinuous silicon carbide reinforced aluminum composites", *Scripta Metallurgica* 20(1), (1986), 43-48.
- [25] Shaffer G.D. "An Archaeomagnetic Study of a Wattle and Daub Building Collapse." *Journal of Field Archaeology*, 20, No. 1. Spring, (1993), 59-75.
- [26] "Minerals commodity summary - cement - 2014", US United States Geological Survey. (2014). <http://minerals.usgs.gov/minerals/pubs/commodity/cement/mcs-2014-cemen.pdf>

[27] Kardos J. L., "Critical issues in achieving desirable mechanical properties for short fiber composites", *Pure & Applied Chemistry*, Vol. 57, No. 1 1, (1985), pp. 1651-1657.

[28] Erhard G., "Designing with Plastics", Trans. Martin Thompson, Hanser Publishers, (2006).

[29] Gurvishal S., Harwinder L., Daljit S. and Gurdeshbir S., "An Approach For Improving Wear Rate Of Aluminum Based Metal Using Red Mud, Sic And Al<sub>2</sub>O<sub>3</sub> Matrix Composites", *International Journal of mechanical engineering and robotics research*, Vol. 2, No. 1, (2013).

[30] Hartaj S., Sarabjit N. J., et.al, "An overview of metal matrix composite processing and SiC based mechanical properties", *Journal of Engineering Research and Studies*, Vol. II, (2011), 72–78.

[31] Rohatgi P. K., "Metal matrix composites." *Defence Science Journal* 43(4), (2013), 323-349.

[32] Mahon G. J., J. M. Howe and Vasudevan A. K., "Microstructural development and the effect of interfacial precipitation on the tensile properties of an aluminum/silicon-carbide composite", *Acta Metallurgica et Materialia* 38(8), (1990), 1503-1512.

[33] Rana R. S., Purohit R. and Das, S., "Review of recent Studies in Al matrix Composites", *International Journal of Scientific & Engineering Research*, Volume 3, (2012).

[34] On the web: <http://bricad.com/aluminium/dur/>

[35] On the web: [http://www.3m.com/market/industrial/mmc/products\\_page.html](http://www.3m.com/market/industrial/mmc/products_page.html)

[36] Cerit A.A., Karamiş M.B., Nair F. and Yildizli K., "Effect of reinforcement particle size and volume fraction on wear behavior of metal matrix composites", Tribology in industry, Volume 30, No. 3&4, (2008).

[37] Muzakkir, A. K., "An overview on effect of reinforcement and process parameters on properties of aluminium based metal matrix", International Journal of Research in Engineering and Science (IJRES), Volume 2 Issue 10, (2014).

[38] Myriounis D. P., Hasan, S. T. and Matikas, T. E., "Microdeformation behaviour of Al-SiC metal matrix composites", Composite Interfaces, 15 (5), 495-514., Vol 15, Issue 5, (2008).

[39] Myriounis D. P., et al., "Effects of heat treatment on microstructure and the fracture toughness of SiCp/Al alloy metal matrix composites", Journal of advanced materials 41(3), (2009), p.18.

[40] Kreider K. G. "Composite Materials", Vol. 4., Metallic Matrix Composites, Academic Press, New York, (1974), 483 p.

[41] Lloyd D.J., "Particle Reinforced Aluminium and Magnesium Matrix Composites", International Materials Reviews 39, (1994), p.1-23.

[42] Shang J.K., Yu W., Ritchie R.O., "Role of silicon carbide particles in fatigue crack growth in SiCp particulate reinforced aluminum alloy composite", Mater Sci Eng.,A102 (1988), p.181-92.

- [43] Hasson D. F., Hoover S. M. and Crowe C. R., "Effect of thermal treatment on the mechanical and toughness properties of extruded SiCw/aluminium 6061 metal matrix composite", *Journal of materials science* 20(11), (1985), p.4147-4154.
- [44] Manoharan M., Lewandowski J. J., "Effects of aging condition on the fracture toughness of 2XXX and 7XXX aluminum composites", *Scripta Met.*, 23, (1989), p.301-305.
- [45] Davidson, D.L., "Fracture surface toughness as a gauge of fracture toughness: Aluminium particulate SiCp composites", *Mat. Sci.*, 24, (1989), p.681- 687.
- [46] Manoharan, M., Lewandowski, J.J., "Effect of microstructure and notch root radius on fracture toughness of an aluminium metal matrix composite", *Int. J. Fract.*, 40 (1989), p.31-34.
- [47] Manoharan, M., Lewandowski, J.J., "Fracture Initiation and Growth Toughness of an Aluminum Metal-Matrix Composite", *Acta Met.*, 38 (1990), p.489-9.
- [48] Mott, N.F., Nabarro, F.R.N., "An attempt to estimate the degree of precipitation hardening, with a simple model", *Proc Phys Soc* 52, (1940), p.85.
- [49] Clyne, T.W., Withers, P.J., "An Introduction to Metal Matrix Composites", Cambridge University Press, Cambridge, (1993).
- [50] Rack H.J., Kumar P. and Vedula K., "Processing and Properties of Powder Metallurgy Composites", the metallurgical society, Warrendale, PA, (1988), p.155.
- [51] Ibrahim I.A., Mohamed F.A. and Lavernia E.J., "Particulate reinforced metal matrix composites-a review." *Journal of materials science* 26(5), (1991), p.1137-1156.

- [52] Srivatsan T. S., Sudarshan T. S. and Lavernia E. J., "Processing of discontinuously-reinforced metal matrix composites by rapid solidification", *Progress in Materials Science* 39(4), (1995), p.317-409.
- [53] Wu Y. and Enrique J. L., "Interaction mechanisms between ceramic particles and atomized metallic droplets." *Metallurgical Transactions A* 23(10), (1992), p.2923-2937.
- [54] Ma Z.Y., Bi J., Lu Y.X., Luo M. and Gao Y.X., "Quench strengthening mechanism of AL-SiC composites." *Scripta metallurgica et materialia* 29(2), (1993), p.225-229.
- [55] Nair S. V., Tien J. K. and Bates R. C., "SiC-reinforced aluminium metal matrix composites." *International Metals Reviews* 30.1 (1985), p.275-290.
- [56] Ma Z.Y., Ning X.G., Lu Y.X., Li J.H., Bi J. and Zhang Y.Z., "Microstructure and properties of SiC whisker reinforced Al-8.5 Fe-1.3 V-1.7 Si alloy composite", *Materials Letters* 21(1), (1994), p.69-72.
- [57] Tjong S. C., Lau K. C. and Wu S. Q., "Wear of Al-based hybrid composites containing BN and SiC particulates", *Metallurgical and Materials Transactions A* 30(9), (1999), p.2551-2555.
- [58] Clyne T.W., "Metallic Composite Materials, in *Physical Metallurgy*", Elsevier, (1996), p.2568-625.
- [59] Gergely V., Degischer H.P. and Clyne T.W., "Recycling of MMCs and Production of Metallic Foams, in *Comprehensive Composite Materials*", (2000) p.797-820.

- [60] Westwood A. R. C. "Materials for advanced studies and devices", Metallurgical Transactions A 19(4), (1988), p.749-758.
- [61] Rawal, Suraj P. "Metal-matrix composites for space applications." JOM 53(4), (2001): 14-17.
- [62] Biselli C., Morris D. G., and Randall N., "Mechanical alloying of high-strength copper alloys containing TiB<sub>2</sub> and Al<sub>2</sub>O<sub>3</sub> dispersoid particles", Scripta metallurgica et materialia 30(10), (1994), p.1327-1332.
- [63] Yong C., Lee J. K. and Mullins M. E., "Densification process of TiCx–Ni composites formed by self-propagating high-temperature synthesis reaction", Journal of materials science 32(7), (1997), p.1717-1724.
- [64] Everett R.K., "Deposition Technologies for MMC Fabrication, in Metal Matrix Composites: Processing and Interfaces", Academic Press, (1991), p.103-19.
- [65] Mortensen A., and Javier L., "Metal Matrix Composites", Annual review of materials research, 40, (2010), p.243-270
- [66] Aghajanian M.K., Rocazella M.A., Burke J.T. and Keck S.D., "The Fabrication of Metal Matrix Composites by a Pressureless Infiltration Technique", J.Mat.Sci., vol.26, (1991) p.447-54.
- [67] Mortensen A., Masur L.J., Cornie J.A. and Flemings M.C., "Infiltration of a Fibrous Preform by Pure Metal", Metall. Trans., vol.20A, (1989), p.2535-63.
- [68] Mortensen A., "Melt infiltration of metal matrix composites", Comprehensive composite materials, volume 3: metal matrix composites, Pergamon Press, Oxford, UK, (2000), p. 521–554.

- [69] Zhou W., Xu Z.M., "Casting of SiCp Reinforced Metal Matrix Composites", Journal of Materials Processing Technology, 63, (1997), p.358-363.
- [70] Gowri Shankar M.C, Jayashree, et.al, "Individual and Combined Effect of Reinforcements on Stir Cast Aluminium Metal Matrix Composites - A Review", International Journal of Current Engineering and Technology, Vol.3, No.3, (2013).
- [71] Kumar R., Bhandare G., Sonawane P. M., "Preparation of Aluminium Matrix Composite by Using Stir Casting Method", International Journal of Engineering and Advanced Technology, Vol, 3, Issue 2, (2013).
- [72] Skibo M. D. and Schuster D. M., "Process for production of metal matrix composites by casting and composite therefrom." U.S. Patent No. 4,759,995.,(1988).
- [73] Saravanan C., "Effect of Particulate Reinforced Aluminium Metal Matrix Composite –A Review", Mechanics and Mechanical Engineering Vol. 19, No. 1, (2015), p.23–30.
- [74] Ray S. "Synthesis of cast metal matrix particulate composites." Journal of Materials Science 28.20, (1993), p.5397-5413.
- [75] Mortensen A. and Jin I., "Solidification Processing of Metal Matrix Composites", Int. Mat. Rev.vol.37, (1992), p.101-28.
- [76] Lloyd D.J. and Jin I., "Melt Processed Aluminium Matrix Particle Reinforced Composites", Comprehensive Composite Materials, Vol. 3: Metal Matrix Composites, Elsevier, (2000) p.555-77.
- [77] Lin Ching-Bin, "Process for making metal-matrix composites reinforced by ultrafine reinforcing materials products", US. Patent Document-Number 5,401,338, (1993).

[78] Willis T. C. "Spray deposition process for metal matrix composites manufacture", *Metals and Materials* 4(8), (1988), p.485-488.

[79] Clyne T. W., "An Introductory Overview of MMC Systems, Types, and Developments", Vol. 3 *Metal Matrix Composites of Comprehensive Composite Materials.* (2000).

[80] Matthews F.L and Rawlings R. D., "Composite materials: engineering and science", Elsevier, (1999) – p.125.

[81] Flemings M. C. "Solidification processing." *Metallurgical transactions* 5(10), (1974), p. 621–633.

[82] Georghe I. and Rack H.J., "Powder Processing of Metal Matrix Composites", *Comprehensive Composite Materials*, Elsevier, (2000), p.679-700.

[83] Peel C., Robertson J. and Tarrant A., "Metal Matrix Composites - UK Trends", *Materials World*, vol. 3, (1995).

[84] Izadia H., Noltingb A. et.al, "Friction stir processing of Al/SiC composites fabricated by powder metallurgy", *Journal of Materials Processing Technology*, (2013), p.1900–1907.

[85] U.S. Congress Office of technology assessment, "Advanced materials by design", OTA- E-351 (1988), Congress Catalog card number 87-619860, Online: <http://ota.fas.org/reports/8801.pdf>

[86] Tjong S. C., "8 Processing and Deformation Characteristics of Metals Reinforced with Ceramic Nanoparticles." *Nanocrystalline Materials: Their synthesis-structure-property relationships and applications*, (2013), p.269.

- [87] Bodunrin M. O., Kenneth K. A. and Lesley H. C., "Aluminium matrix hybrid composites: a review of reinforcement philosophies; mechanical, corrosion and tribological characteristics." *Journal of Materials Research and Technology*, (2015).
- [88] Faulkner R. G. and Shvindlerman L. S., "Thermodynamics of vacancies and impurities at grain boundaries", *Mater. Sci. Forum* 207–209, (1996), p.157–160.
- [89] Lim L.C. and Watanabe T., "Fracture toughness and brittle–ductile transition controlled by grain boundary character distribution (GBCD) in polycrystals", *Acta Met* 38(12), (1990), p.2507–2516.
- [90] Faulkner R.G, Shvindlerman L.S, "Thermodynamics of Vacancies and Impurities at Grain Boundaries", *Materials Science Forum*, 207-209 (Part 1), (1996), p.157-160.
- [91] McMahon Jr. C.J., Vitek V., "Effects of segregated impurities on intergranular Fracture Energy", *Acta Metall*, 27(4), (1979), p.507-513.
- [92] Clyne T.W., "An introductory overview of MMC Systems, Types and Developments, in *Comprehensive Composite Materials*", Elsevier, (2000), p.1-26.
- [93] Clyne T. W. and Withers P. J., "An introduction to metal matrix composites", Cambridge University Press, Cambridge, (1993).
- [94] Torralba J. M., Da Costa C. E., Velasco F., "P/M aluminum matrix composites: an overview", *J Mater Process Technol*, 133, (2003), p.203–206.
- [95] Maruyama B., Hunt W. H. Jr. "Discontinuously reinforced aluminum: status and future direction", *J Met* 51, (1999), p.59–61.
- [96] Chawla N., Shen Y. L., "Mechanical behaviour of particle reinforced metal matrix composites". *Adv Eng Mater* 3, (2001), p.357–370.

- [97] Hong S. J., Kim H. M., Huh D., Suryanarayana C. and Chun B.S., "Effect of clustering on the mechanical properties of SiC particulate reinforced aluminum alloy 2024 metal matrix composites", *Mater Sci Eng A* 347, (2003), p.198–204.
- [98] Narayanasamy R., Ramesh T., Prabhakar M., "Effect of particle size of SiC in aluminum matrix on workability and strain hardening behaviour of P/M composite", *Mater Sci Eng A* 504, (2009), p.13–23.
- [99] Davis L. C. and Allison J. E., "Residual stresses and their effects on deformation in particle-reinforced metal-matrix composites", *Metall. Trans A* 24, (1993), p.2487–2496.
- [100] Rack H. J., "Light-weight, high-performance metal matrix composites, processing and properties for powder metallurgy composites", Annual meeting of metallurgical society, Denver, Colorado, (1987), p.155.
- [101] Fathy A., Sadoun A. and Abdelhameed M., "Effect of matrix/reinforcement particle size ratio (PSR) on the mechanical properties of extruded Al–SiC composites", *Int J Adv Manuf Technol* (2014) 73:1049–1056 DOI 10.1007/s00170-014-5901-9.
- [102] Slipenyuk A., Kuprin V., Milman Y., Goncharuk V. and Eckert J., "Properties of P/M processed particle reinforced metal matrix composites specified by reinforcement concentration and matrix to reinforcement particle size ratio", *Acta Mater* 54, (2006), p.157–166.
- [103] Lewandowski J. J., Liu C. and Hunt W. H., "Effects of matrix microstructure and particle distribution on fracture of an aluminum metal matrix composite", *Materials Science and Engineering: A* 107, (1989), p.241-255.

- [104] Stone I. C., Welson C. E. and Tsakirooulos P., "The dependence of aging on 3-dimensional spatial distribution of reinforcement in Al- 4wt% Cu/SiCP MMCs", *Scr Mater* 37, (1997), p.305–310.
- [105]. Sternowski S. B., Garret E. O'Donnell, and Looney L., "Effect of particle size on the mechanical properties of SiC particulate reinforced aluminium alloy AA6061." *Key Engineering Materials*, Vol. 127, (1996).
- [106]. Krajewski P. E., Allison J. E. and Jones J. W., "The influence of matrix microstructure and particle reinforcement on the creep behaviour of 2219 aluminum", *Metall Mater Trans A* 24, (1993), p.2731–2741.
- [107]. Chawla N., Andres C., Jones J. W. and Allison J. E., "Effect of SiC volume fraction and particle size on the fatigue resistance of a 2080 Al/SiCp composite", *Metall Mater Trans A* 29, (1998), p.2843–2854.
- [108] Llorca J., Needleman A. and Suresh S., "An analysis of the effects of matrix void growth on deformation and ductility in metal-ceramic composites", *Acta Metallurgica et Materialia* 39(10), (1991), p.2317-2335.
- [109] Christman T., A. Needleman and Suresh S., "An experimental and numerical study of deformation in metal-ceramic composites." *Acta Metallurgica* 37.11, (1989), p.3029-3050.
- [110] Bao G., Hutchinson J. W. and McMeeking R. M., "Particle reinforcement of ductile matrices against plastic flow and creep." *Acta metallurgica et materialia* 39(8), (1991), p.1871-1882.

- [111] McHugh P.E., Asaro R.J. and Shih C.F., "Computational modelling of metal matrix composite materials - I. Isothermal deformation patterns in ideal microstructures", *Acta Metall. Mater.* 41, (1993), p.1461-1476.
- [112] Llorca J., Suresh S. and Needleman A., "An experimental and numerical study of cyclic deformation in metal matrix composites", *Metallurgical transaction A* 23 A, (1992), p.919-934.
- [113] Böhm H. J., "Computer based micromechanical investigations of the thermomechanical behavior of metal matrix composites", VDI Verlag, (1991).
- [114] O'Dowd N.P., Tang W.C., Busso E.P. and McHugh P.E., "Modelling of deformation and failure of metal/ceramic composites", *The seventh international symposium on plasticity and its current applications*, Net Press, Maryland, (1999), p.745-748.
- [115] Watt D. F., Xu X. Q. and Lloyd D. J., "Effects of particle morphology and spacing on the strain fields in a plastically deforming matrix", *Acta Metall. Mater.* 44, (1996), p.789-799.
- [116] Albertini G., Bruno G., Carrado A., Fiori F., Rogante M. and Rustichelli, F. "Determination of residual stresses in materials and industrial components by neutron diffraction", *Measurement Science and Technology*, 10(3), R56, (1999).
- [117] Aghdam M. M., Smith D. J. and Pavier M. J., "Finite element micromechanical modelling of yield and collapse behaviour of metal matrix composites", *Journal of the Mechanics and Physics of Solids* 48(3), (2000), p.499-528.
- [118] Lin T.H., Salinas D. and Ito Y.M., "Initial yield surfaces of a unidirectionally reinforced composite", *J. Appl. Mech.* 39, (1972), p.320-326.

- [119] Dvorak G. J., Rao M. S. M. and Tran J.Q., "Yielding in unidirectional composites under external loads and temperature changes", J. Composite Mater. 7, (1973), p.194-216.
- [120] Dvorak G. J., Rao M. S. M. and Tran J. Q., "Generalised initial yield surfaces for unidirectional composites", J. Appl. Mech. 41, (1974), p.249-253.
- [121] Dvorak G.J., "Thermal expansion of elastic-plastic composite materials", J. Appl. Mech. 53, (1986), p.737-743.
- [122] Bruzzi M. S., McHugh P. E., O'Rourke F., and Linder T. (2001). "Micromechanical modelling of the static and cyclic loading of an Al 2124-SiC MMC", International Journal of Plasticity, 17(4), (2001), p.565-599.
- [123] Chawla N. and Yu-Lin S., "Mechanical behaviour of particle reinforced metal matrix composites", Advanced engineering materials 3(6), (2001), p.357-370.
- [124] Taya M., Arsenault R. J., "Metal matrix composites: thermomechanical behaviour", vol. 4. Elmsford, New York, Pergamon Press, (1989).
- [125] Srivatsan T. S. and Al-Hajri M., "The fatigue and final fracture behaviour of SiC<sub>p</sub> particle reinforced 7034 aluminum matrix composites", Composites: Part B 33, (2002), p.391-404.
- [126] Christman T. and Suresh S., "Effects of SiC<sub>p</sub> reinforcement and aging treatment on fatigue crack growth in an Al-SiC<sub>p</sub> composite", Mater Sci. Eng. 102, (1988), p.211-20.

- [127] Shang J. K., Yu W. and Ritchie R.O., "Role of silicon carbide particles in fatigue crack growth in SiCp particulate reinforced aluminum alloy composite", *Mater Sci. Eng. A102*, (1988), p.181–192.
- [128] Bruzzi M. S. and McHugh P. E., "Micromechanical investigation of the fatigue crack growth behaviour of Al–SiC<sub>p</sub> MMCs", *International Journal of Fatigue*, 26, 8, (2004), p.795-804.
- [129] Griffith A. A., "The phenomena of rupture and flow in solids", *Philosophical Transactions of the Royal Society of London*, A 221, (1921), p.163–198.
- [130] Broek D., "Elementary engineering fracture mechanics", Springer Science & Business Media, (1986), p.5-17.
- [131] Faulkner R. G. and Shvindlerman L. S., "Grain boundary thermodynamics, structure and mechanical properties", *Mater. Sci. Forum* 207–209(1), (1996), p.157–160.
- [132] Papazian J. M., "Effects of SiC whiskers and particles on precipitation in aluminum matrix composites", *Metallurgical and Materials Transactions A*, Volume 19, Number 12, (1988), p.2945-2953.
- [133] Myriounis D. P., Hasan S. T. and Matikas T. E., "Predicting Interfacial Strengthening Behaviour of Particulate-Reinforced MMC—A Micro-mechanistic Approach." *Composite Interfaces* 17(4), (2010), p.347-355.
- [134] Shoyxin L., Lizhi S., Huan L., Jiabao L. and Zhongguang W., "Stress carrying capability and interface fracture toughness in SiCp/6061 Al model materials", *Journal of materials science letters* 16, (1997), p.863–869.

- [135] Syed A. A. Shah and S.T Hasan, "An empirical method of calculating interfacial strength in a second phase reinforced alloy system", *Advances in Materials & Processing Technology Journal*, accepted, 2015.
- [136] Wang Z. and Zhang R. J., "Microscopic characteristics of fatigue crack propagation in aluminium alloy based particulate reinforced metal matrix composites", *Acta metal mater.* 42(4), (1994), p.1433-1445.
- [137] Xu X.Q. and Watt D. F., "BaSiCp role of a hard particle in a metal matrix subjected to tensile loading", *Acta Metal Mater.*, 42(11) 3, (1994), p.717-3729.
- [138] Cox H. L. "The elasticity and strength of paper and other fibrous materials", *British journal of applied physics* 3.3 (1952), p.72.
- [139] Faulkner R. G., "Impurity diffusion constants and vacancy binding energies in Solids", *Mater. Sci. Technol.* 1(6), (1985), p.442-447.
- [140] Chawla K. K., "Composite materials: science and engineering", Springer Science & Business Media, (2012), p.102.
- [141] Cox H. L., "The elasticity and strength of paper and other fibrous materials", *British journal of applied physics* 3(3), (1952) p.122.
- [142] Anthony K. and Macmillan N. H., "Strong Solids." Oxford University Press, Walton Street, Oxford OX 2 6 DP, UK, (1986), p.57.
- [143] Nardone V. C. and Prewo K. M., "Comment on a comparison of PM vs melted SiC/Al composites", *Scripta metallurgica* 23(2), (1989), p.291-292.
- [144] Davis L. C. and Allison J. E., "Residual stresses and their effects on deformation", *Metallurgical Transactions A* 24(11), (1993), p.2487-2496.

[145] Chawla N., et al., "The effect of matrix microstructure on the tensile and fatigue behavior of SiC particle-reinforced 2080 Al matrix composites", *Metallurgical and Materials Transactions A* 31(2), (2000), p.531-540.

[146] Chawla K. K. and Metzger M., "Initial dislocation distributions in tungsten fibre-copper composites", *Journal of Materials Science* 7(1), (1972), p.34-39.

[147] Chawla K. K., "Grain boundary cavitation and sliding in copper/tungsten composites due to thermal stresses", *Philosophical Magazine* 28(2), (1973), p.401-413.

[148] Vogelsang M., Arsenault R. J. and Fisher R. M., "An in-situ HVEM study of dislocation generation at Al/SiC interfaces in metal matrix composites", *Metallurgical Transactions A* 17(3), (1986), p.379-389.

[149] Arsenault R. J. and Shi N., "Dislocation generation due to differences between the coefficients of thermal expansion", *Materials Science and Engineering* 81, (1986), p.175-187.

[150] Suresh S. and Chawla K. K. "Aging characteristics of reinforced metals", *Fundamentals of metal-matrix composites (A 95-25875 06-24)*, Stoneham, MA, Butterworth-Heinemann, (1993), p.119-136.

[151] Krajewski P. E., Allison J. E. and Jones J. W., "The influence of matrix microstructure and particle reinforcement on the creep behavior of 2219 aluminum", *Metallurgical Transactions A* 24(12), (1993), p.2731-2741.

[152] Mital S. K., Murthy P. L. N. and Goldberg R. K., "Micromechanics for particulate reinforced composites", *Mechanics of Advanced Materials and Structures*, 4(3), (1997), p.251-266.

[153] Subodh K. M., "Micromechanics for Particulate Reinforced Composites", NASA Technical Memorandum 107276, (1996).

[154] MC-21, Inc, Carson City, NV, USA, Technical Report, [www.mc21inc.com](http://www.mc21inc.com)

[155] Ellermann A. and Scholtes B., "The Bauschinger Effect in Different Heat Treatment Conditions of 42CrMo4", International Journal of Structural Changes in Solids – Mechanics and Applications Volume 3, Number 1, (2011), p.1-13,

[156] Yu W. and Tang T., "Variational asymptotic method for unit cell homogenization of periodically heterogeneous materials", International Journal of Solids and Structures 44(11) (2007), p.3738-3755.

[157] Tang T., "Variational Asymptotic Micromechanics Modeling of Composite Materials", All Graduate Theses and Dissertations, (2008), Paper 72.

[158] Neto M. A., Yu W. and Tang T., "Analysis and optimization of heterogeneous materials using the variational asymptotic method for unit cell homogenization", Composite Structures 92(12), (2010), p.2946-2954.

[159] Myriounis D. P., Hasan S. T. and Matikas T. E., "Heat Treatment and Interface Effects on the Mechanical Behaviour of SiC-Particle Reinforced Aluminium Matrix Composites", Journal of ASTM International, Vol. 5, No. 7, Paper ID JAI101624, (2008).

[160] Sowerby R., Uko D. K. and Tomita Y., "A review of certain aspects of the Bauschinger effect in metals", Materials Science and Engineering, 41(1), (1979), p.43-58.

[161] Prager W., "A New Method of Analysing Stress and Strain in Work Hardening Plastic Solids", ASME Journal of Applied Mechanics, 78, (1956), p.493.

- [162] Armstrong P. J. and Frederick C. O., "A Mathematical Representation of the Multiaxial Bauschinger Effect", CEGB Report, RD/B/N731, Berkeley Nuclear Laboratories, (1966).
- [163] Ohno N. and Wang J. D., "Kinematic Hardening Rules with Critical State Dynamic Recovery, Part II: Application to Experiments of Ratcheting Behaviour", *International Journal of Plasticity*, 9, (1991), p.391.
- [164] Chaboche J. L., Dang-Van K. and Cordier G., "Modelization of the Strain Memory Effect on the Cyclic Hardening of 316 Stainless Steel", SMIRT-5, Division L Berlin, (1979).
- [165] Chaboche J. L., "Constitutive Equations for Cyclic Plasticity and Cyclic Viscoplasticity", *International Journal of Plasticity*, 5, (1989), p.247-302.
- [166] Chaboche J. L., "Time-Independent Constitutive Theories for Cyclic Plasticity", *International Journal of Plasticity* 2(2), (1986), p.149-188.
- [167] Mroz, Z., "On the Description of Anisotropic Work-Hardening", *Journal Mech. Phys. Solids*, 15, (1967), p.163-175.
- [168] Dafalias Y. F. and Popov E. P., "Plastic Internal Variables Formalism of Cyclic Plasticity", *Journal of Applied Mechanics* 43(4), (1976), p.645-651
- [169] Chaboche J. L., "On Some Modifications of Kinematic Hardening to Improve the Description of Ratchetting Effects", *International Journal of Plasticity* 7, (1991), p.661-678.
- [170] Carolan R. A. and Faulkner R. G., "Grain boundary precipitation of M 23 C 6 in an austenitic steel", *Acta Metallurgica* 36(2), (1988), p. 257-266.

[171] Sinclair J. E. and Fletcher R., "A new method of saddle-point location for the calculation of defect migration energies", *Journal of Physics C: Solid State Physics* 7(5), (1974), p.864.

[172] Chaboche J. L. and Rousselier G., "On the plastic and viscoplastic constitutive equations—Part I: Rules developed with internal variable concept", *Journal of Pressure Vessel Technology* 105(2), (1983), p.153-158.  
DOI: 10.1115/1.3264257

[173] Chawla N. and Yu-Lin Shen. "Mechanical behaviour of particle reinforced metal matrix composites", *Advanced engineering materials* 3(6), (2001), p.357-370.

[174] Segurado J., Gonzalez C. and Llorca J., "A numerical investigation of the effect of particle clustering on the mechanical properties of composites", *Acta Materialia* 51(8), (2003), p.2355-2369.

[175] Lewandowski J. J., "Fracture and fatigue of particulate MMCs", *Comprehensive Composite Materials, Metal Matrix Composites* 3, (2000), p.151-187.

[176] Chawla, N., et al., "Effect of SiC volume fraction and particle size on the fatigue resistance of a 2080 Al/SiCp composite", *Metallurgical and Materials Transactions A* 29(11), (1998), p.2843-2854.

[177] Couper M. J. and K. Xia., "Development of microsphere reinforced metal matrix composites", *Metal Matrix Composites- Processing, Microstructure and Properties. Proc. 12<sup>th</sup> Riso Int. Symp. on Materials Science Roskilde. Vol. 206.* (1991).

[178] Brockenbrough J. R., Suresh S. and Wienecke H. A., "Deformation of metal-matrix composites with continuous fibers: geometrical effects of fiber distribution and shape", *Acta metallurgica et materialia* 39(5), (1991), p.735-752.

[179] Arsenault R. J. and Wu S. B., "The strength differential and Bauschinger effects in SiC<sub>p</sub> Al composites", *Materials Science and Engineering* 96, (1987), p.77-88.

[180] Shen Y-L., et al., "Effective plastic response of two-phase composites", *Acta Metallurgica et Materialia* 43(4), (1995), p.1701-1722.

[181] Corbin S. F. and Wilkinson D. S., "The influence of particle distribution on the mechanical response of a particulate metal matrix composite", *Acta metallurgica et materialia* 42(4), (1994), p.1311-1318.

## Appendix A: Getting to know ANSYS

The 1<sup>st</sup> set of experiments performed on ANSYS workbench was consisting of a structural steel beam, this simple geometry was chosen to get hands on with the softwares environment. A simple force was then applied and stress, strain and reaction forces were observed. This basic first experiment consisted of a single material and was performed in the Static structural environment, figure A1(i) shows the beam after the force has been applied and the stresses while figure A1(ii) gives a closer view of the beam and the stresses been observed in a bit more depth.

The following material data input without any thermal effects were used,

Temperature	Young's Modulus	Poisson's	Bulk Modulus	Shear Modulus
C	Pa	Ratio	Pa	Pa
	6.8948e+006	0.3	5.7456e+006	2.6518e+006

Table A1: Material properties used as input for structural steel

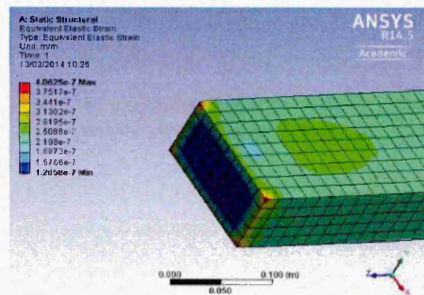
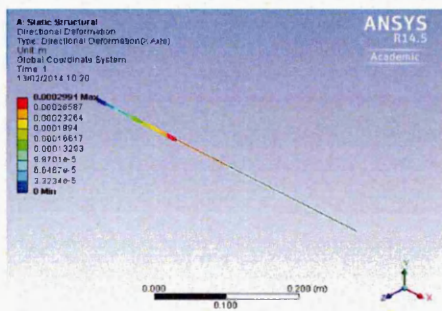


Figure A1 (i) Force been applied to a structural steel beam and stresses observed  
A1(ii) A close up of the beam section

Time [s]	Force (X) [N]	Reaction (Y) [N]	Force (Z) [N]	Reaction (Total) [N]
1.	-5.2381	0.	0.	5.2381

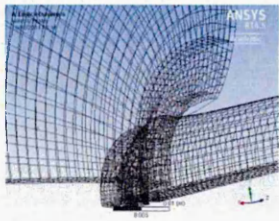
Table A2: Model (A4) > Static Structural (A5) > Solution (A6) > Force Reaction

2<sup>nd</sup> Series of Experiments was done by considering a plate and a beam, and then the beam dynamically hits the plate so that at the point of contact the plate loses the part where it was hit. The simulation was run in real time, two different materials were used and the properties of the materials for the plate (Al 2024 - T4) with a Density of 2785 Kg m<sup>-3</sup> and specific heat 863 J kg<sup>-1</sup> C<sup>-1</sup> and the beam (Copper) with a Density of 8900 kg m<sup>-3</sup>, Specific heat of 1.e-012 J kg<sup>-1</sup> C<sup>-1</sup> and a Shear Modulus of 4.64e+010 Pa were used with the following mechanical properties,

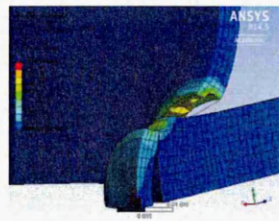
Initial Yield Stress Pa	Maximum Yield Stress Ymax Pa	Hardening Constant B	Hardening Exponent n	Derivative dG/dP G'P	Derivative dG/dT Pa C <sup>-1</sup>	Derivative G'T dY/dP Y'P	Melting Temperature Tmelt C
2.6e+008	7.6e+008	310	0.185	1.8647	- 1.762e+007	1.695e- 002	946.85

Table A3: Al 2024-T4 > Steinberg Guinan Strength

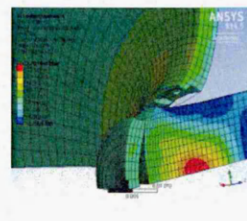
Some of the results from the simulation of the Explicit Dynamics mode of ANSYS are shown below;



(i)



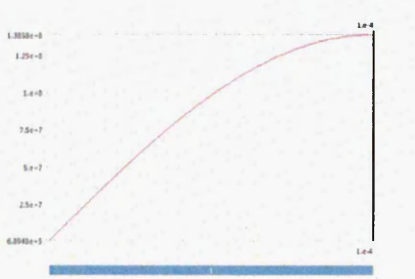
(ii)



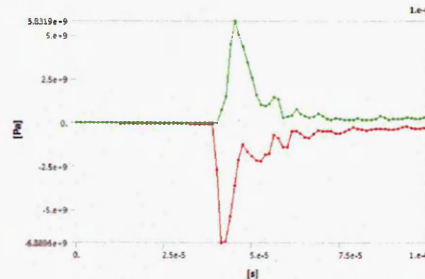
(iii)

Figure A2: (i) Mesh (ii) Stresses (iii) Strains

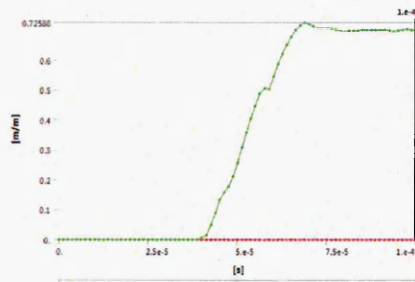
The following results showed in figure A3, were gathered and analysed for understanding purposes.



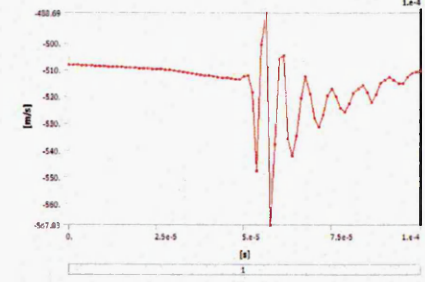
(i)



(ii)



(iii)



(iv)

Figure A3 (i) Pressure (ii) Equivalent Elastic Strain (iii) Normal Stress (iv) Velocity Probe

The 3<sup>rd</sup> series of experiments consisted of multiple different geometries, stresses and strains were recorded, also different meshing techniques were applied to test which

is best for a particular geometry. The following grid patterns (figures A4 - A6) show a few of the experiments done during the practice.

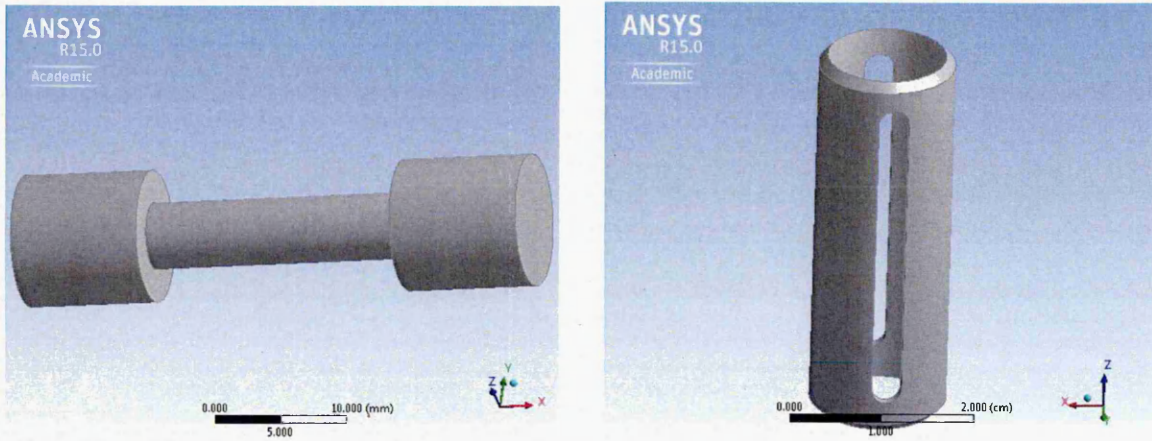


Figure A4 (i) A dog bone structure (ii) A cylindrical structure with slits and chamfer.

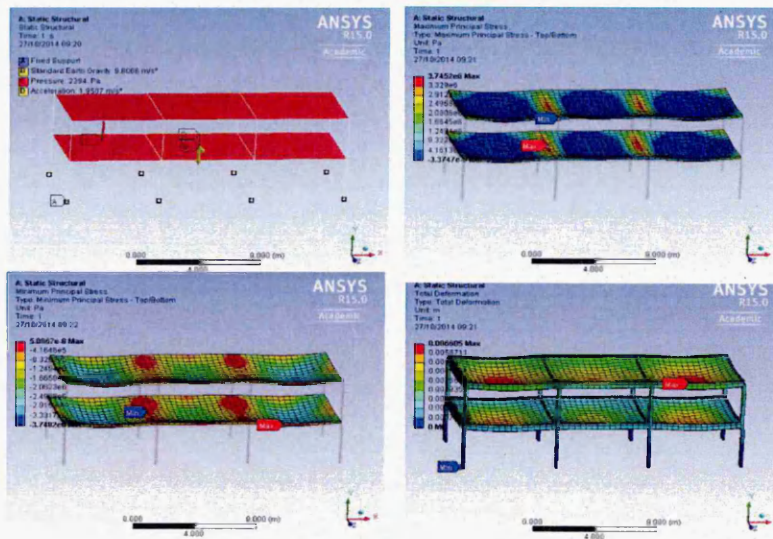


Figure A5 (i) A double story structure with boundary conditions (ii) Max Principal stresses (iii) Min Principal stresses (iv) Total deformation.

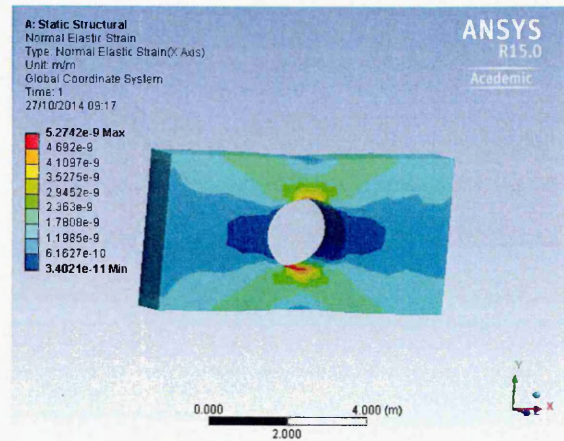
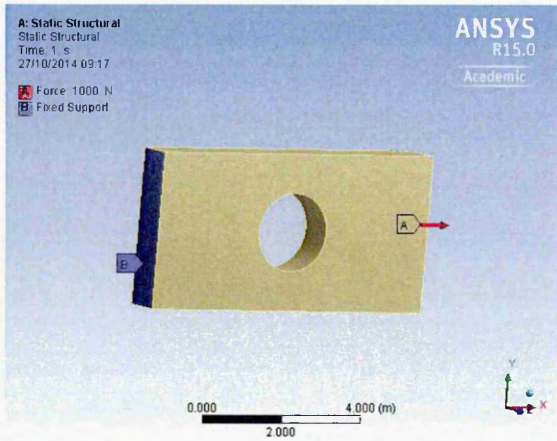


Figure A6 (i) A Plate with a hole with boundary conditions (ii) Normal elastic strain on x-axis.

## Appendix B: Initial Experiments on the Unit Cell Concept

The unit cell as described in section 4.2.1 was then developed and the first experiment was done, the geometry was made and the stress was applied on the right and left side of the unit cell, but as seen in the grid patterns below it was observed that the boundary conditions needed to be changed as the whole geometry was moving with the applied forces deforming the unit cell, hence the top and bottom sides of the unit cell were fixed, making then the boundaries of the interface and applying stress to the other two sides mimicking a unit cell as if it's actually a part of the big material.

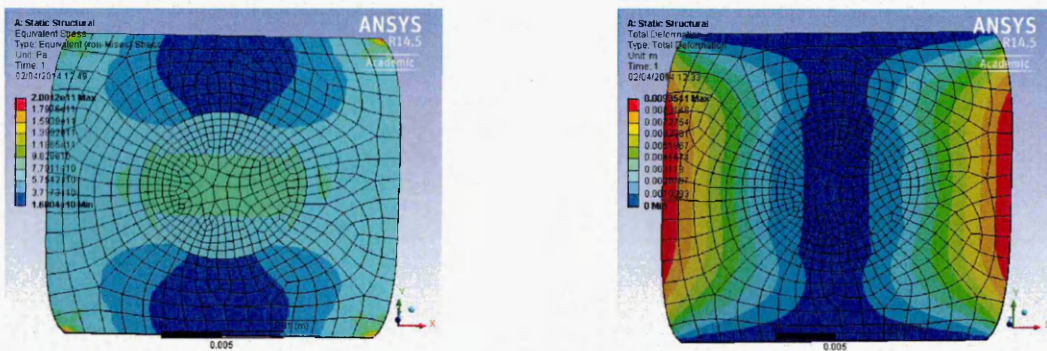


Figure B7 (i) stresses (ii) Total deformation

The next set of experiments were conducted with fixing the boundaries as mentioned in the earlier experiment, the problem was solved but this time it was observed as also can be seen in the grid patterns that the stresses did not completely effect the particulate part of the unit cell and at higher stresses, debonding can be seen taking place and eventually failure of the matrix can be seen without any effect on the particulate, this actually ment that the matrix and the particulate were not properly attached to each other.



first layer and in some cases used the second layer. The following grid patterns show the non convergent meshes while observing the total deformation, and equivalent von-Mises stresses when applied with stresses of 1500N.

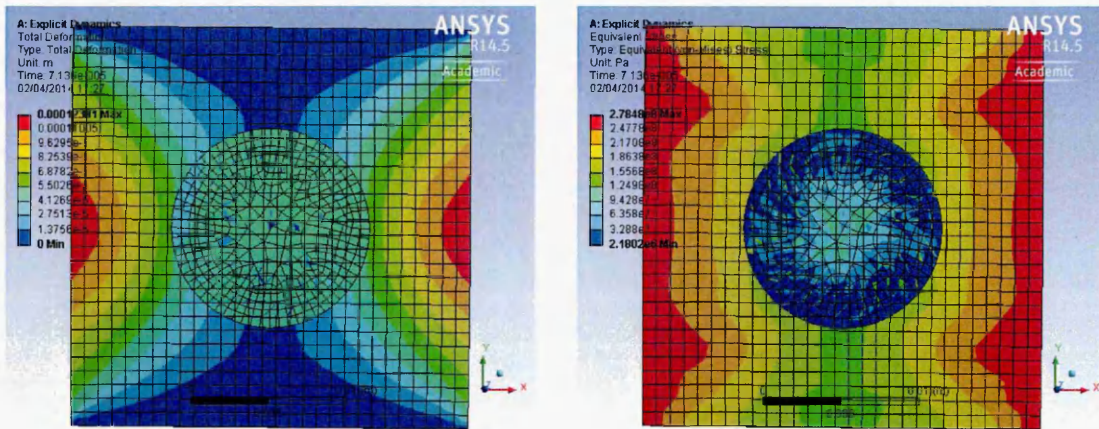


Figure B10: total deformation and equivalent von-Misses stresses with a non-convergent mesh when applied with 1500N stresses on the positive and negative x-axis.

Other simulations followed to take care of the meshing issues and some of the grids are shown in figure B11 and B12 for reference the simulations were done while applying stresses from 1N to 4000N to cater for different solutions for the mesh.

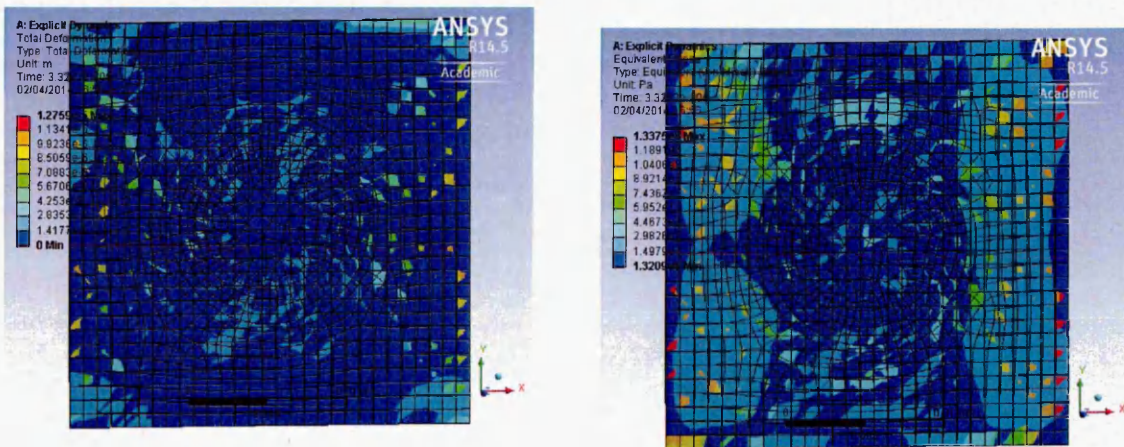


Figure B11: Total deformation and equivalent von-Misses stress at 1000N

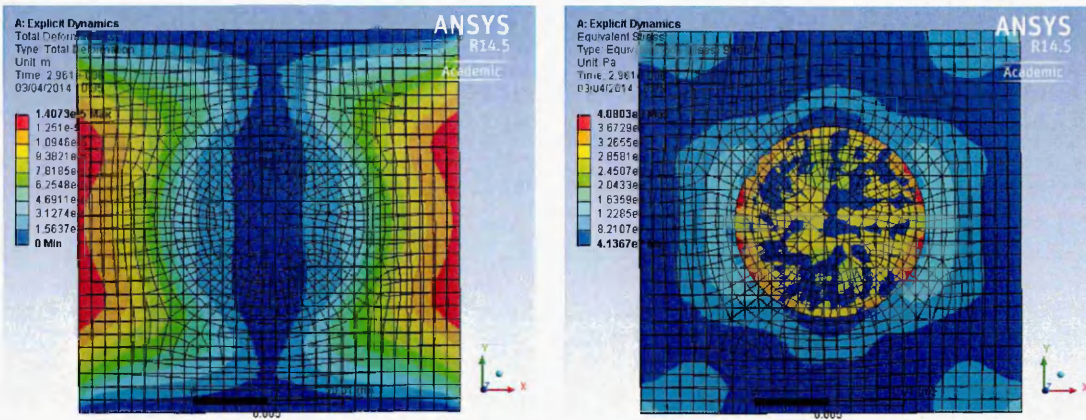


Figure B12: Different techniques applied, the above two grids show the deformation and Stress at 1000N when Body Interaction Was Bonded

Finally the model was corrected and the mesh became convergent, the problem was solved by considering the boundary conditions as described earlier and the two separate materials were made and then bonded frictionless to form one part and then mesh together so that the mesh could converge. The following results were presented in a Poster Appendix F.

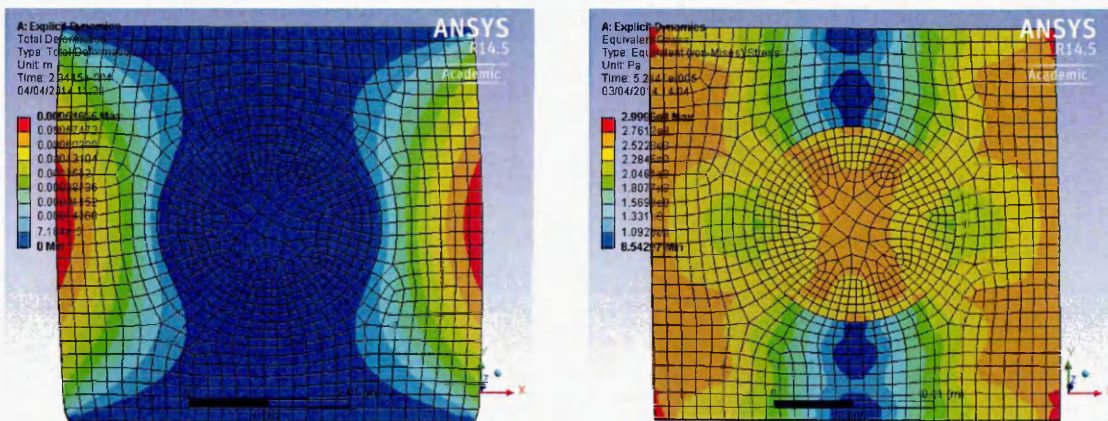


Figure B13: Total deformation and equivalent von-Mises stress at 2000N

The following two grid patterns as shown in figure 13 show the convergence of the mesh and also show the total deformation and equivalent von-Misses stresses, detailed description on the results is mentioned in chapter 4.

The experiments on refining the mesh continued and a unit cell was made keeping the dimensions 1x1 but this time the mesh was sized using the sizing controls and infiltrations, the problem with very fine mesh was that as seen in the grid patterns in figure 15 the mesh again did not converge on the interface as was expected since the two different material properties were treated as two separate materials by ANSYS. These tests were done using very small stresses for the reason of saving the processing time of the simulations.

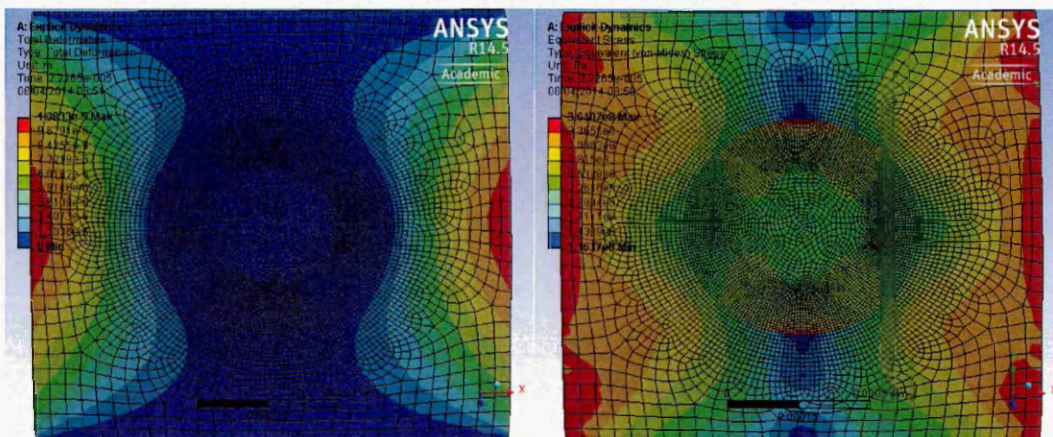


Figure B14: Refined mesh and total deformation and equivalent von-Misses stress at 1N

Again attempts were made to refine the mesh and to make the mesh as fine as possible, the problem still continued that when two different materials were put together and the mesh made finer ANSYS would automatically consider them as two separate materials and hence when the materials were combined and it can be observed at the interface the mesh did not coincide and became non convergent as

can be seen in figure 15. The problem in this experiment was that there was no effect on the particulate when the forces were applied as can be seen in figure 16 that when the stresses were applied the matrix and the particulate separated.

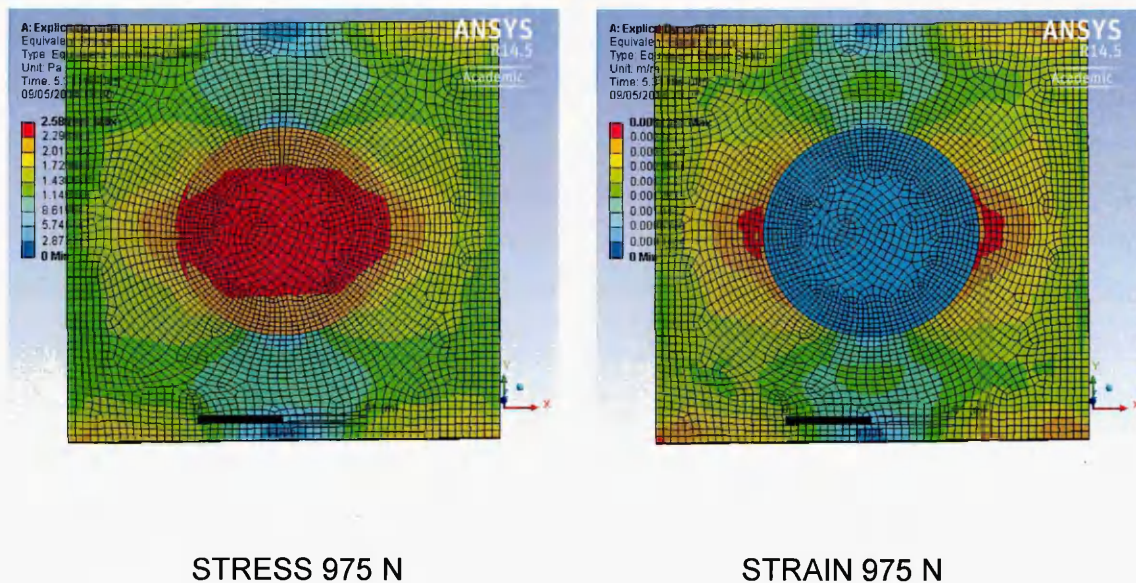


Figure B15: Total deformation

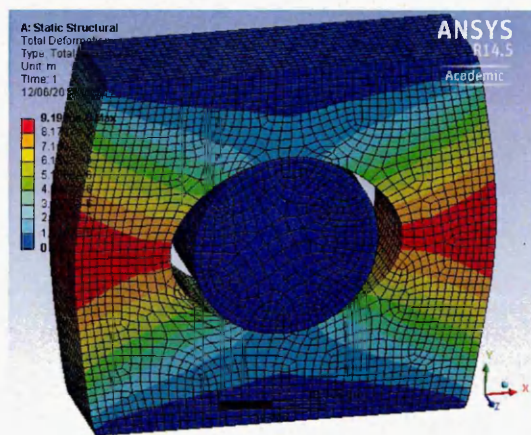


Figure B16: IF NOT BONDED

In the third attempt both of the materials i.e. the matrix and the particulate were bonded together and meshed together the results were pretty good as the effect of

the forces went straight through both of the materials and as required both the materials for the matrix and the particulate behaved as one material as a composite, the following grid patterns show the mesh, coordinate system, contact region of the bonded interface and the boundary conditions of the final unit cell been used in this research for further analysis.

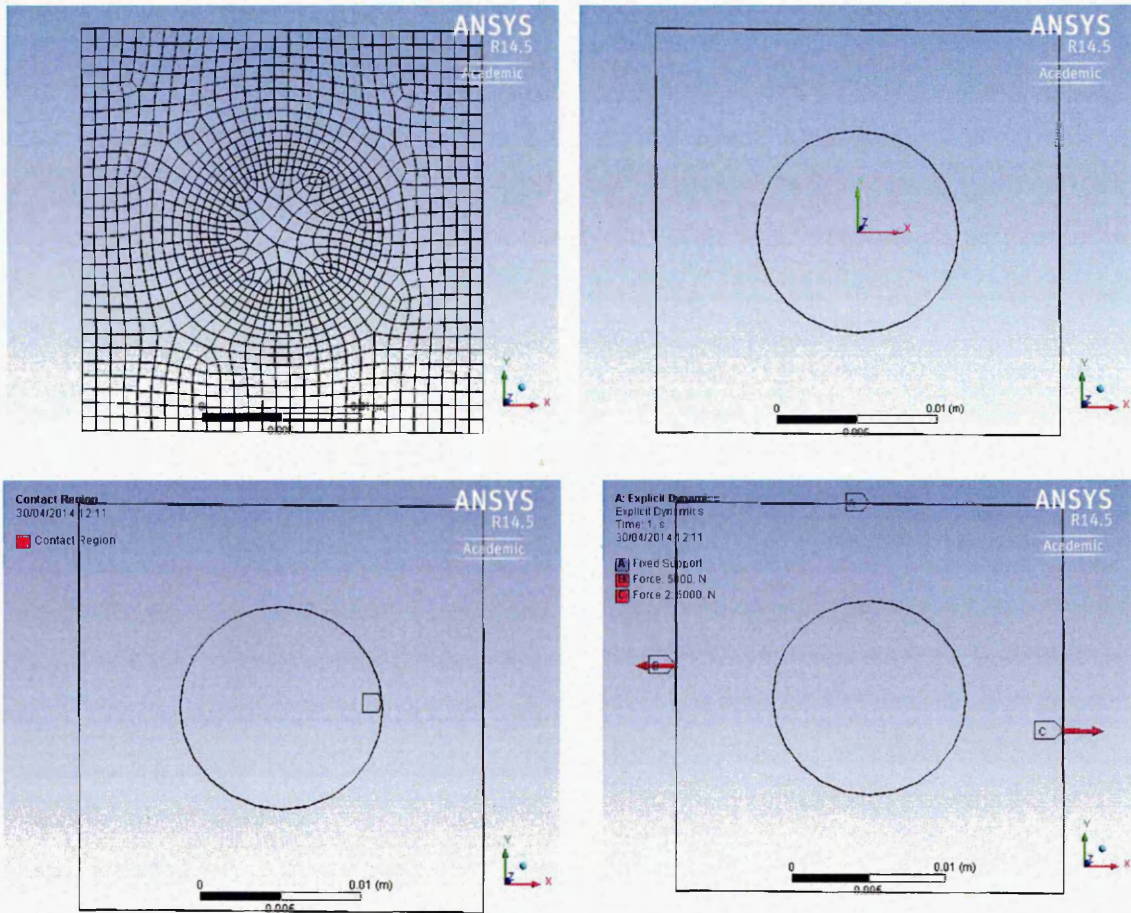


Figure B17 (i) MESH (ii) COORDINATE SYSTEM (iii) CONTACT REGION BONDED (iv) BOUNDARY CONDITIONS

The preliminary results as shown in the grid patterns in figure B18 show the strains recorded with increasing stress values and from the grid patterns it can clearly be seen the effect on the interface changes with the increasing stresses on the edges of

the unit cell and as the stresses increase the strains increase on the interface, in the grid patterns shown in figure B19 clearly shows the failure of the particulate as the stresses go beyond the ultimate tensile strength of the material.

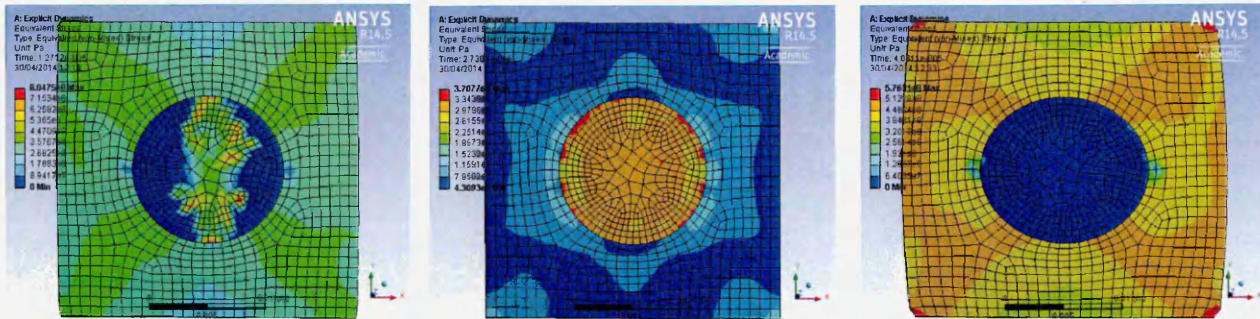


Figure B18: Strains

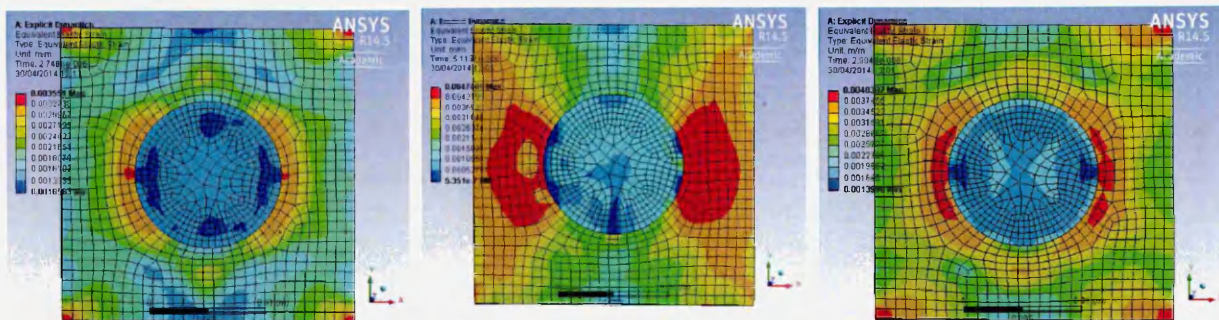


Figure B19: Stresses

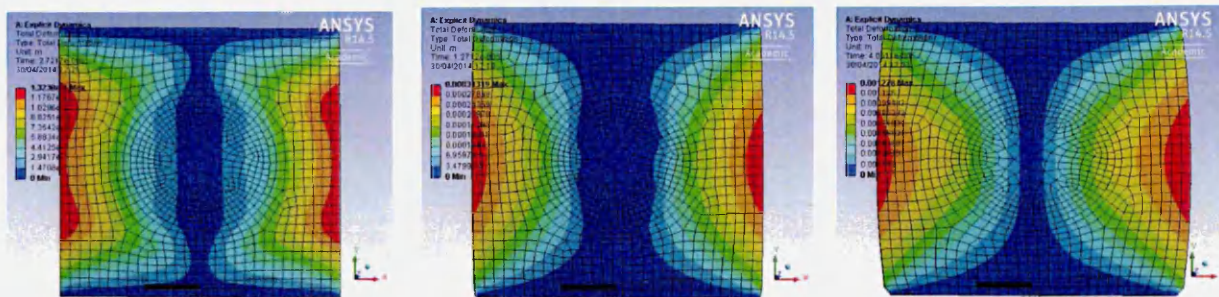


Figure B20: Total deformation

## **Appendix C: ANSYS APDL Code for Non-Linear Analysis**

The ANSYS APDL code is written for the non-linear analysis of particulate unit cell using finite element analysis. The code starts off with defining the file "PUZ" which is defined to store the results. The variables are then defined along with the number of subsets to be tested upon; in this study 400 subsets were considered. The unit cell shape is then defined and meshing controls are set (mapped meshing with tetrahedral element shape). Material properties are input in the system and then the composite unit cell is meshed. The whole composite unit cell is then symmetrized and display controls set. The non-linear hardening model which in our case is CHABOCHE is set. The problem is then solved by entering into the solution processor. Convergence is performed during the solution processor with a time stepping of 4 and the number of subsets defined are 400, in this step the type of analysis is defined, time stepping and the number of subsets is defined and finally before solving the degree of freedom are defined. The results are obtained by entering the time-history results post processor, the output array displays the results as defined according to the data file.

The layout of the program is given below,

-User Input

Define Variables

Define shape of unit cell

Meshing defined

input material properties

Non-linear hardening function defined

Mesh the whole composite

Symmetrize to make the whole volume

Display controls defined

Apply displacement controls

Define coupled nodes

-Output file setup

Define the displacement-time, table

-Solving the problem

Enter solution processor

Type of analysis defined

Convergence performed

Time stepping defined

No. of subsets

Degree of freedom defined

Solve

-Post processing

Enter the time-history results post processor

Define the no. of variables allowed

Specify the data file

Define output array

-Output results

Close down files

**!For Particulate unit cell Finite Element ANSYS**

**!Code for non linear analysis**

!EXPLANATION

!\*CREATE,PUZ,mac

FINISH

/CLEAR

/FILNAM,PUZ

/Title,PUZ                   !Name of output file

/OUTPUT, , data, ,           !Type of output file

/UIS,MSGPOP,3

PI=3.141592654

LENGTH=2.34299734756583

AREA=LENGTH\*LENGTH

VOF=0.1

    !\*IF,VOF,GT,0.523,OR,VOF,LT,0,THEN

!OR means true if either  
!clause is true, GT and LT  
!mean greater & lower than

    !\*MSG,ERROR

    !The volume fraction of fibers is invalid,%/&

    !\*ENDIF

R=(0.75\*VOF\*LENGTH\*LENGTH\*LENGTH/PI)\*(1/3)

!R=0.850000001

! Variables

!=====

EMAX=0.005

UMAX=EMAX\*LENGTH

UULT=0.0\*LENGTH

NSBSTMIN=400               !100

NSBST=NSBSTMIN

NSBSTMAX=2\*NSBST

/PREP7

!PREP7 commands are used to mesh solid models with  
!nodes and elements.

!-----Flexible function-----

!\*ASK,VOF,Enter the volume fraction (0 < VOF < 0.523),0.2

!\*ASK,LENGTH,Enter the side length of the single unit cell in real composite structure,100

! Define 1/8 shape

!=====

BLC4,,,LENGTH/2,LENGTH/2,LENGTH/2 . !BLC4, xcorner, ycorner, width, height,  
depth !creates a rectangular area

SPHERE,R,0,0,90

VSBW,2 !subtracts intersection of the working plane  
!from volumes (divides volumes)

VDELE,3, , ,1 !deletes unmeshed volumes

!0 - deletes volumes only

!1 - deletes volumes as well as keypoints, lines and areas attached to the specific volume

VOVLAP,ALL !overlaps volumes

VGLUE,ALL !Glue volumes

NUMCMP,VOLU !Compresses the numbering of defined  
items, volume to be compressed

! Meshing

!=====

ASEL,,,2,6,2 !Selects a subset of areas !ASEL, Type,  
!Item, Comp, vMIN, VMAX, VINC, KSWP

!VMIN - Minimum value of item range.

!VMAX - Maximum value of item range.

VMAX !defaults to VMIN.

!VINC - Value increment within range. Used  
!only with integer

!ranges (such as for area numbers). Defaults to 1.

!VINC cannot be negative.

!KSWP - Specifies whether only areas are to be  
!selected:

!0 - Select areas only.

!1 - Select areas, as well as keypoints, lines, Inodes, and elements associated with selected lareas. Valid only with Type = S.

ACCAT,ALL !Concatenates (join like a string ball+joint=balljoint) multiple lareas in preparation for mapped meshing  
ALLS !Selects all entities with a single command  
LCCAT,8,12 !Concatenates multiple lines into one line for mapped meshing  
LCCAT,5,10  
LCCAT,2,3  
MSHAPE,0,3D !For elements that support multiple shapes, specifies the lelement shape to be used for meshing  
MSHK,1 !type of meshing, 0-free meshing, 1-mapped meshing, 2-if possible used mapped otherwise free  
!Tetraheadral shaped elements  
  
ET,1,SOLID185 !ET is element type  
ESIZE,LENGTH/12 !element size

! Define material properties  
!=====

! Material #1  
!-----

MPTEMP,,,,,,,,  
MPTEMP,1,0  
MPDATA,EX,1,,450E9  
MPDATA,PRXY,1,,0.19

! Material #2  
!-----

MPTEMP,,,,,,,,  
MPTEMP,1,0  
MPDATA,EX,2,,71e9  
MPDATA,PRXY,2,,0.33

! Nonlinear Kinematic Hardening Specifications (CHABOCHE)

!=====

INTEMP - !Number of temperatures for which data will be provided. Default = 1. The maximum value of NTEMP is such that

NTEMP x (1 + 2NPTS) = 1000.

INPTS - Number of kinematic models to be superposed. Default = 1. Maximum = 5.

ITBOPT - Not used.

TB,CHAB,2,1,1.0,            !TB - Activates a data table  
                              !,material ref no, NTEMP-No.of temp's data will be  
                              !provided, NPTS-No. of data points,

TBTEMP,0  
TBDATA,,154,7019,118.6  
TB,NLIS,2,1,4,  
TBTEMP,0  
TBDATA,,154,0,140.2,7.094,,

! Mesh composites  
!=====

MAT,1  
VMESH,1                    !VMESH, NV1, NV2, NINC  
                              !Generates nodes and volume elements within volumes.  
                              !Mesh volumes from NV1 to NV2 (defaults to NV1) in steps of  
NINC                        !(defaults to 1).  
MAT,2  
VMESH,2

! Symmetrize to make whole volume  
!=====

VSYMM,X,ALL                !Generates volumes from a volume pattern by symmetry  
                              !reflection.  
VSYMM,Y,ALL  
VSYMM,Z,ALL

NUMMRG,NODE                !Merges coincident or equivalently defined Nodes  
NUMMRG,ELEM                !Merges coincident or equivalently defined Elements

NUMCMP,NODE                !Compresses the numbering of defined items.  
NUMCMP,ELEM

! Display control

!=====

/NUMBER,1           !Specifies whether numbers, colors, or both are used for  
displays.  
!0 - Color (terminal dependent) the numbered items and show  
numbers.  
!1 - Color the numbered items. Do not show the numbers.  
!2 - Show the numbers. Do not color the items.  
!-1 - Do not color the items or show the numbers.

/PNUM,MAT,1           !/PNUM, Label, KEY           !Controls entity  
numbering/coloring           !on plots.           !0-off, 1-on  
EPLOT           !Produces an element display.  
/UIS,MSGPOP,1       !/UIS, Label, VALUE       !Controls the GUI behaviour.  
!MSGPOP — Controls which messages from the ANSYS  
error message subroutine       are displayed in a  
message dialog box.  
!Values controlling behaviour if Label = MSGPOP:  
!0 - All messages displayed.  
!1 - Only notes, warnings, and errors displayed.  
!2 - Only warnings and errors displayed (default).  
!3 - Only errors displayed.

!Apply displacement constraints

!-----

NSEL,S,LOC,Z,-LENGTH/2           !NSEL, Type, Item, Comp, VMIN, VMAX,  
VINC, KABS  
!Selects a subset of nodes.  
!S - Select a new set (default).

D,ALL,UZ,  
NSEL,ALL

D,NODE(0,0,-LENGTH/2),ALL

!Define coupled nodes

!-----

NSEL,S,LOC,Y,-LENGTH/2  
CP,1,UY,ALL           !CP, NSET, Lab, NODE1, NODE2, ..... ,NODE17

!Defines (or modifies) a set of coupled degrees of freedom.

!NSET - Set reference number   In - Arbitrary set number.

!Lab - Degree of freedom label for coupled nodes

NSEL,ALL

NSEL,S,LOC,Y,LENGTH/2  
CP,2,UY,ALL  
NSEL,ALL

NSEL,S,LOC,X,-LENGTH/2  
CP,3,UX,ALL  
NSEL,ALL

NSEL,S,LOC,X,LENGTH/2  
CP,4,UX,ALL  
NSEL,ALL

! Obtain the numbers of the nodes on the top  
!=====

NSEL,S,LOC,Z,LENGTH/2  
\*GET,NTCOUNT,NODE,,COUNT

\*GET, Par, Entity, ENTNUM, Item1, IT1NUM, Item2, IT2NUM  
!Retrieves a value and stores it as a scalar parameter or part of  
!an array parameter.

\*DIM,NTNUM,ARRAY,NTCOUNT

!\*DIM, Par, Type, IMAX, JMAX, KMAX, Var1, Var2, Var3, CSYSID  
!Defines an array parameter and its dimensions.

\*GET,NTNUM(1),NODE,,NUM,MIN  
\*DO,I,2,NTCOUNT  
    NTNUM(I)=NDNEXT(NTNUM(I-1))  
\*ENDDO  
NSEL,ALL

! Define the displacement-time table

!=====

\*DIM,DISPL,TABLE,5,1,1

\*SET,DISPL(0,1,1),0

!\*SET, Par, VALUE, VAL2,....., VAL10

!Assigns values to user-named parameters.

\*SET,DISPL(1,0,1),0

\*SET,DISPL(2,0,1),1

\*SET,DISPL(2,1,1),UMAX

\*SET,DISPL(3,0,1),2

\*SET,DISPL(3,1,1),0

\*SET,DISPL(4,0,1),3

\*SET,DISPL(4,1,1),-UMAX

\*SET,DISPL(5,0,1),4

\*SET,DISPL(5,1,1),UULT

! Solve the problem

!=====

SAVE,MODEL

!SAVE, Fname, Ext, --, Slab

!Saves all current database information.

!The extension defaults to DB if Fname is blank.

!Slab - Mode for saving the database:

!ALL - Save the model data, solution data and post data

!(element tables, etc.). Default Value.

/SOLU

!enter the solution processor

!RESUME,MODEL

ANTYPE,STATIC

!ANTYPE, Antype, Status, LDSTEP, SUBSTEP, Action

!Specifies the analysis type and restart status.

!STATIC or 0 - Perform a static analysis. Valid for all

!degrees of freedom.

AUTOTS,ON

!AUTOTS, Key !Specifies whether to use automatic

!time stepping or load stepping.

!Key - Automatic time stepping key

!OFF - Do not use automatic time stepping.

!ON - Use automatic time stepping.

!AUTO - The program determines whether to use

!automatic time stepping. This option is recommended.



!Specifies the data file where results are to  
!be found.

\*DIM,UZTOP,ARRAY,NSBSTMAX           !Defines an array parameter and its  
!dimensions.

NSOL,2,NODE(0,0,LENGTH/2),U,Z,UZ\_2   !NSOL, NVAR, NODE, Item, Comp,  
!Name, SECTOR  
!Specifies nodal data to be stored  
!from the results file.

VGET,UZTOP,2,0                   !VGET, Par, IR, TSTRT, KCPLX  
!Moves a variable into an array parameter  
!vector.  
!Par - Array parameter vector in the  
!operation.  
!IR - Reference number of the variable (1 to  
!NV [NUMVAR]).  
!TSTRT - Time (or frequency)  
!corresponding to start of IR data.  
!If between values, the nearer value is used.  
!KCPLX - Complex number key:  
!0 - Use the real part of the IR data.  
!1 - Use the imaginary part of the IR data.

\*VOPER,UZTOP(1),UZTOP(1),DIV,LENGTH   !\*VOPER, ParR, Par1, Oper, Par2,  
!CON1, CON2  
!Operates on two array parameters.

\*DIM,RFTMP,ARRAY,NSBSTMAX           !\*DIM, Par, Type, IMAX, JMAX, KMAX,  
!Var1, Var2, Var3, CSYSID  
!Defines an array parameter and its  
!dimensions.

\*DIM,RFSUM,ARRAY,NSBSTMAX           !Defining an array named RFSUM

\*DO,I,1,NTCOUNT  
RFORCE,3,NTNUM(I),F,Z,FZ\_3           !RFORCE, NVAR, NODE, Item,  
!Comp, Name  
!Specifies the total reaction force data to be stored.  
!NVAR - Arbitrary reference number assigned to  
!this variable (2 to NV [NUMVAR]).  
!Overwrites any existing results for this variable.  
!NODE - Node for which data are to be stored.

!Item - Label identifying the item. Some items also  
!require a component label.  
!Comp - Component of the item (if required).  
!Name - name identifying the item on printouts and  
!displays.  
!Defaults to an eight character label formed by  
!concatenating the first four characters of the Item  
!and Comp labels.

VGET,RFTMP,3,0  
VARDEL,3

!VARDEL, NVAR  
!Deletes a variable (GUI).  
!NVAR - The reference number of the variable to  
!be deleted.  
!NVAR is as defined by NSOL, ESOL, etc.

\*VOPER,RFSUM(I),RFSUM(I),ADD,RFTMP(I) !\*VOPER, ParR, Par1, Oper, Par2,  
CON1, CON2

!Operates on two array parameters.

\*ENDDO

\*VOPER,RFSUM(1),RFSUM(1),DIV,AREA

!\*CFOPEN,Z,txt,,  
!\*VWRITE,UZTOP(1),RFSUM(1)  
!(F10.5,X,F10.5)  
!\*CFCLOSE

!\*END

## Appendix D: ANSYS APDL Code with Cohesive Zone Element Analysis

A sample APDL code is listed below for the addition of the cohesive zone element in the unit cell as the interface.

```
! Define material properties
!=====

MP,EX,1,450E9!      ! Define material properties of particles
MP,PRXY,1,0.19
MP,ALPX,1,5E-6

MP,EX,2,71e9      ! Define material properties of matrix
MP,PRXY,2,0.33
MP,ALPX,2,54E-6

ET,3,204          !Introducing a cohesive zone material
                  !204=3D 16 Node quadratic element

TB,CZM,1,2,,CBDD  !CBDD= A linear elastic material behavior with linear
                  !softening characterized by maximum traction and
                  !maximum separation (OTHER OPTION = EXPO)

TBDATA,1,1,1,1,1  !TBDATA,1,smax, ,tmax, ,?,β

MP,EX,3,100E9     ! Define material properties of interface
MP,PRXY,3,0.19
MP,ALPX,3,54E-6

! Define element type and size
!=====

et,1,95           !SOLID95 is a higher order version of the 3-D 8-node solid
                  !element (SOLID45)
```

esize,Length/12

!original Length/4

! Mesh composites

!=====

MAT,1

VMESH,1

!VMESH, NV1, NV2, NINC

!Generates nodes and volume elements within volumes.

!Mesh volumes from NV1 to NV2 (defaults to NV1) in steps of

!NINC (defaults to 1).

MAT,2

VMESH,2

CZMESH,1,2,,,

!Meshing the cohesive zone material

EGEN,1,100,ALL,,,,,,,,,

MAT,2

VMESH,3

## **Appendix E: Fatigue Analysis**

### **SUMMARY**

After the finalization of the unit cell as described in chapter 4, fatigue analysis was conducted; the same model of the unit cell is used here but in the ANSYS APDL environment, as this gives a much better control if cyclic loadings are applied. The following experiments on simulations were done and the ductility of the composite was studied with 20% and 31% volume fraction of SiC in Al matrix. It was observed that as the volume fraction of the reinforcement was increased the ductility was decreased.

### **E.1 Introduction**

A lot of development of Metal Matrix Composites has been done of monolithic lightweight alloys having inadequate fatigue resistance for many demanding applications. The use of a high stiffness ceramic reinforcement in particulate form, such as SiC, can result in a substantial increase in fatigue resistance while maintaining low cost. The fatigue resistance of particulate MMCs depends on a variety of factors, including volume fraction of the reinforcement, particle size, matrix microstructure, the presence of inclusions or defects that arise from processing, and testing environment.[173-175] The effect of some of these factors on the fatigue behaviour of particle reinforced MMCs is summarized in this chapter. Here stress versus number of cycles (S-N) fatigue behaviour is focused.

In the composite, most of the load is carried by the high strength reinforcement, so for a given stress, the composite undergoes a lower average strain than the

unreinforced alloy, thus improving the fatigue lives of particle reinforced MMCs as compared to unreinforced metals. These improvements are most pronounced at lower stresses, in the high cycle fatigue regime, while at high stress the differences between reinforced and unreinforced materials are reduced. This can be attributed to "ductility exhaustion" of the composites in the low cycle fatigue regime. With decreasing particle size, for a given reinforcement volume fraction, the reinforcement inter-particle spacing decreases, resulting in more barriers for the reversible slip motion that takes place during fatigue, and a decrease in strain localization by cyclic slip refinement [176]. Narrowing of the particle size range distribution also results in higher fatigue life, particularly when eliminating larger particles that are more prone to cracking [177].

In addition to particle reinforcement, the matrix microstructure also significantly influences the fatigue behaviour of the composite. Factors affecting the matrix microstructure include shape, size and spacing of precipitates and grain size. The normal trend in composites with regards to grain size is similar to monolithic materials, and hence for a given matrix alloy composition and volume fraction of reinforcement, finer grain sizes generally result in improved properties. Contrary to conventional monolithic materials, in MMCs high matrix yield and ultimate tensile strength do not necessarily reflect high fatigue strength.

Precipitates should be of sufficient size to not be susceptible to precipitate shearing, but completely coherent with the matrix to impose repulsive stress fields against dislocation motion [167]. These mentioned defects increase the local stress intensity in the material and promote easy crack nucleation acting as stress concentrators. Studies show that crack initiation during fatigue takes place at these defects, which

are typically located at the surface of the specimen [177]. This is because inclusions at the surface are more highly stressed than inclusions completely within the matrix (where more load is borne by the reinforcement), so a higher stress concentration and, thus, higher probability for crack initiation is present at the surface. In a composite where the inclusion is surrounded by high stiffness reinforcement particles the stress concentration is lower than in the unreinforced alloy. Since more of the load is being shared by the high stiffness SiC particles in the composite.

To understand the fatigue performance, cyclic stress-strain behaviour needs to be analysed. In short-fibre reinforced composites [178], even when the matrix is assumed to exhibit isotropic hardening behaviour, the particle reinforced composites shows a distinct Bauschinger effect upon reversed loading [179-180], through the examination of the evolution of local stress field, that the apparent early reversed yielding for the composite arises from the non-uniformity of deformation in matrix caused by the constraint imposed by the brittle reinforcement. Thus, high local effective stresses trigger early local yielding after the load is reversed. The above micro-plasticity effect in the composite is the same mechanism that causes the experimentally observed early deviation from linearity of the tensile stress-strain curve for metal matrix composites compared to the monolithic matrix material observed experimentally [181]. Hence, although the composite shows much higher macroscopic yield strength the proportional limit for the composite is actually lower than that of monolithic matrix material.

## **E.2 Model**

In order to adequately model the stabilized cyclic response without encountering elastic shake-down, in the modelling presented below kinematic hardening was

assumed for the matrix with its elastic-plastic behaviour taken from the experimental stress-strain behaviour of the unreinforced Al alloy. A unit-cell model was used for the analysis. Using the symmetry conditions, a quarter model was observed for faster analysis. As seen in figure E21 (A) it can clearly be seen the two materials Al which is represented in red and the SiCp which is represented in in blue and both the materials for the sake of analysis are glued together and the measurements are taken on the interface where the two materials meet. Figure E21 (B) shows the meshing which was used during the analysis. Figure E21 (C) shows the symmetry used for the model and the fixed supports and all the measurements were recorded on zero degrees on the interface in the direction of the forces applied on the key-point as shown in figure E21 (D). The stress amplitude imposed is 350 MPa, which is well below the elastic limit of 489 MPa for the unreinforced alloy.

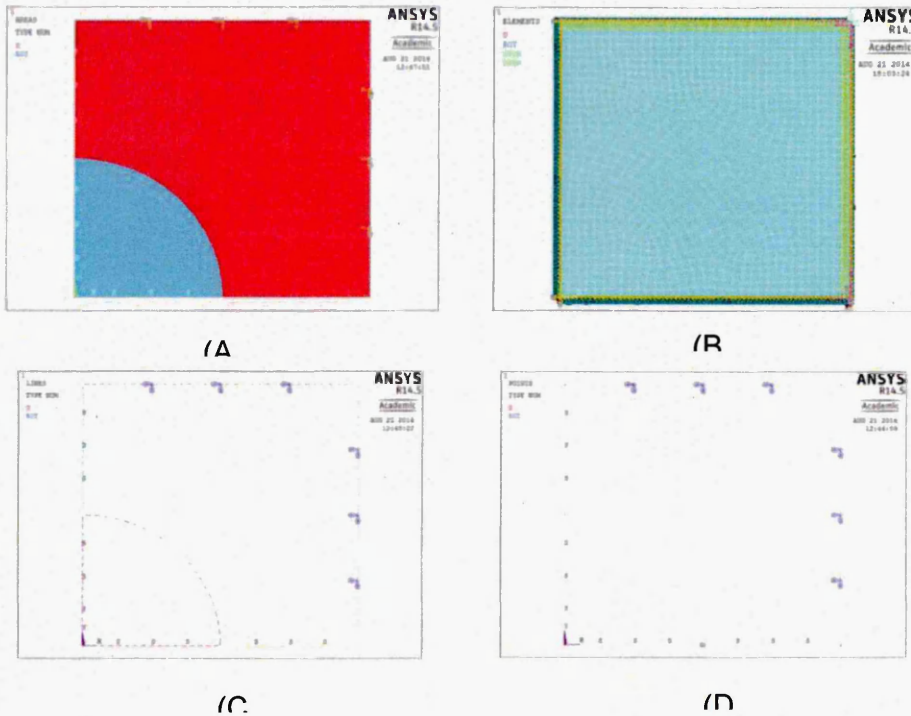


Figure E21: (A) A quarter model of the unit cell (Al in red and SiCp in blue) (B) The Meshing (C) Symmetry used for the model and the fixed supports (D) Key point at 0 degrees.

### E.3 The Strain Life Approach

The Strain Life approach is widely used as it can be directly measured and has been shown to be an excellent quantity for characterizing low-cycle fatigue. Strain Life is typically concerned with crack initiation, whereas Stress Life is concerned with total life and does not distinguish between initiation and propagation. In terms of cycles, Strain Life typically deals with a relatively low number of cycles and therefore addresses Low Cycle Fatigue (LCF), but works with high numbers of cycles as well. Low Cycle Fatigue usually refers to fewer than  $10^5$  cycles. Stress Life is based on S-N curves (Stress – Cycle curves) and has traditionally dealt with relatively high numbers of cycles and therefore addresses High Cycle Fatigue (HCF), greater than  $10^5$  cycles inclusive of infinite life.

The Strain Life Relation equation is shown below which is used by ANSYS:

$$\frac{\Delta\varepsilon}{2} = \frac{\sigma_f}{E} (2N_f)^b + \varepsilon_f (2N_f)^c \quad (71)$$

The two cyclic stress-strain parameters are part of the equation below:

$$\Delta\varepsilon = \frac{\Delta\sigma}{E} + 2 \left( \frac{\Delta\sigma}{2K} \right)^{\frac{1}{n}} \quad (72)$$

Where:

$$\frac{\Delta\varepsilon}{2} = \text{Total Strain Amplitude}$$

$$\Delta\sigma = 2 \times \text{the stress amplitude}$$

$$E = \text{Modulus of elasticity}$$

$N_f$  = Number of cycles of failure

$2N_f$  = Number of reversals to failure

And the parameters required for the strain life analysis are:

$\sigma_f$  = Fatigue strength Coefficient

B = Fatigue strength Exponent (Basquin's Exponent)

$\varepsilon_f$  = Fatigue Ductility Coefficient

C = Fatigue Ductility Exponent

K = Cyclic Strength Coefficient

n = Cyclic Strain Hardening Exponent

Note that in the above equation, total strain (elastic + plastic) is the required input. However, running an FE analysis to determine the total response can be very expensive and wasteful, especially if the nominal response of the structure is elastic. An accepted approach is to assume a nominally elastic response and then make use of Neuber's equation to relate local stress/strain to nominal stress/strain at a stress concentration location.

According to Neuber's rule, the strain and stress can be related as,

$$\varepsilon\sigma = K_t^2 eS \quad (73)$$

Where:

$\varepsilon$  = Local (Total) Strain

$\sigma$  = Local Stress

$K_t$  = Elastic Stress Concentration Factor

$e$  = Nominal Elastic Strain

$S$  = Nominal Elastic Stress

Thus by simultaneously solving Neuber's equation along with cyclic strain equation, the local stress/strains (including plastic response) given only elastic input can be calculated. Note that this calculation is nonlinear and is solved via iterative methods. Also note that ANSYS fatigue uses a value of 1 for  $K_t$ , assuming that the mesh is refined enough to capture any stress concentration effects. This  $K_t$  is not be confused with the Stress Reduction Factor option which is typically used in Stress life analysis to account for things such as reliability and size effects.

#### **E.4 Inputs for the Fatigue Analysis**

The following inputs were chosen for the cyclic loading experiments

##### **E.4.1 Cyclic Loading**

Unlike static stress, which is analysed with calculations for a single stress state, fatigue damage occurs when stress at a point changes over time. There are essentially four classes of fatigue loading supported by ANSYS:

- Constant amplitude, proportional loading
- Constant amplitude, non-proportional loading
- Non-constant amplitude, proportional loading
- Non-constant amplitude, non-proportional loading

The loading is a variant of a sine wave with a single load ratio, with the load ratio changing with time. Secondly the proportionality describes whether the changing load causes the principal stress axes to change. If the principal stress axes do not change, then it is proportional loading. If the principal stress axes changes, then the cycles cannot be counted and it is non-proportional loading.



Figure E22: An example of constant Amplitude Fully Reversed cycle.

Constant amplitude, proportional loading is the classic, calculation describing whether the load has a constant maximum value or continually varies with time. Constant amplitude proportional loading is used and hence only one set of FE stress results along with a loading ratio is required to calculate the alternating and mean values. The loading ratio is defined as the ratio of the second load to the first load ( $LR = L2/L1$ ). Loading is proportional since only one set of FE results are needed (principal stress axes do not change over time). Common types of constant amplitude loading are fully reversed (apply a load, then apply an equal and opposite load; a load ratio of  $-1$ ) and zero-based (apply a load then remove it; a load ratio of  $0$ ). Since loading is proportional, looking at a single set of FE results can identify critical fatigue locations. Likewise, since there are only two loadings, no cycle counting or cumulative damage calculations need to be done.

#### **E.4.2 Multiaxial Stress Correction Factors**

The Experimental test data which was to be compared was uniaxial whereas the FE results obtained were multi-axial, for this reason the stresses were converted from a multi-axial stress state to a uniaxial one. Von-Mises, and maximum principal stress component of the stresses were used to compare against the experimental uniaxial stress values. A "signed" Von-Mises stress was chosen where the Von-Mises stress takes the sign of the largest absolute principal stress.

#### **E.4.3 Value of Infinite Life**

Another available option when conducting a variable amplitude fatigue analysis is the ability to set the value used for infinite life. In constant amplitude loading, if the alternating stress is lower than the lowest alternating stress on the fatigue curve, the fatigue tool in ANSYS uses the life at the last point. This provides for an added level of safety because many materials do not exhibit an endurance limit. However, in non-constant amplitude loading, cycles with very small alternating stresses may be present and may incorrectly predict too much damage if the number of the small stress cycles is high enough. To help control this, the infinite life value was set as, if the alternating stress goes beyond the limit of the SN curve. Setting a higher value makes small stress cycles less damaging if they occur many times, the first damage matrix was calculated with an infinite life of  $1e^6$  cycles and the second was calculated with an infinite life of  $1e^9$  cycles.

#### E.4.4 Fatigue Strength Factor

Fatigue material property tests are usually conducted under very specific and controlled conditions. If the service part conditions differ from the as tested conditions, modification factors can be applied to try to account for the difference. The fatigue alternating stress is usually divided by this modification factor and can be found in design handbooks. (Dividing the alternating stress is equivalent to multiplying the fatigue strength by  $K_f$ .) Fatigue Strength Factor ( $K_f$ ) reduces the fatigue strength and must be less than one. Note that this factor is applied to the alternating stress only and does not affect the mean stress.

#### E.5 Predictions and Correlations

For the Fatigue analysis the quarter model of the unit cell as described in chapter 4 was used and the model along with its meshing is shown in figure E22. The figure also demonstrates the unloaded and the loading conditions with its deformations.

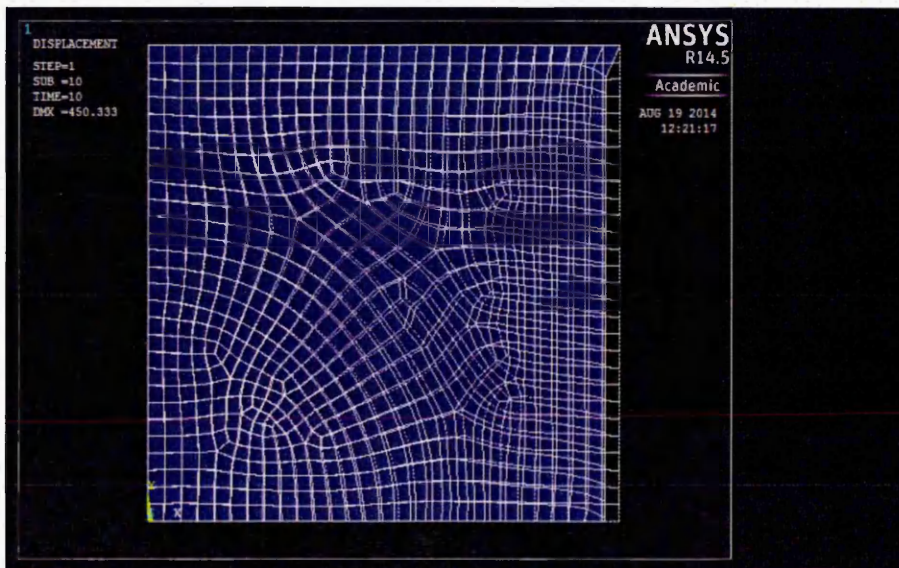


Figure E23: Meshing, Loaded and Unloaded condition of the quarter model unit cell.

A Constant amplitude, proportional loading was applied with a magnitude of 260 and Eq. 74 was used on the right side of the quarter section for applying the load, as the quarter model was symmetrical the load was automatically applied on the opposite side, giving us a uniform model of a unit cell analysed with loading on both sides.

$$Y = 260 \times \text{Cos}(\text{time}) \tag{74}$$

Von Mises Stresses were observed for the purpose of cancelling out the multi-axial stress correction factors at  $10^0$ ,  $10^1$  and  $10^2$  cycles with a step of 1 for low frequency, then for  $10^3$ ,  $10^4$ ,  $10^5$  and  $10^6$  cycles the step was increased to 1000 for High frequency and it can clearly be seen in figure E24 where the stresses are compared with the number of cycles and as expected as the stresses increase, the number of cycles to failure reduce.

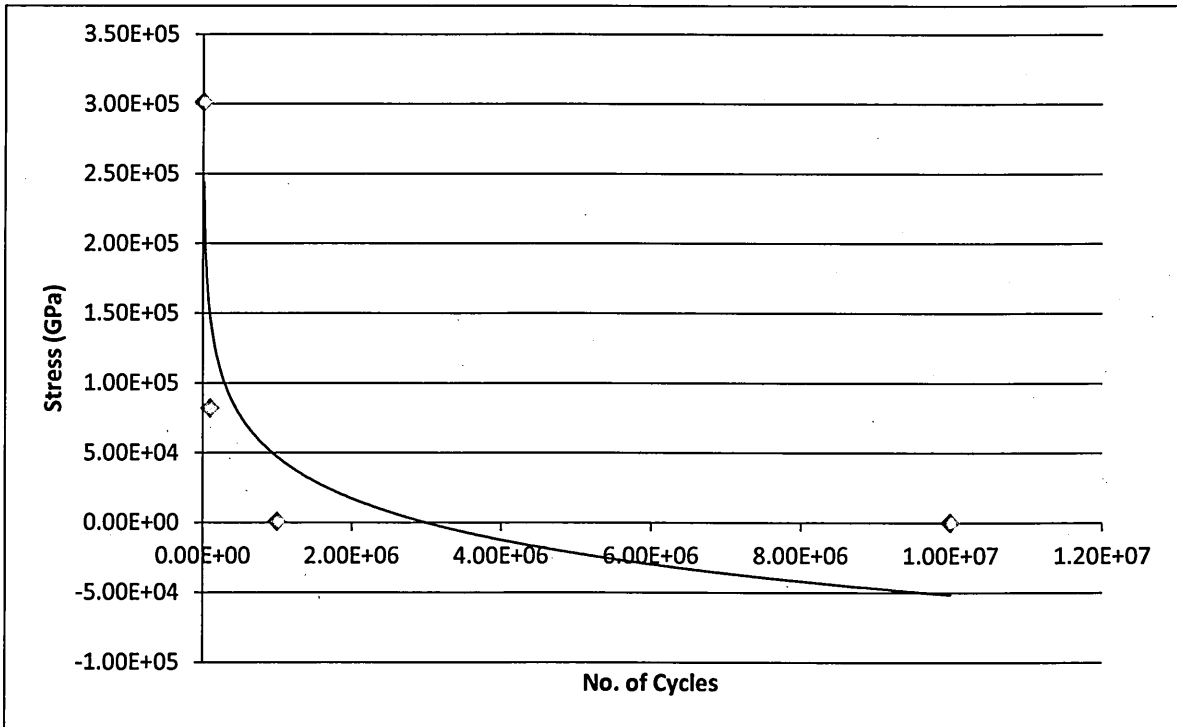


Figure E24: Stress vs Number of cycles, SN Curve.

Another analysis was done with the quarter section with a transient cyclic load of  $260 \cdot \cos(\text{time})$  where the number of cycles were kept constant at 1,000,000 ( $10^6$ ) and the frequency of the results were varied from  $10^3$ ,  $10^2$  and  $10^1$  and stresses were recorded. An important factor noted was the confirmation of the strain levels around the matrix, reinforcement and the interface. Using the same quarter model of the unit cell, strain levels were measured at the 3 points indicated by the red arrows in figure E26 (A). The center arrow is on the interface, the arrow to its right is on the matrix and the one on extreme left is on the reinforcement. All the measurements are done very close to the interface to get a good idea of the strain levels on the three different areas. As expected the strain levels were much higher in the matrix as compared to the reinforcement, but the maximum levels of strain were observed on the interface. The strain levels are also shown in figure E25 (B).

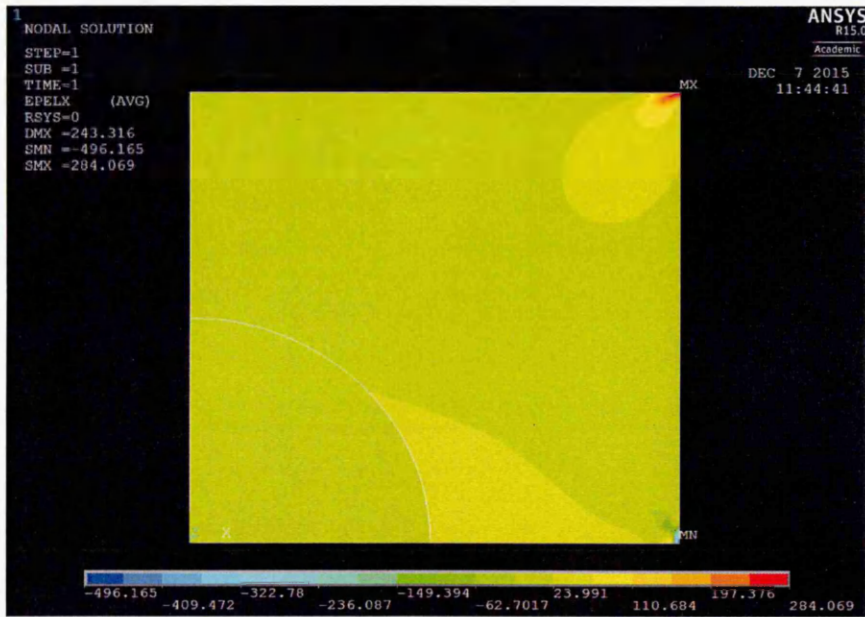
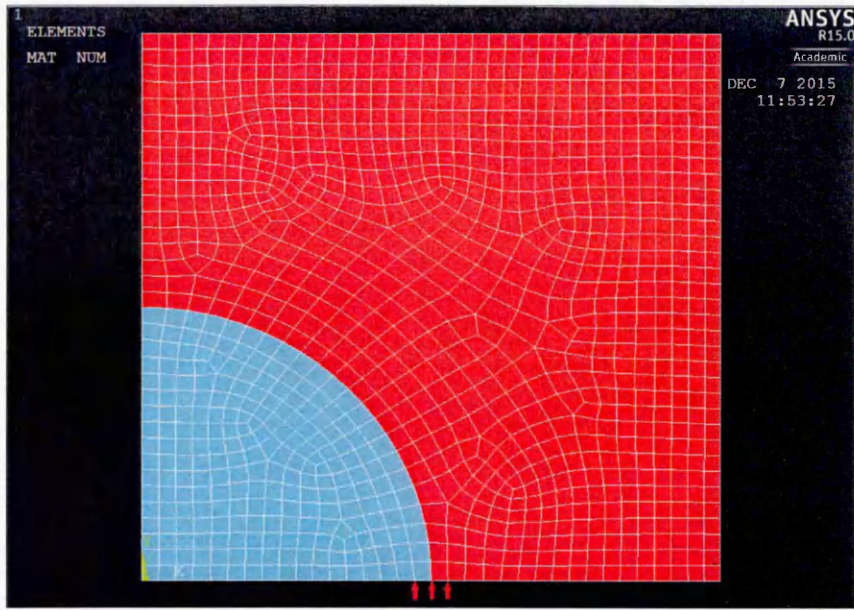


Figure E25: (A) Quarter model of Unit cell showing the points where strains were measured (B) Strain levels in the same quarter model of the unit cell

## **Appendix F: List of Publications and Posters**

1. "A Micromechanics Model for the Determination of Interfacial Fracture Toughness in Particulate Composites", Syed A. A. Shah, S. T. Hasan, Wenbin Yu, Hamsasew. M. Sertse. Submitted, International journal of engineering science, Elsevier, 2016, under review.
2. "Modelling non-linear response of SiC reinforced aluminium alloy", To be published in Elsevier special Journal issue, in press.
3. "Numerical Simulation and Modelling of Al/SiC" Accepted for oral presentation at Advances in Materials & Processing Technology Conference, 14-17-Dec-2015, Madrid, Spain.
4. "Predicting micro-mechanics damage behaviour at a metal-ceramic interface in a reinforced alloy" Accepted for publishing in Key Engineering Materials, Vol.665 in 2016. The title of the Vol. is Advances in Fracture and Damage Mechanics XIV.
5. "Numerical Simulation and Modelling of Al/SiC" presented at the MERI Symposium Sheffield Hallam University, UK, 19-20 May 2015.

6. "An Empirical Method Of Calculating Interfacial Strength In A Second Phase Reinforced Alloy", S. A. A. Shah and S. T. Hasan, Advances in Materials and Processing Technology (AMPT) Journal, in press.
7. "Analytical Solution of Isothermal Fatigue Crack Growth in Solid Cylinder", M.A.Nasser, S.T.Hasan and Syed A A Shah. Advances in Materials and Processing Technology (AMPT) Journal,2015.
8. "Modelling Strain on the Interface of Al/SiC", S.A.A.Shah, S.T.Hasan and M.D.Brahmhall , MERI/BMRC Winter Poster Event, Sheffield Hallam University, UK, 11 November 2014
9. "Micro-Mechanics modelling of Smart Structures", S.A.A.Shah, S.T.Hasan and M.D.Brahmhall, MERI Symposium, Sheffield Hallam University, Sheffield, United Kingdom.13-14 May 2014.
- 10."Modelling and Simulation of Interfacial Strengthening Behaviour of a Metal Matrix Composite System", S.A.A.Shah and S.T.Hasan, National Student Conference in Metallic Materials, 26-27 June 2014, The Ridge, University of Sheffield, Sheffield, United Kingdom.

## PUBLICATIONS

1. Syed A A Shah and Syed T Hasan, "An empirical method of calculating interfacial strength in a second phase reinforced alloy", *Advances in Materials & Processing Technology Journal*, accepted, 2015. DOI: 10.1080/2374068X.2015.1121719.

### **Abstract:**

Innovations in MMCs are beginning to pay off with new military and commercial developments underway. Engineered solutions, capitalising on the advantages of light weight and effective thermal performance, are proving the superiority of MMCs over traditional approaches and materials. As a technology-driven 21st century dawns, demand for better performance, productivity and/or efficiency in transportation, aerospace and industrial processes/products will increasingly require the use of these remarkable composite materials. The understanding of the interfacial strengthening mechanisms, therefore, is the key factor for optimising the properties of these remarkable new advanced materials.

A method of calculation has been applied in order to predict the interfacial fracture strength of aluminium, in the presence of silicon segregation. The interface fracture toughness was determined as a function of the macroscopic experimental measurements (mechanical properties of the composite) and the microscopic modification parameters (tailoring of interface properties). The model shows success in making prediction possible of trends in relation to segregation and interfacial fracture strength behaviour in SiC particle-reinforced aluminium matrix composites.

The model developed here can be used to predict possible trends in relation to segregation and the interfacial fracture strength behaviour in metal matrix composites. The results obtained from this work conclude that the role of precipitation and segregation on the mechanical properties of Al/SiC composites is crucial, affecting overall mechanical behaviour.

2. M.A.Nasser, Syed T Hasan and Syed A A Shah, " Analytical Solution of Isothermal Fatigue Crack Growth in Solid Cylinder", Advances in Materials & Processing Technology Journal, accepted, 2015, in press.

**Abstract:**

Nowadays many industries deal with components which are subjected to high loads at elevated temperatures than before due to the increasing requirements regarding weight and performance. The simplest process to check the behaviour of the material at high temperature is the isothermal fatigue (IF), by designing a fatigue cycle at constant and uniform temperature to estimate stress-strain required to predict fatigue life of the material. Generally it is assumed that the maximum temperature in the loading cycle represents the most damaging condition likely to be experienced during service life of the component.

An empirical isothermal fatigue model for solid cylinder subjected to constant temperature superimposed with sinusoidal mechanical load applied at different stress levels is being proposed. Linear equations are developed to describe the severity of the temperature gradient, thermal stresses, and stress and strain intensity factors through the solid cylinder wall as function of time. Results show the effect of

temperature can be explained as increase in von-Mises thermal stress increase as a function of increasing temperature. The highest stress at 400 °C recorded is due to inherent hardness increased of the material indicated by high modulus of elasticity. The mechanical stress is more effective than thermal loading and results show that the stress intensity factor decreases with temperature, except at 400 °C (due to hardness increase).

3. Syed A A Shah and Syed T Hasan, "Numerical Simulation and Modelling of Al/SiC", Accepted for oral presentation at Advances in Materials & Processing Technology Conference (AMPT), 14-17-Dec-2015, Madrid, Spain

**Abstract:**

Metal Matrix Composites (MMCs) have educed a lot of interest for many high temperature and aerospace applications as structural materials, due to their strong strength and light weight. Depending upon the processing of the MMC the performance can vary, but is significantly dependent upon the matrix-reinforcement interface. As the MMC attempts to deform during processing, at micro-level the development of local concentration gradients around the reinforcement can be very different to the nominal conditions and play a crucial role in important micro structural events such as segregation and precipitation at the matrix-reinforcement interface. These events dominate the cohesive strength and subsequent mechanical properties of the interface; hence it is important to understand the interfacial strengthening mechanisms of metal matrix composites.

In this study a modest attempt has been made to simulate a hard particulate reinforced Al alloy system using ANSYS. The results indicate an increasing trend of hardness and impact strength with increase in percentage of SiC, Since the linear part of the stress strain data forms the basis of maximum design load for structural data, the linear part of the stress strain curve has been studied in depth and verifications of the results have been made on three different heat treated Al-SiC metal matrix composites, using 20% and 31% volume fraction of SiC in Al. This research will help to identify the key processing parameters controlling the fracture at matrix-reinforcement interface and simplify the dependency of large number of variables proposed in the constitutive model to predict interfacial strength of reinforced MMC. The stress-strain response at matrix reinforcement interface will form the basis of correlating empirical to numerical results. The method of analysis proposed will help the design engineers to incorporate advanced MMC's in real life applications.

4. Syed A A Shah and Syed T Hasan, "Predicting micro-mechanics damage behaviour at a metal-ceramic interface in a reinforced alloy ", Key Engineering Materials, Vol.665, 2016. Vol. Advances in Fracture and Damage Mechanics XIV.

**Abstract:**

The performance of metal matrix composites (MMCs) depends critically on the quality of the matrix-reinforcement interface. The nature of the interface in turn depends on the processing of the MMCs. At the micro-level, local concentration

gradients around the reinforcement are being developed during processing and due to the metal matrix attempting to deform during deformation which can be very different to the nominal conditions. This plays a crucial role in the development of micro-structural events such as segregation and precipitation at the matrix-reinforcement interface. Micro-deformation characteristics of matrix reinforcement interface are modelled using commercial FE software and compared with analytical and experimental data. A method of calculation has been applied to predict the interfacial fracture strength of aluminium silicon carbide (Al-SiC) with 20% and 31% Vol fraction. Preliminary results show that the model succeeds in predicting the trends in relation to segregation and intergranular fracture strength behaviour in these materials. The proposed hypothesis will help the design engineers to select and use the materials in structural/load bearing applications. Interfacial strengthening characteristics will in turn give more accurate life predictions of such smart composite systems.

5. Syed T Hasan and Syed A A Shah, "Modelling non-linear response of SiC reinforced aluminium alloy ", accepted, Elsevier special Journal issue, Under Review, December

**Abstract:**

Metal matrix composites (MMCs) such as Al/SiC have received considerable attention within a number of different industries including the aerospace, automobile, sports equipment and many others on account of their enhanced structural performance such as their high strength to weight ratio, ease of manufacturing and

recyclability. Silicon carbide (SiC) is a ceramic material and is used widely in high temperature structural applications and utilised as reinforcement in composite material to improve the mechanical properties.

This paper reports a finite element study of non-linear response effect of load on silicon carbide (SiC) reinforced Aluminium alloys interfacial Stress/Strain characteristics. The non-linear behaviour of the composite is simulated by using ANSYS finite element package, using a unit cell model and applying appropriate boundary conditions. An attempt is made to study the influence of different volume fractions of the reinforcement on the stress transfer from matrix to particle analysis, it is found that the volume fraction of the particulate plays an important role in the ductility and overall fracture toughness of the composite, also the results show that de-bonding is more pronounced in the interfacial element near the axis of symmetry.

6. Syed A A Shah, Syed T Hasan, Wenbin Yu and Hamsasew. M. Sertse, "A Micromechanics Model for the Determination of Interfacial Fracture Toughness in Particulate Composites", Submitted, International journal of engineering science, Elsevier, 2016, under review.

**Abstract:**

The fracture at the interface of particulate-reinforced metal matrix composites (MMCs) are influenced by several factors like volume fraction of the reinforcement, the particle size of the reinforcement and inter-particle spacing of the reinforcement. In this paper a method of calculation has been applied to predict the interfacial

fracture toughness in a particulate reinforced composite. The composite used in this study is silicon carbide (SiC) reinforced with aluminum (Al) matrix, in the presence of silicon segregation. The model presented here shows success in predicting trends in relation to segregation and interfacial fracture strength behavior in particulate MMCs. The numerical simulation is done based on strain rather than stress which has proven to be more accurate when compared with the experimental data. Due to segregation small changes in surface energy are caused which in return changes the interfacial fracture stress tremendously. The importance of interface in MMCs is for a lot of reasons like in determining the amount of predicted segregation and hence the change of the interfacial energy caused by the segregation. In this paper equations have been predicted to forecast the energy change in terms of the coincidence site stress which is the value describing the interface, along with the energies formed due to the impurities particularly at the interface. Software simulation is also done using VAMUCH and ANSYS to cater for the linear and non-linear behavior of the composite respectively. In the end we have tried to predict the interfacial strength based on the fracture toughness properties of the interface of the MMC.

7. M.A.Nasser, S.T.Hasan and Syed A A Shah. "Analytical Solution of Isothermal Fatigue Crack Growth in Solid Cylinder", Advances in Materials and Processing Technology (AMPT) Journal,2015.

### **Abstract.**

Nowadays many industries deal with components which are subjected to high loads at elevated temperatures than before due to the increasing requirements regarding

weight and performance. The simplest process to check the behaviour of the material at high temperature is the isothermal fatigue (IF), by designing a fatigue cycle at constant and uniform temperature to estimate stress-strain required to predict fatigue life of the material. Generally it is assumed that the maximum temperature in the loading cycle represents the most damaging condition likely to be experienced during service life of the component.

An empirical isothermal fatigue model for solid cylinder subjected to constant temperature superimposed with sinusoidal mechanical load applied at different stress levels is being proposed. Linear equations are developed to describe the severity of the temperature gradient, thermal stresses, and stress and strain intensity factors through the solid cylinder wall as function of time. Results show the effect of temperature can be explained as increase in von-Mises thermal stress increase as a function of increasing temperature. The highest stress at 400 °C recorded is due to inherent hardness increased of the material indicated by high modulus of elasticity. The mechanical stress is more effective than thermal loading and results show that the stress intensity factor decreases with temperature, except at 400 °C (due to hardness increase).

**POSTERS**

8. Syed A A Shah, Syed T Hasan, M. D. Bramhall, "Micro-Mechanics modelling of Smart Structures", MERI Symposium, Sheffield Hallam University, Sheffield, United Kingdom. 13-14 May 2014.

**MICRO-MECHANICS MODELING OF SMART MATERIALS**

S. A. A. Shah, S. T. Hasan and M. D. Bramhall

Materials and Engineering Research Institute, Sheffield Hallam University, S1 1WB, UK. Email: sasimalishah@gmail.com

**Abstract**

Metal Matrix Composites (MMCs) are rapidly becoming strong candidates as structural materials for many high temperature and aerospace applications. The satisfactory performance of MMC depends entirely on their integrity, the heart of which is the quality of the matrix-reinforcement interface. The nature of the interface depends on the processing of the MMC component. As the MMC attempts to deform during processing, at micro-level the development of local concentration gradients around the reinforcement can be very different to the nominal conditions and play a crucial role in important micro structural events such as segregation and precipitation at the matrix-reinforcement interface. These events dominate the cohesive strength and subsequent mechanical properties of the interface.

**Key Objective**

**"To simulate & predict the interfacial strengthening mechanism at the matrix-reinforcement interface in a Metal Matrix Composite."**

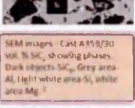
**Objectives**

1. Estimate the interfacial fracture energy.
2. Develop an algorithm to model a hard ceramic in a soft matrix with a clear distinct interface.
3. Set the boundary conditions
4. Numerical simulation of reinforced alloy deformation under a point load.
5. Predict and correlate the interfacial strengthening behaviour of ceramic reinforced alloy.

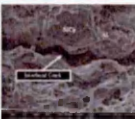
**Concept**



SEM Mapping Analysis of Cast A356/30 vol.% SiC, microstructure showing four distinct phases: Al, SiC, Si<sub>3</sub>N<sub>4</sub> and Magnesium<sup>1</sup>



SEM images - Cast A356/30 vol.% SiC, showing SiC particles. Dark objects: SiC, Grey area: Al, Light white area: Si<sub>3</sub>N<sub>4</sub>, white area: Mg<sup>2</sup>



HTS heat treatment condition: cracking through the interface.<sup>3</sup>

**Theoretical Modelling**

The effect of stress and strain history on the micro-mechanisms is likely to be of greatest importance to the segregation and precipitation phenomena and in turn on interfacial strengthening behaviour of particulate reinforced metallic alloy system. The methods of incorporating stress into the description of the segregation process is based on Raub-Bullough theory [4] and also use the concept of misfit-related impurity-boundary binding energies developed by Carolan and Faulkner [5].

The precipitation kinetics modelling uses Russell's arguments [6] and by evaluating the effect of the misfit term in the free energy of nucleus formation equation. Attempts have been made to quantify the effects of strain on diffusion constants using the saddle point configuration volume method [7] and by performing an iteration loop using the diffusion constant data with the stress induced segregation data, this gives a complete picture of the effect of strain on growth and distribution of precipitates in a reinforced alloy system.

The Micro-mechanics model, based on thermodynamics principles developed by Myrland-Hasan [8], will be used to simulate the fracture strength of the interface at segregated state in MMC.

$$K_{ic} = \frac{K}{L_p} V_p + \frac{2K_m}{L_p} (V_m - V_p) + \frac{K}{L_m} 2V_m + K_m (1 - 3V_p)$$

This model uses energy consideration to express the fracture toughness of the interface in terms of interfacial critical strain energy release rate and elastic modulus. Mechanical data such as fracture strength, elastic modulus and fracture toughness of the composite will be used as inputs to the model. Based on the experimental data and the analysis, the interfacial strength can be determined for SiC particle-reinforced aluminum composites as [9].

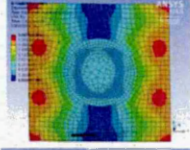
$$\sigma_{ic} = \sqrt{\frac{100G_c E_m}{\pi d}}$$

This model considers the interfacial energy caused by segregation of impurities at the interface and uses Griffith crack-type arguments to forecast the energy change in terms of the coincidence site stress describing the interface and the formation energies of impurities at the interface. Based on Griffith's approach, the fracture toughness of the interface is expressed in terms of interfacial critical strain energy release rate and elastic modulus. The interface fracture toughness and mechanical properties of the composite using two different approaches, a toughening mechanism model based on crack deflection and interface cracking and a stress transfer model. These approaches show success in making prediction possible of trends in relation to segregation and interfacial fracture strength behaviour in SiC particle-reinforced aluminum matrix composites. The proposed model can be used to predict possible trends in relation to segregation and the interfacial fracture strength behaviour in MMC.

**References:**

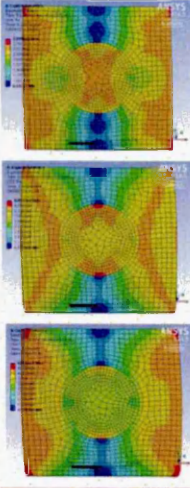
1. J. E. Smith and R. W. Rice, "The Mechanical Behavior of Al<sub>3</sub>Si<sub>2</sub> Intermetallics", *Journal of Intermetallics*, Vol. 1, No. 1, pp. 1-15, 1993.
2. J. E. Smith and R. W. Rice, "The Mechanical Behavior of Al<sub>3</sub>Si<sub>2</sub> Intermetallics", *Journal of Intermetallics*, Vol. 1, No. 1, pp. 1-15, 1993.
3. J. E. Smith and R. W. Rice, "The Mechanical Behavior of Al<sub>3</sub>Si<sub>2</sub> Intermetallics", *Journal of Intermetallics*, Vol. 1, No. 1, pp. 1-15, 1993.

**Numerical Simulation**



**Unit Cell Designed in ANSYS**

As we go down we can see that the stress in the centre part of the cell (SiC) starts increasing till the second grid pattern and then starts decreasing from the third to very low in the fourth grid pattern which shows the failure of the material as tensile forces are increased on both sides of the unit cell.



The increasing stress levels on the edges and decreased levels in the centre.

**Program of Work**

This research will apply the numerical simulation of hard particulate reinforced Al alloy system using ANSYS. The stress-strain history will be predicted at micro-level and fracture toughness behaviour will be correlated with numerical simulation.

This research will help to identify the key parameters controlling the fracture at matrix-reinforcement interface and simplify the constitutive model to predict interface strength of reinforced MMC. The stress-strain response at matrix reinforcement interface will form the basis of correlating empirical to numerical results.

A method of analysis will be proposed to predict the accurate state of matrix-reinforcement interface and the analysis of micro-deflection mechanism supporting at the interface boundary and to help in identifying the strengthening of second phase reinforcement.

**The method of analysis proposed will help the design engineers to incorporate advanced MMC's in real life applications.**

• Completed numerical ANSYS modeling.  
 • Completed the theoretical analysis of the model.  
 • Abstract submitted to the 13th International Conference on MMC.  
 • Theoretical & numerical results to be submitted to the Annual Publication.

9. Syed A A Shah, Syed T Hasan, M. D. Bramhall, "Modelling and Simulation of Interfacial Strengthening Behaviour of a Metal Matrix Composite System ", National Student Conference in Metallic Materials, The Ridge, University of Sheffield, Sheffield, United Kingdom. 26-27 June 2014

## MODELLING AND SIMULATION OF INTERFACIAL STRENGTHENING BEHAVIOUR OF A METAL MATRIX COMPOSITE SYSTEM

**Abstract**

Metal Matrix Composites (MMCs) are rapidly becoming strong candidates as structural materials for many high temperature and aerospace applications. The main objective of using a MMC system is to increase overall temperature of specific mechanical properties of structural components by replacing existing super alloys. The satisfactory performance of MMC depends critically on their strength, the level of which is the quality of the matrix-reinforcement interface. The nature of the interface depends on the processing of the MMC component. As the MMC strength is defined during processing, at micro-level the development of local concentration gradients around the reinforcement can be very different to the nominal conditions and play a critical role in important stress structural events such as segregation and precipitation at the matrix-reinforcement interface. These events determine the ultimate strength and subsequent mechanical properties of the interface.

**Objectives**

1. Estimate the interfacial fracture energy.
2. Develop an algorithm to model a hard ceramic in a soft matrix with a clear distinct interface.
3. Set the boundary conditions.
4. Numerical simulation of reinforced alloy deformations under a point load.
5. Predict and compare the interfacial strengthening behaviour of ceramic reinforced alloy.

**Concept**

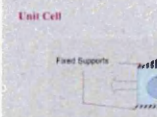


Figure 1: The Unit Cell showing where the forces were acting and the fixed supports.

**Theoretical Modelling**

The effect of stress and strain history on the micro-mechanisms is likely to be of greater importance in the segregation and precipitates phenomena and in turn on interfacial 'recognition' behaviour of particulate reinforced metallic alloy systems. The method of incorporating stress into the description of the segregation process is based on Rate-Independent theory [1].

The thermo-mechanics model, based on Eshelby's principles developed by Mura [2], will be used to simulate the fracture strength of the interface at a given state in MMC.

$$K_p = \frac{K_m}{L_p} \left( 1 + \frac{2K_m}{L_p + L_m} (1 - \nu_p - \nu_m) \right) + \frac{K_m}{L_p} 2\nu_p + K_m (1 - 3\nu_p)$$

This model uses energy concentration to express the fracture toughness of the interface in terms of non-linear critical strain energy release rate and elastic modulus. Mechanical data such as fracture strength, elastic modulus and fracture toughness of the composite will be used to input to the model. Based on the experimental data and the analysis, the interfacial strength can be determined for SiC particle-reinforced aluminium composites as [3].

$$\sigma_{cr} = \sqrt{\frac{1000 \cdot E \cdot \gamma}{\pi l}}$$

This model considers the interfacial energy stored by segregation of impurities at the interface and uses Griffith crack-type arguments to forecast the energy change in terms of the concentration and stress describing the interface and the fracture energy of impurities at the interface. Based on Griffith's approach, the fracture toughness of the interface is expressed in terms of interfacial critical strain energy release rate and elastic modulus. The interface fracture toughness and mechanical properties of the composite using two different approaches, a strengthening mechanism model based on crack deflection and interface cracking and a stress transfer model. These approaches show success in making predictive models of stress to segregation and interfacial fracture strength behaviour in SiC particle-reinforced aluminium matrix composites. The proposed model can be used to predict possible trends in relation to segregation and the interfacial fracture strength behaviour in MMC.

**Numerical Simulation**

A unit cell was designed in ANSYS, representing a small part of the composite which has Aluminium as the base material with a hard reinforcement of Silicon Carbide (SiC) in the centre. It is assumed to be in a symmetric configuration. The dimensions of the unit cell were taken as 1 x 1 with a 0.5 dia for the reinforcement. The top and bottom edges were fixed and loads were varied from 100N to 2000N, equivalent to 50% of the UTS of the composite, and were applied on the right and left side of the composite to visually see the effects of the composite. The interface between the matrix and the reinforcement was bonded (Discretized Grid pattern 1-4 show stresses which can be seen changing in the grid pattern especially in the part of SiC where the stress levels start very small and then gradually get to a point where they are at the peak level and then start decreasing again which shows the failure of the material. Grid patterns 9-16 show corresponding Strain and the values can be seen on the grid pattern.

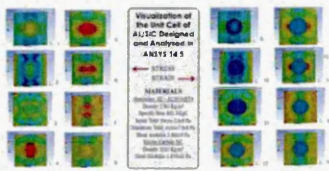


Figure 2: Visualization of the Unit Cell of Al/SiC Composite and Analysis in ANSYS 14.5

**Future Work**

This research will apply the numerical simulation of hard particulate reinforced Al alloy systems using ANSYS. The concentration history will be produced at micro-level and fracture toughness behaviour will be simulated with numerical simulation. This research will help to identify the key parameters controlling the fracture at matrix-reinforcement interface and simplify the constitutive model to predict interface strength of reinforced MMC. The interfacial impurity at matrix-reinforcement interface will form the basis of extending empirical to numerical results.

A method of analysis will be proposed to predict the accurate data of matrix-reinforcement interface and the analysis of micro-deformation mechanisms operating at the interface boundary and some controlling the strengthening of matrix-reinforcement systems.

The method of analysis proposed will help the design engineers to incorporate advanced MMC's in real life applications.

**References**

1. J. E. Shyne, "Design of Metal Matrix Composites: Progress and Prospects," *Materials Science and Engineering: Part B*, vol. 10, pp. 1-10, 1993.
2. E. Eshelby, "The Elasticity of a Particulate Composite," *Proceedings of the Royal Society London, Series A, Mathematical and Physical Sciences*, vol. 251, pp. 37-40, 1959.
3. S. A. Shah, S. T. Hasan, M. D. Bramhall, "Modelling and Simulation of Interfacial Strengthening Behaviour of a Metal Matrix Composite System," *National Student Conference in Metallic Materials*, The Ridge, University of Sheffield, Sheffield, United Kingdom, 26-27 June 2014.
4. S. A. Shah, S. T. Hasan, M. D. Bramhall, "Modelling and Simulation of Interfacial Strengthening Behaviour of a Metal Matrix Composite System," *National Student Conference in Metallic Materials*, The Ridge, University of Sheffield, Sheffield, United Kingdom, 26-27 June 2014.
5. S. A. Shah, S. T. Hasan, M. D. Bramhall, "Modelling and Simulation of Interfacial Strengthening Behaviour of a Metal Matrix Composite System," *National Student Conference in Metallic Materials*, The Ridge, University of Sheffield, Sheffield, United Kingdom, 26-27 June 2014.

Figure 2: The interfacial strengthening behaviour of the Al/SiC composite using the finite element method (FEM) in ANSYS 14.5. The figure shows the stress distribution in the unit cell under increasing loads. The stress is concentrated at the interface between the matrix and the reinforcement, especially in the part of SiC where the stress levels start very small and then gradually get to a point where they are at the peak level and then start decreasing again which shows the failure of the material. Grid patterns 9-16 show corresponding Strain and the values can be seen on the grid pattern.

S. A. Shah, S. T. Hasan and M. D. Bramhall,  
Materials and Engineering Research Institute,  
Sheffield Hallam University, 51 TOWER, U.K.  
Email: s.a.shah@student.shu.ac.uk



10. Syed A A Shah, Syed T Hasan, M. D. Bramhall, "Modelling Strain on the Interface of Al/SiC ", MERI/BMRC Winter Poster Event, Sheffield Hallam University, UK, 11 November 2014

## MODELLING STRAIN ON THE INTERFACE OF AL/SiC

S. A. A. Shah, S. T. Hasan and M. D. Bramhall  
 Materials and Engineering Research Institute, Sheffield Hallam University, S1 1WB, UK.  
 Email: syed.a.shah5@student.shu.ac.uk

### Abstract

Abstract text describing the research objectives and findings.

### Unit Cell



Figure 1: The Unit Cell showing, when the beam was using with fixed supports.

### ANSYS

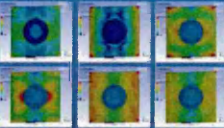


Figure 2: The stress on the interface of Al/SiC.

### Future Work

- To investigate the mechanical strength of Al/SiC interface under various conditions...
- To determine the effect of various parameters on the mechanical strength of the interface...

### Concept

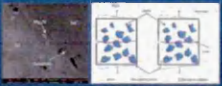


Figure 1: A schematic diagram showing the Al/SiC interface and the unit cell.

### Theoretical Modeling

The method of interfacial energy is described by the equation:

$$\sigma = \frac{1}{2} \rho \left( \frac{d\sigma}{d\rho} \right)^2$$

The interfacial energy is defined as:

$$\sigma = \frac{1}{2} \rho \left( \frac{d\sigma}{d\rho} \right)^2$$

where  $\rho$  is the interfacial energy per unit area,  $\sigma$  is the stress, and  $d\sigma/d\rho$  is the derivative of stress with respect to interfacial energy.

### RESULTS

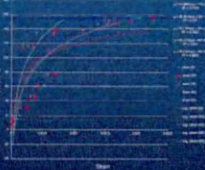


Figure 3: Stress-Displacement curve showing the mechanical behavior of the interface.

### References

1. Syed A A Shah, Syed T Hasan and M. D. Bramhall, "Modelling Strain on the Interface of Al/SiC", MERI/BMRC Winter Poster Event, Sheffield Hallam University, UK, 11 November 2014.
2. ...

Sheffield Hallam University